Structure of three-body hypernuclei

Hildenbrand, Fabian

(2020)

DOI (TUprints): https://doi.org/10.25534/tuprints-00014248

Publikationstyp: Dissertation
Fachbereich: 05 Fachbereich Physik
Quelle des Originals: https://tuprints.ulb.tu-darmstadt.de/14248

Structure of Three-Body Hypernuclei

Zur Erlangung des Grades eines Doktors der Naturwissenschaften (Dr. rer. nat.)
genehmigte Dissertation von Fabian Hildenbrand aus Heidelberg
Tag der Einreichung: 12. Mai 2020, Tag der Prüfung: 17. Juni 2020

1. Gutachten: Prof. Dr. Hans-Werner Hammer
2. Gutachten: Prof. Dr. Jens Braun
Darmstadt – D 17

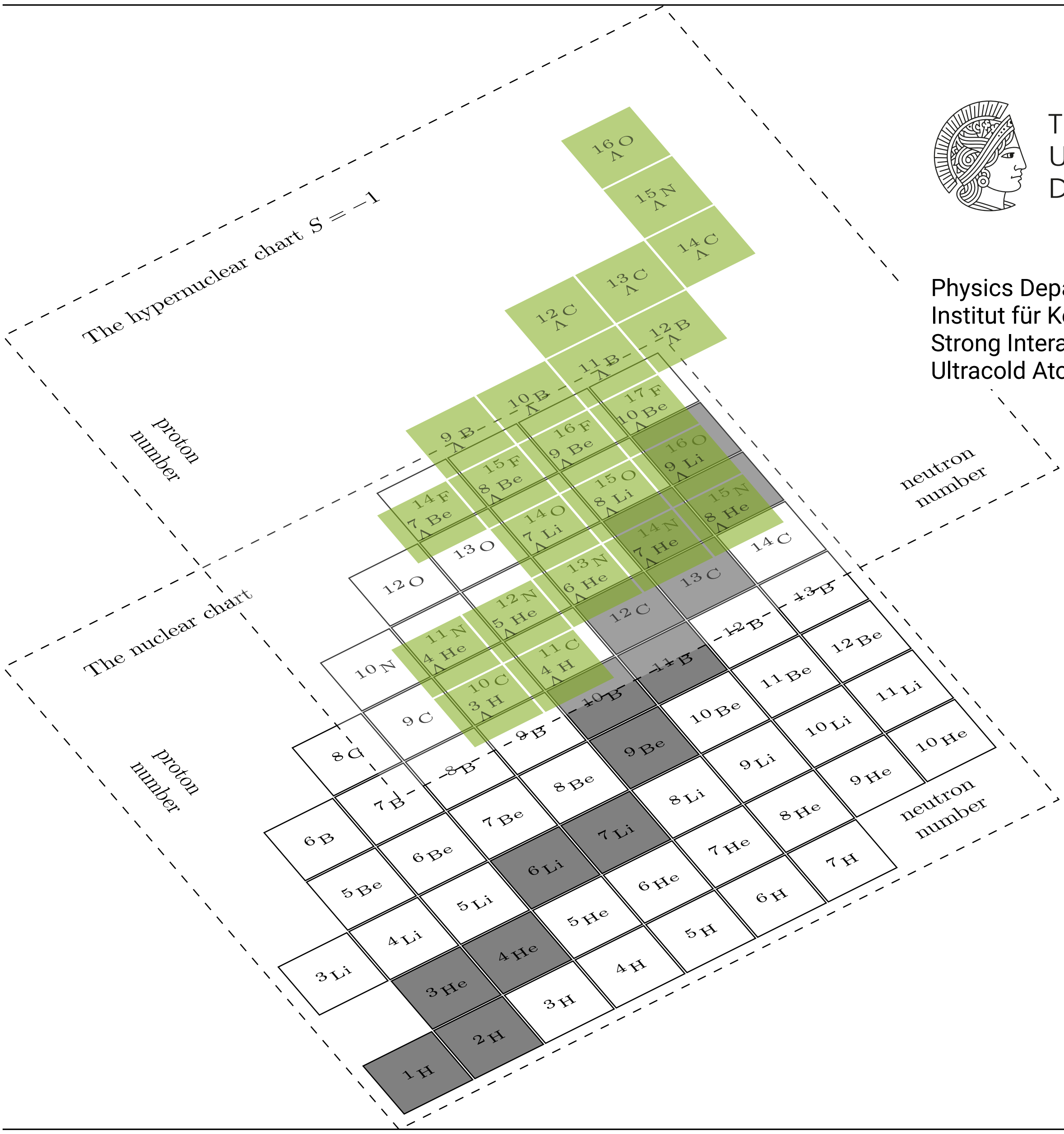

TECHNISCHE
UNIVERSITÄT
DARMSTADT

Physics Department
Institut für Kernphysik
Strong Interactions and
Ultracold Atoms

Structure of Three-Body Hypernuclei

Doctoral thesis by Fabian Hildenbrand

1. Review: Prof. Dr. Hans-Werner Hammer
2. Review: Prof. Dr. Jens Braun

Date of submission: 12. Mai 2020
Date of thesis defense: 17. Juni 2020

Darmstadt – D 17

Bitte zitieren Sie dieses Dokument als:
URN: urn:nbn:de:tuda-tuprints-142483
URL: http://tuprints.ulb.tu-darmstadt.de/14248

Erklärungen laut Promotionsordnung

§8 Abs. 1 lit. c PromO

Ich versichere hiermit, dass die elektronische Version meiner Dissertation mit der schriftlichen Version übereinstimmt.

§8 Abs. 1 lit. d PromO

Ich versichere hiermit, dass zu einem vorherigen Zeitpunkt noch keine Promotion versucht wurde. In diesem Fall sind nähere Angaben über Zeitpunkt, Hochschule, Dissertationsthema und Ergebnis dieses Versuchs mitzuteilen.

§9 Abs. 1 PromO

Hiermit versichere ich, dass ich die vorliegende Dissertation selbstständig angefertigt und keine anderen als die angegebenen Quellen und Hilfsmittel verwendet habe. Alle wörtlichen und paraphrasierten Zitate wurden angemessen kenntlich gemacht.

§9 Abs. 2 PromO

Die Arbeit hat bisher noch nicht zu Prüfungszwecken gedient.

Darmstadt, 12. Mai 2020

Fabian Hildenbrand

Abstract

Hypernuclear physics offers a unique playground for understanding the physics of the strong interaction beyond the up- and down-quark sector. A particularly attractive feature is that hyperons, particles containing at least one strange quark, offer us an opportunity to probe nuclear interior without being affected by the Pauli principle. Due to the lack of two-body bound systems, three-body NNΛ systems take a prominent role for understanding hypernuclear physics. In recent years the focus has been on two particular systems, the hypertriton and the Λnn system in the isospin $I = 0$ and $I = 1$ sector respectively. Although the first has been known for many decades it is still not fully understood. Recent results by the STAR Collaboration question the binding energy established in the past. In addition experimental results for the hypertriton width vary over a large range and are therefore inconsistent. The hypertriton is considered to be a shallow S-wave bound state with a Λ separation energy of a few hundred keV at most.

The nature of the Λnn, however, remains controversial. In 2013 first results have shown evidence that this system might be bound, however the possibility of a resonance or a virtual state are also up for debate. Since typical momenta of these systems are small compared to the pion mass, we can utilize pionless effective field theory to explore these systems.

In the first part of this thesis we exploit this separation of scales within the systems in an effective field theory approach analyzing the structure of these hypernuclei. Effective field theory offers a unique model-independent approach with controllable uncertainties. Utilizing this method we calculate scattering properties for both systems. Since the scattering lengths of the two-body systems are large, both systems show universal behavior due to the Efimov effect. We therefore calculate universal relations for both systems, connecting different observables. In a next step we extend our efforts by calculating matter radii and wave functions.

In the second part of this work, we focus on the other open question about the lifetime of the hypertriton against the weak interaction. We calculate the four most important

mesonic decay channels in a fundamental deuteron approximation. For this part, we utilize isospin symmetry to connect charged and uncharged channels. In light of the new resuls for the binding energy, we discuss the lifetime and related properties relating binding energy data to lifetime date. In addition we take recent results for the weak Λ decay parameters into consideration.

Kurzfassung

Hypernukleare Physik bietet einmalige Möglichkeiten die starke Wechselwirkung über den Up- und Down-Quarksektor hinausgehend zu verstehen. Besonders nützlich ist dabei, dass Hyperonen, Teilchen, welche aus mindestens einem Strange Quark bestehen, es erlauben Kernmaterie ohne den Einfluss des Pauli-Prinzips zu studieren. Da es keine gebundene Zwei-Teilchensysteme gibt, sind Drei-Teilchen NNΛ Systeme von herausstehender Bedeutung. In den letzten Jahren lag der Fokus insbesondere auf zwei Systemen, dem Hypertriton und dem Λnn im Isopin $I = 0$ und $I = 1$ Sektor. Das Erste ist bereits seit Jahrzehnten bekannt, allerdings immer noch nicht vollends verstanden. Vor kurzem publizierte Ergebnisse der STAR Kollaboration ziehen den über Jahre benutzten Wert für die Lambda-Separationsenergie in Zweifel. Zusätzlich sind experimentelle Ergebnisse für die Lebensdauer inkonsistent und decken einen großen Wertebereich ab. Das Hypertriton wird dabei als ein schwach gebundener S-Wellen-Zustand mit einer Lambda-Separationsenergie von maximal wenigen hundert keV angenommen.

Die Natur des Λnn wird hingegen kontrovers diskutiert. Im Jahr 2013 haben experimentelle Ergebnisse darauf hingewiesen, dass dieses System möglicherweise gebunden ist. Allerdings werden auch andere Möglichkeiten, wie zum Beispiel eine Resonanz oder ein virtueller Zustand diskutiert. Da typische Impulse klein gegenüber der Pion Masse sind, können wir pionenlose effektive Feldtheorie benutzten, um diese Systeme zu erforschen.

Im ersten Teil der Dissertation wird diese Skalenseparation ausgenutzt, um die Struktur dieser Hyperkerne zu analysieren. Effektive Feldtheorie bietet dabei einen Modell unabhängigen Ansatz mit kontrollierbaren Unsicherheiten an. Mithilfe dieser Methode werden Streuobservablen berechnet. Da Streulängen der involvierten Zwei-Teilchensyteme groß sind, zeigen beide Systeme den Efimov-Effekt und daher universelles Verhalten. Es werden daher universelle Korrelationen für beide Systeme berechnet, welche verschiedene Messgrößen miteinander verknüpfen. In einem weiteren Schritt wird die Analyse durch die Berechnung von Wellenfunktionen und Massenradien erweitert.

Im zweiten Teil der Arbeit wird der Fokus auf die offene Frage der Lebenszeit des Hypertritons bevor es durch die schwache Wechselwirkung zerfällt gelegt. In einer Näherung eines fundamentalen Deuterons werden die vier wichtigsten Zerfallskanäle berechnet. Dabei wird die Isospin Symmetrie von geladenen und ungeladen Kanälen ausgenutzt. Die Ergebnisse für die Lebensdauer und damit verbundender Eigenschaften werden dabei unter Berücksichtigung der neuen Ergebnisse für die Bindungsenergie diskutiert. Dabei werden Verknüpfungen zwischen Resultaten für die Bindungsenergie und die Lebensdauer hergestellt. Zusätzlich wird der Einfluss der neuesten Ergebnisse für den schwachen Λ Zerfallsparameter beleuchtet.

Contents

1. Introduction

Most everyday life phenomena can be explained using what we call normal matter i.e. neutrons, protons and electrons. However, these are not all constituents of matter we know of. With the discovery of the kaon in 1947 by Rochester and Butler [1], the picture of normal matter needed to be extended. The kaon, a meson, consists of a strange quark and an anti-up or -down quark. It introduced a new type of matter, strange matter. Over the years more families of quarks have been added to the fundamental particle zoo and the picture was extended even further.

The most advanced theory describing physical phenomena and aspects is the standard model of particle physics. Quantum Chromodynamic (QCD), which is part of the standard model, describes strong interactions among quarks and gluons [2]. Since the late 2000s ab-initio calculations of nucleon masses at near physical poin masses are available [3]. Although QCD is the best possible description of the strong force available, calculating compound particles - especially light (hyper)nuclei - to a precise level is challenging or at least computationally expensive. This becomes particular challenging due to the confinement of quarks at low energies and the strong coupling.

Another approach for calculating light nuclei observables uses so-called effective field theories (EFT). The basic idea here is that the quarks are confined at the energy level of nucleons. Therefore phenomena on the level of quark physics cannot be resolved and are not relevant degrees of freedom. Identifying the relevant degrees of freedom at a certain scale allows us to systematically approach compound systems of quarks. For example nuclei can be described in terms of neutrons and protons[1]. In contrast to the microscopic attempt to solve the standard model directly, this approach is based on fixing interaction observables to experimental results or, if available, more fundamental theories.

---

[1] Note: In principle this method can be applied to many fields, for an comprehensive introduction see also Ch. 2.3.

Having neutrons and protons now at hand, we can combine them to built up the nuclear chart, the normal matter the world around us consists of. However, as mentioned earlier, we can extend this chart by including hyperons, particles that contain at least one strange quark. The inclusion of hyperons in nuclear bound states extends the nuclear chart to a third dimension, as already illustrated on the title page. These so-called hypernuclei offer a unique playground for testing our understanding of the strong interactions beyond the u and d quark sector. A particularly attractive feature of hypernuclei is that hyperons probe the nuclear interior without being affected by the Pauli principle.

However, hypernuclei are not stable. They are often short-lived, with life spans of only hundreds of picoseconds. Although stable against the strong interaction, they are unstable against the weak interaction. This interaction, being part of the standard model as well, allows particle transitions between different quark families, opening up decays of hypernuclei into normal matter baryons and mesons. Typical for hypernuclei discussed in this thesis are decays into nucleons and pions. Although generally described in terms of the Weinberg-Salam theory of weak interaction, a frequently and for our cases sufficient effective low-energy field theory is given by the Fermi theory.

There is a vigorous experimental and theoretical program in hypernuclear physics that dates back as far as the 1950s exploring the understanding of those nuclei. (See Ref. [4] for a comprehensive review of past and current efforts.)

1.1. Three-Body Hypernuclei

There is no bound two-body system consisting of two hyperons or a nucleon and a hyperon. Thus three-body systems are a gateway to understanding hypernuclear physics and therefore the interaction between hyperons and nucleons. The most prominent example of such a three-body hypernucleus is the hypertriton, consisting of a proton, a neutron and a Λ particle. This system has been known to be bound in a shallow S-wave state for about 60 years. The binding energy is expected to be $B = 2.35 \pm 0.05$ MeV [5]. The state is shallow because the binding energy can be separated into the binding of the deuteron with about $B_d \approx 2.22$ Mev and a weakly attached Λ with a binding energy of only $B_\Lambda = 0.13 \pm 0.05$ MeV [5]. However, this system is still not fully understood yet. In particular results for the lifetime have remained a puzzle until today [6]. Due to the shallowness of the Λ it is expected that the decay is mainly driven by the decay of the free Λ, which has a lifetime of about $\tau_\Lambda = 263.2$ ps [7]. The lack of data for the two-body Λ-N systems at the low energies relevant for hypernuclei make this puzzle even more challenging. Further on new results on the hypertriton binding energy [8] suggests that the state might not be as shallow as we have initially thought. For a further introduction to the hypertriton see also Ch. 4.1.

In 2013 the HypHI collaboration at GSI found evidence that a second three-body hypernucleus, the Λnn, might be bound [9]. Immediately after publication an intensive discussion of the nature of this new state started. Is it bound, a resonance, and should we not see it in other experiments as well, and how does this influence other hypernuclear data? Furthermore the Λnn would be the first bound many-baryon state that does not include a proton since all states including only neutrons are considered to be unbound. In addition, this would directly imply that the Λnn is a boromean state since, as stated before, all hyperonic two-body states and the di-neutron are unbound. For a further introduction to the Λnn system see also Ch. 4.2.

The goal of this thesis is to address the challenges and open questions of the two three-body systems the hypertriton and Λnn applying EFT methods exploiting the separation of scales available.

1.2. Structure of this Thesis

This thesis is structured in four main parts. In the first part general physical concepts are introduced in a compact fashion covering the theoretical foundation on which calculations in this thesis are based on. The chapter covers basic concepts of scattering theory and interactions, but also the concepts of EFTs and universality. Following up Ch. 2 a short introduction on hypernuclear physics and its unique properties is given. The focus will be on the basic ideas which are important for this work. After having laid the physical foundation, we discuss the structure of three body hypernuclei in detail in a pionless effective field theory in the next chapter. The focus will be on the calculations of phase shifts and the $\Lambda - d$ scattering length as a function of the binding energy of the hypertriton. Further on we calculate three-body wave functions as well as matter radii. This will be done in Ch. 4. We then shift our efforts towards the lifetime of the hypertriton and the associated puzzle in a deuteron closure approximation. We calculate the widths and therefore the lifetime of the hypertriton for the important mesonic decay channels at the same time introducing the weak interaction in the system. We will conclude our findings of Ch. 6 with a summary of this work in Ch. 7.

2. Theoretical Background

In this chapter we introduce the most important physical concepts relevant for this thesis in comprehensive fashion. We draw our attention towards scattering theory and universal effects before discussing the specialties of hyperon physics in the next chapter. The introduction of scattering theory will mostly follow the book by Sakurai [10] and the review by Braaten and Hammer [11].

2.1. Low-Energy Physics

Describing quantum mechanical problems on a fundamental level implies an explicit treatment of all its constituents. This means especially a simple nuclear two-body problem becomes a complicated many-body problem involving all quarks and leptons of the standard model. Such standard model calculations are not accessible with today's computational power.

At low-energy scales we fortunately do not need to access the substructure of a complex object, for example a nucleus or a nucleon, since it is not resolved at a low-energy scale. This reduces the system again to a few-body problem of point-like particles. The picture of a complex object like a nucleon as a system without substructure holds particularly well if the typical momentum $\boldsymbol{p}$ becomes so small so that the *de Broglie* wave length $\lambda = 2\pi/p$ is large compared to the object itself. The wavelength then cannot resolve the internal structure of the object. Since the relative momenta of the involved particles are small, the relativistic energy-momentum relation $E^2 = \boldsymbol{p}^2 + m^2$ can be expanded for small $\boldsymbol{p}$ compared to rest mass m of the particle. We obtain

$$E = \sqrt{\boldsymbol{p}^2 + m^2} \approx m + \frac{\boldsymbol{p}^2}{2m} + \mathcal{O}\left(\boldsymbol{p}^4\right) . \tag{2.1}$$

The typical momenta in this thesis are small compared to the mass of the pion, the lightest meson. Thus this expansion holds and we can neglect all relativistics corrections to the non-relativistic dispersion relation Eq. (2.1).

2.2. Basic Concepts of Scattering Theory

For the calculation of basic properties of the hypertriton (Λpn) and the Λnn two concepts are of utter importance: The scattering length a and the scattering amplitude f. Since we are interested in low-energy[1] scattering, we want to restrict ourselves to the non-relativistic case. The scattering amplitude is the starting point for calculations of physical properties like the matter radius of a system. At low energies the scattering of two particles is mainly determined by their S-wave scattering length[2]. This scattering length can be defined by the partial wave expansion of the scattering amplitude, connecting both of the concepts. In order to do so, we consider the wave function solution Ψ^+ of the elastic scattering problem for two particles with opposite momenta. In the asymptotic limit for large distances $r \to \infty$ we obtain the sum of a plane wave and an outgoing wave

$$\left\langle \boldsymbol{r} \middle| \Psi^+ \right\rangle \Rightarrow e^{ikz} + f_k\left(\theta\right) \frac{e^{ikr}}{r}. \tag{2.2}$$

The prefactor of the outgoing spherical wave $f_k\left(\theta\right)$ is defined as the scattering amplitude, depending on the scattering angle θ and the wave number k. The scattering amplitude is directly connected to the amount of particles scattered towards a specific area Ω encoded in the cross section $\mathrm{d}\sigma$. For distinguishable particles we find for example

$$\frac{\mathrm{d}\sigma}{\mathrm{d}\boldsymbol{\Omega}} = \left|f_k\left(\theta\right)\right|^2. \tag{2.3}$$

At low-energies S-wave scattering becomes isotropic and therefore does not depend on the angle anymore. We therefore define the scattering length a as the low-energy limit of the scattering amplitude

$$\lim_{k \to 0} f_k\left(\theta\right) = -a. \tag{2.4}$$

---

[1] Low-energy to be understood in the sense introduced before.

[2] We will from now on only refer to it as the scattering length.

This definition offers us an experimental approach to determine the scattering length of a two particle system. Since relation Eq. (2.3) connects the scattering length directly to the low-energy limit of the cross section, we obtain for distinguishable particles

$$\lim_{E\to 0} \sigma\left(E\right) = 4\pi a^2. \tag{2.5}$$

The resulting relation is quadratic in the scattering length. Therefore only the magnitude is measurable directly. The sign of the scattering length is therefore only accessible in interference experiments. In order to take corrections and higher orders in the angular momentum $\boldsymbol{L}$ into account it is useful to expand the scattering amplitude in partial waves. We obtain the scattering amplitude in terms of Legendre polynomials

$$f_k\left(\theta\right) = \frac{1}{k}\sum_{l=0}^{\infty}\left(2l+1\right) f_l\left(k\right) P_l \cos\left(\theta\right) \tag{2.6}$$

with $P_l \cos\left(\theta\right)$ the l-th Legendre polynominal. The coefficients f_l can be expressed in terms of scattering phase shifts. Analyzing again the outgoing behavior of the spherical wave we obtain the following relation between f_l and the corresponding phase shifts δ_l

$$\begin{aligned} f_l\left(k\right) =& e^{i\delta_l(k)} \sin\left(\delta_l\left(k\right)\right) \\ =& \frac{1}{\cot\left(\delta_l\left(k\right)\right) - i} \, . \end{aligned} \tag{2.7}$$

For sufficiently low energies it is possible to expand the phase shifts in powers of k^2 since they are analytic in the energy. For S-waves ($l = 0$) we obtain the effective range expansion

$$k \cot \delta_0 = -\frac{1}{a} + \frac{1}{2} r_s k^2 + \ldots \tag{2.8}$$

with r_s the effective range of the interaction [12, 13]. Similar expressions can be obtained for higher partial wave phase shifts since $k^{2l+1} \cot \delta_l$ in analytic in the energy. At sufficiently low momenta k the phase shift is then only determined by the scattering length a. At this point the effective range introduces a momentum scale M_{High} at which it becomes relevant. For the remainder of this thesis we will be only interest in momenta $p < M_{\text{High}}$.

2.2.1. Interactions at Low Energies

Having identified the typical momentum scale of the non-relativistic physics we want to discuss, we now need a way to describe the interaction between them. This can be done in terms of two-body potentials $V\left(\boldsymbol{r},\boldsymbol{r}'\right)$ in position space. The eigenenergies of such a two-body system are then determined by the stationary Schrödinger equation for the relative wave function $\psi\left(r\right)$. In position space with the usual conventions it is given by

$$-\frac{\boldsymbol{\nabla}_r^2}{2\mu}\psi\left(\boldsymbol{r}\right)+\int \mathrm{d}^3\boldsymbol{r}'\,V\left(\boldsymbol{r},\boldsymbol{r}'\right)\psi\left(\boldsymbol{r}'\right)=E\psi\left(\boldsymbol{r}\right). \tag{2.9}$$

In this thesis we will only study so-called short-range potentials. Such potentials fall of as $r\mapsto\infty$ faster than any power law. For example the potential might drop to zero at a specific point (finite range potential) or have an exponential tail. At small energies it is possible to approximate any short-range potential, for example a square well potential, in terms of contact interactions, resulting in a sum of delta distribution and derivatives thereof. Before returning to our general discussion about scattering theory we discuss the important interactions for our causes utilizing the just introduced concept of the scattering length and contact interactions.

2.2.2. Nucleon-Nucleon Interaction

Baryons consist of quarks and gluons. Interactions between those fundamental particles are described by QCD description, the fundamental theory of the strong interaction. Since the interactions is strong and therefore the coupling constant of QCD becomes large in the case of low energies, quarks and gluons are confined into so-called hadrons. This means that no free quark or gluon can be observed. Hence at a nuclear level hadrons, especially neutrons and protons, are the effective and therefore relevant degree of freedom. The underlying physics cannot be resolved. Since it is not possible to resolve quark physics directly within an experiment, it is very challenging to derive a description of nucleon-nucleon interactions directly from QCD. Extracting features from scattering experiments and symmetry considerations leads to a wide range of phenomenological interaction potentials for nucleons that reproduce nuclear data correctly. Since there is no strict prescription how to obtain a two-body or three-body force within such a potential, there is no systematic way to improve it.

A way to avoid this problem of having no systematic improvement is to implement an EFT to access the nucleon-nucleon interaction. In the nucleon-nucleon case chiral EFT introduced by Weinberg is the theory of choice. It describes the low-energy dynamics of QCD and is consistent with the approximate chiral symmetry of QCD as well as parity and charge conjugation symmetry. It features the typical properties of any EFT described in Ch. 2.3. In particular, its power counting sorts the interaction terms according to an expansion in low momenta and low quark masses. The Goldstone bosons of the theory arise then as a derivative coupling. As for the theory used later in this thesis this expansion, however, is non-pertubative. Therefore many-body interactions enter the theory in comparison to model potentials in a systematic, natural way. Compared to the pionless EFT later used within this thesis chiral EFT includes pions as explicit degree of freedom. A different approach would be to calculate nuclear properties on the lattice (lattice QCD), as mentioned in the introduction.

For our purposes enough scattering data for the nucleon-nucleon interaction is available. Therefore we can obtain the needed scattering properties directly from experiment. At low energy all interactions are considered to be of S-wave type, corresponding to $l = 0$. As indicated by the effective range expansion Eq. (2.8) at very low energy the scattering phase shift is then only determined by the scattering length a.

Another approximate symmetry, the isospin symmetry, comes in handy when dealing with nucleons. Both nucleons have isospin $I = 1/2$ with the projection in z-direction $I_3 = 1/2$ for protons and $I_3 = -1/2$ for neutrons respectively. Analyzing the structure of two nucleons we obtain an isospin singlet $I = 0$ and an isospin triplet $I = 1$. The isospin quantum number encodes the relative up- ($I = \frac{1}{2}$) and down-quark ($I = -\frac{1}{2}$) content of a hadron. Respective scattering lengths are given in Fig. 2.1. Without any isospin breaking we would expect all three scattering lengths in the triplet channel to be equal. For the proton-proton scattering length due to the Coulomb interaction we would expect a deviation. Even when removing the pure Coulomb part for the proton-proton scattering length, different values appear in the literature because of interference terms between the the strong and the Coloumb force. In the following calculations we will address nucleon-nucleon interactions in terms of a simple contact interaction associated to the scattering lengths given in Fig. 2.1. The limit of this implementation in momentum space is then given by the momentum that is needed to exchange a pion, which is a natural breakdown scale for pionless theories. This scale is large compared to the scales relevant for hypernuclear systems discussed in this thesis.

2.2.3. Hyperon-Nucleon Interaction

In a similar fashion as before we introduce a contact interaction for the hyperon-nucleon interaction only driven by the scattering length. In contrast to the interaction in the nucleon-nucleon sector, hyperons and nucleons are distinguishable particles. This changes the interaction type on a fundamental level, since restrictions due to the Pauli principle do not exist. Unfortunately at low energy the amount of scattering data is

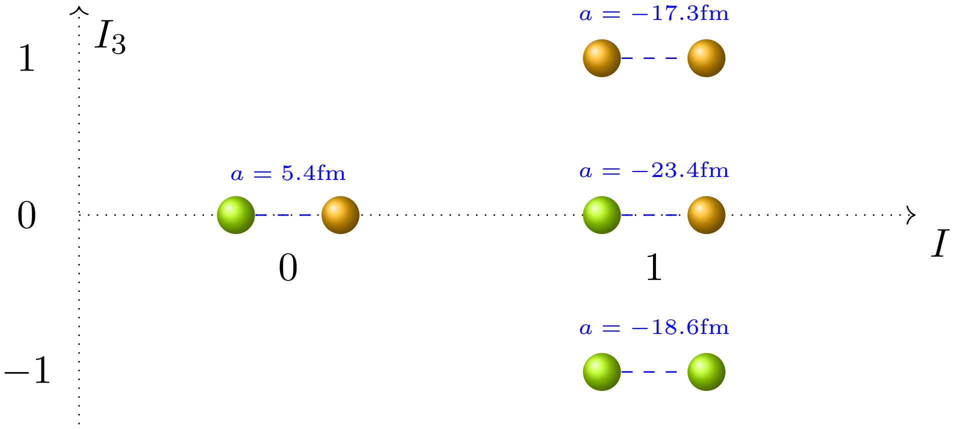

Figure 2.1.: Isospin singlet and triplet for the nucleon-nucleon interaction with corresponding scattering lengths a taken from Refs. [14–16] in the $I-I_3$ plane. The proton is depicted orange and the neutron is depicted greenish.

not sufficient to directly obtain the necessary scattering parameters from experiments. Therefore we will use theoretical results as input parameters for our theory. We use calculations done by Haidenbaur et al. at next to leading order in chiral-EFT [17]. The relevant contributions are depicted in Fig. 2.2. For the for our cases relevant scattering processes in the $p - \Lambda$ channels they obtained for the scattering lengths $a_1^{\Lambda p} = -2.90 - (-2.91)$ fm and $a_3^{\Lambda p} = -1.48 - (-1.70)$ fm. Since there are no direct calculations for the $n - \Lambda$ case available, we will enforce isospin symmetry and use the same values for the scattering lengths in the Λn channels. Please note that the scattering lengths calculated by Haidenbauer et al. are constructed in such a way that they explicitly reconstruct the binding energy of the hypertriton [17] of $B = 2.35$ MeV. These results for the scattering lengths are comparable with the results obtained by meson-exchange potentials [18, 19]. This fixing to a three-body bound state is needed due to the fact that there is no two-body bound state and insufficient scattering data, making the hypertriton the lightest three-body bound state.

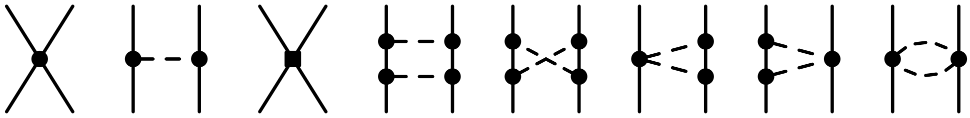

Figure 2.2.: Relevant chiral EFT contributions up to NLO according to Ref. [17]. Octet baryons are depicted by straight lines, pseudo-scalar mesons by dashed lines.

2.2.4. The Lippmann-Schwinger Equation

If we want to calculate the scattering amplitude and hence the phase shifts directly for a given potential, we will enforce the Lippmann-Schwinger equation for the two-body problem. In an abstract form the Schrödinger equation Eq. (2.9) for the time-independent two-body problem is given by

$$\hat{H}\left|\psi\right\rangle = E\left|\psi\right\rangle \tag{2.10}$$

with $\hat{H} = \hat{H}_0 + \hat{V}$ the Hamiltonian consisting of a potential part $\hat{V}$, which one could for example express through diagrams as shown in Fig. 2.2, and $\hat{H}_0$ the Hamiltonian for a free particle. In configuration space this Hamiltonian is then given by

$$\langle \boldsymbol{r}|\hat{H}|\psi\rangle = -\frac{\boldsymbol{\nabla}_r^2}{2\mu}\psi\left(\boldsymbol{r}\right) + \int \mathrm{d}^3\boldsymbol{r}'\, V\left(\boldsymbol{r},\boldsymbol{r}'\right)\psi\left(\boldsymbol{r}'\right) \ , \tag{2.11}$$

with μ the reduced mass of the two-body system. Since we are interested in returning back to our discussions about the scattering amplitude and phase shifts, we are particularly interested in states which reproduce a plane wave $|\boldsymbol{p}\rangle$ if V vanishes, see also Eq. (2.2). Therefore we choose $\left(E - \hat{H}_0\right)|\boldsymbol{p}\rangle = 0$ with $E = \boldsymbol{p}^2/(2\mu)$ and obtain the Lippmann-Schwinger equation

$$\left|\psi^+\right\rangle = |\boldsymbol{p}\rangle + \left(E - \hat{H}_0 + i\epsilon\right)^{-1}\hat{V}\left|\psi^+\right\rangle \tag{2.12}$$

with the usual $+i\epsilon$ prescription shifting the singular expression $E - \hat{H}_0$ slightly into the complex plane, hence it is invertible. The Lippmann-Schwinger equation is self-consistent and to be understood in the limit $\epsilon \mapsto 0$ after all mathematical operations. For the free solution we obtain the Greens-function of the Lippmann-Schwinger equation

$$G_0\left(E\right) = \left(E - \hat{H}_0 + i\epsilon\right)^{-1}. \tag{2.13}$$

Projecting the Lippmann-Schwinger equation (2.12) onto configuration space, we obtain

$$\psi^+\left(\boldsymbol{r}\right) = e^{i\boldsymbol{pr}} - \frac{\mu}{2\pi}\int \mathrm{d}^3\boldsymbol{r}'\frac{e^{i\bar{k}(r-r')}}{\left|\boldsymbol{r}-\boldsymbol{r}\right|}\left\langle\boldsymbol{r}'\middle|\hat{V}\middle|\psi^+\right\rangle. \tag{2.14}$$

In the limit of $r \mapsto \infty$ we obtain the asymptotic solution given in Eq. (2.2) which was our starting point for the discussion of the scattering amplitude and length

$$\psi^+\left(\boldsymbol{r}\right) = e^{i\boldsymbol{pr}} - \frac{\mu}{2\pi}\left\langle\boldsymbol{p}'\middle|\hat{V}\middle|\psi^+\right\rangle\frac{e^{i\bar{k}r}}{r}, \tag{2.15}$$

connecting the potential V directly to the scattering amplitude via

$$\frac{\mu}{2\pi}\left\langle\boldsymbol{p}'\middle|\hat{V}\middle|\psi^+\right\rangle \equiv f\left(\boldsymbol{p}',\boldsymbol{p}\right). \tag{2.16}$$

Eq. (2.12) also allows us to find a direct formal solution for the scattering state $|\Psi^+\rangle$. Defining the T-Matrix to be $\hat{T}\left|\boldsymbol{p}\right\rangle \equiv \hat{V}\left|\psi^+\right\rangle$ a formal solution for the Lippmann-Schwinger equation is given by

$$\left|\psi^+\right\rangle = \left(\boldsymbol{1} + G_0\left(E\right)T\right)\left|\boldsymbol{p}\right\rangle. \tag{2.17}$$

Application of $\hat{V}$ from the left side lets us shift the original problem from finding a wave function fulfilling Eq. (2.12) towards determining the T-matrix. The Lippmann-Schwinger equation for the T-Matrix reads

$$\hat{T}\left(E\right) = \hat{V} + VG_0\left(E\right)\hat{T}\left(E\right). \tag{2.18}$$

Implementing our definition of the T-Matrix for Eq. (2.16) now yields

$$f\left(\boldsymbol{p}',\boldsymbol{p}\right) \equiv \frac{\mu}{2\pi}\left\langle\boldsymbol{p}'\middle|T\middle|\boldsymbol{p}\right\rangle \equiv \frac{\mu}{2\pi}t\left(\boldsymbol{p}',\boldsymbol{p}\right) \tag{2.19}$$

In the remainder of this thesis we will often deal with the momentum space representation of Eq. (2.18) not for the two-body, but for the three-body case, called the Faddeev-equations [20].

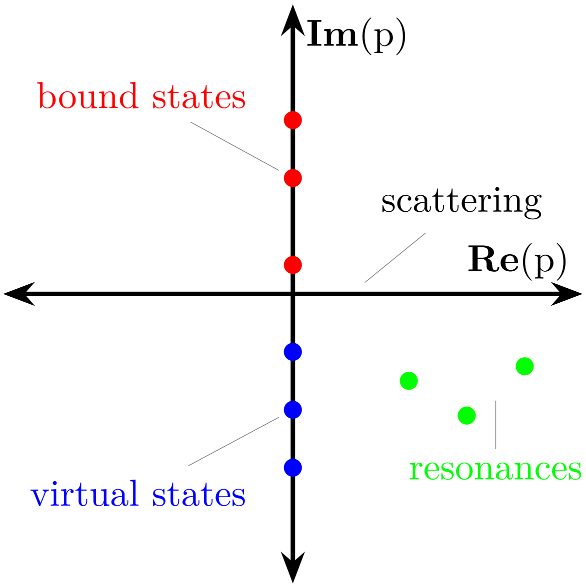

Figure 2.3: The complex $\boldsymbol{p}$-plane. Bound states (red states) arise at the positive imaginary axis with a binding momentum $\gamma = -ip$. States close to the origin are considered shallow states. Virtual states are on the negative imaginary axis (blue states). Scattering occurs at real positive momenta. Resonances are in the fourth quadrant (green states)

2.2.5. Bound States

Since we are not only interested in scattering properties but particularly for the hypertriton also in the bound state of the three-body system, we now look at energies smaller than zero. Let us consider momenta fulfilling

$$\boldsymbol{p}^2 = 2\mu E < 0 \tag{2.20}$$

and analyze the complex $\boldsymbol{p}$ plane Fig. 2.3. Bound states then occur on the positive imaginary axis at a momentum $i\gamma$ with $\gamma > 0$. States on the negative imaginary axis we call virtual states. From now on we will call γ the binding momentum. We obtain as the bound state condition for the scattering phase shifts

$$\cot\left(\delta_l\left(p = i\gamma\right)\right) = i \tag{2.21}$$

2.3. Effective Field Theory

The general idea of an effective theory is to approach a certain phenomenon or effect in a specified energy regime without understanding the underlying theory. Indeed it is even unnecessary to know the theory lying beyond the regime of interest. The huge advantage compared to a model approach is that EFTs are systematic. The accuracy of a model depends mainly on its pre-made assumptions and input parameters, there is no systematic way of improvement. An effective theory in contrast offers a systematic procedure to obtain results at arbitrary accuracy. Such an effective theory can be obtained by exploiting separation of scales in the studied systems. Typical scales are given by masses, distances or excitation energies. The idea is now to use the fact that low-energy physics cannot resolve details of high-energy phenomena. Therefore we can separate those two regimes and can perform an expansion in terms of those scales, sorting the contributions into leading and next to leading parts.

The concept of effective theories can be applied to classical as well as to modern theories. In a quantum mechanical framework this idea allows us for example to describe the leading order scattering length a through a simple effective separable potential, eg. a coupling constant g. This can be solved analytically; we obtain for example for g as a function of the cutoff Λ_c and the scattering length a. The typical behavior of $g\left(\Lambda_c\right)$ for a fixed a and the nonpertubative result for a as a function of g for a fixed cutoff is shown in Fig. 2.4.

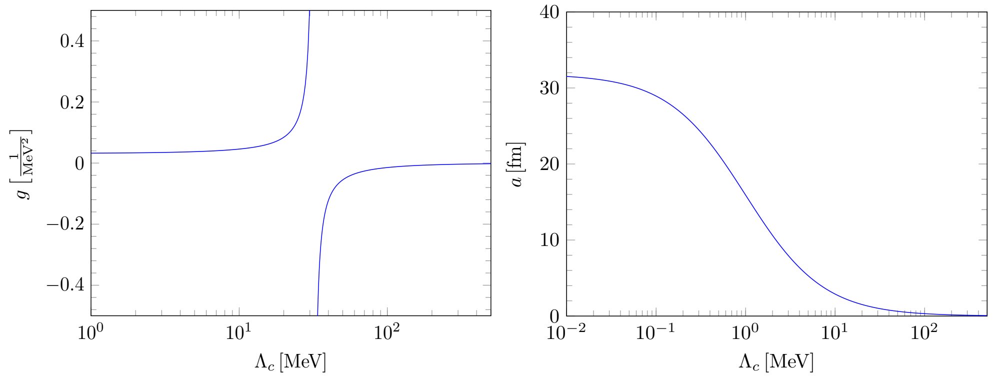

Figure 2.4.: Left panel: Behavior of the coupling constant $g\left(\Lambda_c\right)$ for fixed scattering length $a = 1$fm. Right panel: $a\left(\Lambda_c\right)$ for a fixed coupling constant. For further details see also App. A.1.

The general prescription to construct an EFT is to write down the most general Lagrangian that respects all the symmetries of the problem (e.g. Galilean invariance). In a second step we use the effective theory approach and utilize a separation of scales within the system. We then introduce a power-counting which allows us to make an expansion in powers of the ratio between the low momentum scale μ_{low} and the high momentum scale μ_{high}. It thereby sorts interactions and diagrams by their importance and hence their contribution, since $\mu_{\text{low}}/\mu_{\text{high}} < 1$ assuming that the expansion parameters scale naturally (prefactors of $\mu_{\text{low}}/\mu_{\text{high}}$ are of order 1). Such a power-counting offers a systematic prescription how to improve the theory up to arbitrary precise results as first suggested by Weinberg [21].

Let us consider for example a halo nucleus, weakly bound nuclei which received increasing interest in the recent years. A halo nucleus consists of a tightly bound core and one or more weakly bound particles which are far away R_H from the core compared to the core's size R_C. We can exploit this separation of scale to construct an effective field theory in terms of $\mu_{\text{low}} = R_H^{-1}$ and $\mu_{\text{high}} = R_C^{-1}$. At leading order we can then calculate properties up to an accuracy of $\mu_{\text{low}}/\mu_{\text{high}}$. Typical ratios for halo nuclei range between $\mu_{\text{low}}/\mu_{\text{high}} \sim 0.1 - 0.4$ which would make our theory precise to up to $10 - 40\%$ at leading order. Indeed one can to describe certain hypernuclei with weakly bound hyperons as a halo nucleus.

Since we use pionless EFT in this thesis to describe the systems of interest and integrate pions out of the theory, we look at systems with very large mass difference to understand why pions can be neglected at low energies. Let us consider a theory with two interacting particle types, light particles with the mass M_{light} and a heavy particle with the mass M_{heavy}. If we now want to resolve physics determined by the energy range of the light particle, we are insensitive of the physics generated by the exchange of heavy particles. Since $M_{\text{light}} \sim q \ll M_{\text{heavy}}$ we can expand the corresponding propagator for the exchange of a heavy particle

$$\frac{g^2}{M_{\text{heavy}}^2 - q^2} \approx \frac{g^2}{M_{\text{heavy}}^2} + \frac{g^2 q^2}{M_{\text{heavy}}^4} + \dots . \tag{2.22}$$

The coupling constant g here represents the coupling between a light and a heavy particle. For sufficiently small momenta we can abort this expansion and absorb all high-energy physics into low-energy constant

$$C_0 \equiv \frac{g^2}{M_{\text{heavy}}^2}. \tag{2.23}$$

This exchange then can be represented by contact interactions. The full mechanism of an interaction conducted by heavy particles was integrated out of the theory for scales of the light particle.

2.3.1. Pionless Effective Field Theory

The fundamental degrees of freedom in this thesis will be nucleons and hyperons, in particular the Λ particle. At low energy we can integrate the lightest meson, the pion, out of the theory, as described before. It is then possible to describe physics at a scale $\mu \ll m_\pi \approx 135$ MeV via pure contact interactions. This means all interaction can be written in terms of δ functions and derivatives of them relating pionless EFT back to our description of low-energy short-range quantum mechanics at the beginning of the chapter.

Pionless EFT is an ideal playground of testing universal properties of nuclear problems. The deuteron arises as a universal shallow dimer within pionless EFT. This is the case since the scattering length $a_d = 5.42$ fm is much larger compared to the scale of pionless EFT given by the inverse pionmass $1/m_\pi \sim 1.4$ fm [14]. Since the hypertriton arises as a shallow bound state as well, it is worthwhile looking a little bit deeper into the deuteron as a shallow bound state, results that we will use later as a benchmark test for our results in the three-body sector.

2.3.2. Dimer Fields

In order to utilize the concept of two-body scattering lengths in the three-body sector as well, we will construct effective dimer fields in this thesis [22]. A dimer field combines two fields to a composite effective dimer field, which will then be included in the theory explicitly. Dealing with three-body systems, we then can apply the formalism of a two-body scattering length between those effective dimers and a third single particle.

It can be shown that Lagrangians with dimer fields describe the same physics as those without. Higher particle interactions are generated by construction but are irrelevant due to the lack of particles. Therefore the so-called diatomic field trick allows us to abuse scattering concepts from the two-body sector. The typical procedure to obtain the full dimer propagator is to either sum up an expansion in the coupling constant to all orders (Fig. 2.5 upper line) or to solve the corresponding integral equation (Fig. 2.5 bottom line). For an application of this formalism to three identical bosons, see for example Ref. [11].

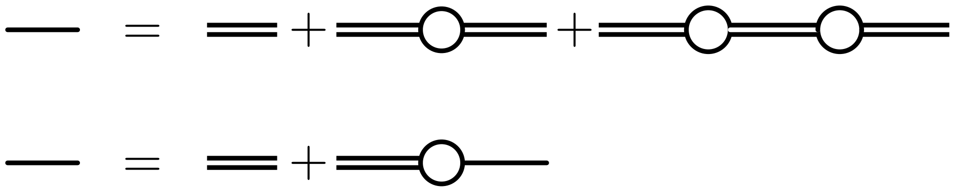

Figure 2.5.: Diagrammatic equations for the complete dimer propagator. The upper line is the pertubative expansion in terms of the coupling constant. In the lower line the corresponding integral equation is depicted. See also Refs. [11, 22].

2.4. Universality

Particles with a large scattering length and short-range interactions show universal properties. As universal we understand that the properties do not depend on the details of the particle structure or the interaction. For the two-body problem the physics are completely determined by the scattering length a, while in the three-body sector for example a sequence of three-body shallow bound states depends only on a and a three-body parameter. Furthermore all important scattering quantities are log-periodic. Since the scattering lengths in the hyperon-nucleon interactions are large compared to the two-pion exchange and we only consider short-range interactions, those universal properties also arise for three-body hypernuclei.

2.4.1. The Shallow Dimer

As mentioned in the introduction on pionless effective field theory the deuteron emerges as universal dimer within this theory. As a universal dimer we understand a dimer with a binding momentum γ_d much smaller than the ultraviolet cutoff Λ_{uv} or a scattering length a much larger than the range of the potential R. For $a > 0$ a single shallow dimer state exists while for $a < 0$ there is only a virtual state. The binding energy is determined fully by the phase shift at threshold and therefore by the scattering length. Utilizing the bound state condition Eq. (2.21) and the effective range expansion Eq. (2.8) we obtain that the binding momentum γ at leading order is given by

$$\gamma \approx \frac{1}{a}$$

if the effective range r_s is small compared to the scattering length a. We then receive a simple expression for the binding energy of a dimer

$$E_d \approx \frac{1}{2\mu a^2}. \tag{2.24}$$

A second universal property, the mean square separation of the two particles reads

$$\langle r^2 \rangle \approx \frac{1}{2} a^2, \tag{2.25}$$

only depending on a as well. Typical corrections to the universal relations given in Eq. (2.24) and Eq. (5.47) are of the order R/a. Going back to the deuteron with a large scattering length $a_d = 5.42$ fm, we can calculate the binding energy for the deuteron up to an accuracy of 35% [11, 14, 23]. Extending our description to the second term in the effective range expansion we can improve our calculation to 16% accuracy. These two expressions also allow us to relate the mean square separation directly to the binding energy of two particles. Furthermore we can use the dimer field formalism from Fig. 2.5 to express the deuteron as a dimer field. For the deuteron the binding momentum is very well known to be $\gamma_d = 45.68$ MeV.

In addition the wave function of such a dimer is universal, therefore it exhibits the universal properties dicussed before. In coordinate space we find for the wave function

$$\psi_D(r) = \frac{1}{r} e^{r/a}, \tag{2.26}$$

which is once again fully determined by the scattering length. The same wave function in momentum space, with $\boldsymbol{k}$ the relative wave number between the two particle, is given by

$$\psi_D(k) = \frac{4\pi}{k^2 + \frac{1}{a^2}}. \tag{2.27}$$

We will later calculate the width of the hypertriton in dependence of such wave functions, since they only depend on the scattering length, we expect this width to be rather insensitive to corrections to such a universal wave function.

2.4.2. The Efimov Effect

In three-body systems of non-relativistic particles a curious effect might occur. In 1970 Efimov discovered that if for at least two two-particle subsets the scattering length a is large compared to the range of the potential r_0, there is a series of geometrically spaced bound states [24]. As illustrated in Fig. 2.6 more and more new bound trimer states, dashed blue states, appear at the dimer-particle (atom) threshold, thick solid line, for increasing a. The respective thresholds and states are so visualized by the associated pictogram.

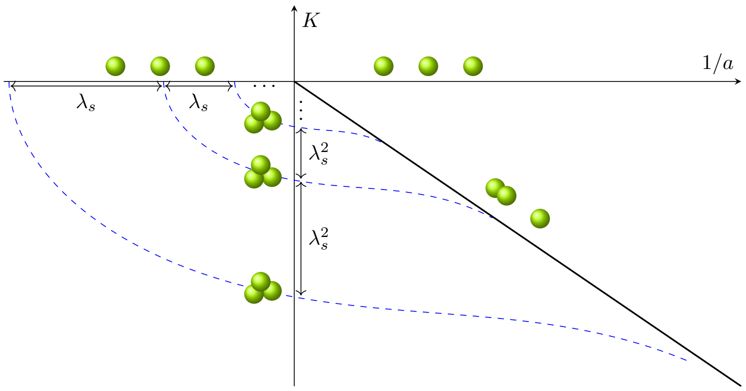

Figure 2.6.: Typical Efimov plot for trimers, blue dashed lines, with the dimer-atom (black) and single particle thresholds depicted graphically in the $K - 1/a$ plane with $K = \text{sgn}(E)\sqrt{|E|}$. The typical scaling between the states is indicated by the arrows. Note that K and $1/a$ are scaled to show more states within this figure and an infinite amount of states arises near the origin. For the binding energies we use the bound state condition from Ref. [11] with the universal function from Ref. [25]. For further details see also App. A.2.

These bound states appear for specific values of a all differing by a factor $\lambda_s = e^{\pi/s_0}$ where s_0 is a parameter determined by the mass ratio and particle statistics of the three-body system. For the often referenced case of three identical bosons, depicted in Fig. 2.6, or three distinguishable particles with equal mass, the parameter is given by the transcendental equation [26]

$$1 = \frac{8}{s_0\sqrt{3}} \frac{\sinh\left(\frac{\pi s_0}{2}\right)}{\cosh\left(\frac{\pi s_0}{6}\right)}. \tag{2.28}$$

The numerical values for this case reads $s_0 = 1.00624$ resulting in a scaling factor of $e^{\pi/s_0} \approx 22.69$. We will find Eq. (2.28) later as result of our three-body calculations, see Ch 5.4. Similar to the geometrical spacing found for the scattering length, it is also possible to find such a relation for the corresponding binding energies B_i^{Ef},i.e.

$$B_{i+1}^{\mathrm{Ef}} = \lambda_s^2 B_i^{\mathrm{Ef}}, i \geq 1$$

Fig. 2.6 also gives us an indication how many states in a particular system exist. Entering the plot from small scattering lengths as mentioned before gradually more and more bound states appear. In the limit of an infinitely large scattering length $a \mapsto \pm\infty$ an infinite amount of three-body states appear right at the three-body threshold. The most curious thing about those states is that they are insensitive to the details of the underlying short-range two-body potential.

While a formal proof of the existence of Efimov states is known since its discovery [27,28], an experimentally confirmed Efimov state was first observed in 2005 in an ultracold gas of caesium atoms [29]. Since then the Efimov effect has been observed in different systems like helium trimers or ultracold gas mixtures [30–32]. For a deeper and more detailed discussion of Efimov physics, see for example Ref. [11]. The effect discovered by Efimov can also be extended beyond the three-body sector. Up to two tetramers can be attached to each three-body state [33], which was observed experimentally as well as five-body Efimov states. For an overview of past and current theoretical as well as experimental efforts see Ref. [34].

2.5. Unstable Particles

Physical systems go into the energetically most favorable state. This is on the one hand the reason for bound states, on the other hand particles become unstable against certain interactions if an energetically better configuration is available. Therefore any particle can decay if a suitable many-particle threshold is available. How long a particle exists until it decays into an energetically more favorable state is typically measured in terms of the lifetime τ.

2.5.1. Lifetime

The lifetime is the average time a state exists before decaying into one different or more different states. It is related to the decay rate Γ by the following relation

$$\tau = \frac{1}{\Gamma}. \tag{2.29}$$

Starting from the general formula for exponential decay

$$\frac{\mathrm{d}N}{\mathrm{d}t} = -\Gamma N, \tag{2.30}$$

where N describes the number of particles, the mean lifetime of such a particle therefore can be derived from the solution $N(t) = N_0 \exp(-\Gamma t)$ in terms of the expectation value

$$\tau =< t >= \int \mathrm{d}t\, \Gamma t \exp(-\Gamma t) = \frac{1}{\Gamma}, \tag{2.31}$$

where we used integration by parts after normalizing the probability distribution. The lifetime τ is therefore the time after which the original number of particles reduced itself to $1/e$. Another value often used in the literature, especially for heavier nuclei, is the half-life time $t_{1/2}$. For this quantity this discussion is done in terms of the factor 2 and not with respect to e. Hence the lifetime and the half-life time are connected by the relation $t_{1/2} = \ln(2)\tau$.

So far we only discussed the decay by one process or into one specific state. In principle and indeed for us important is the case when a system can decay via more than one process. We therefore need to adapt Eq. (2.30) to include more than one process. We obtain

$$-\frac{\mathrm{d}N}{\mathrm{d}t} = N \sum_i \Gamma_i \Rightarrow \tau = \frac{1}{\Gamma_1 + \Gamma_2 + \ldots}, \tag{2.32}$$

with Γ_i the decay rates for different processes. We directly observe that decay constants are additive, since we can replace the sum by a new decay constant Γ_{tot}. Another consequence is that the lifetimes shrinks if more decay processes are involved. This directly implies the naive intuition that a particle becomes more and more unstable the more open decay channels are available.

2.5.2. Inclusion into Theory

Starting from the general two-point function $S^{(2)}$ of a relativistic bosonic particle

$$S^{(2)} = \frac{i}{p^2 - m_0^2 - M^2\left(p^2\right)}, \tag{2.33}$$

we recapitulate the case for stable particles (for example bosons) [2]. In this case the propagator has a pole on the real p^2 axis below the many-particle threshold, m_0 denotes here the bare mass and $M\left(p^2\right)$ the physical one. This simple structure however changes if a decay channel into two or more lighter particles is available. In this case the resulting propagator pole is shifted into the complex plane, hence $M\left(p^2\right)$ becomes complex. This shift to the complex plane reminds us of our discussion of structures in the complex plane earlier. In case of a narrow resonance approximation we can neglect the p depencence of M and the cross section shows the typical behavior of a so-called relativistic Breit-Wigner shape,

$$\sigma \sim \left| \frac{1}{p^2 - m^2 + im\Gamma} \right|^2, \tag{2.34}$$

with m the particle mass and Γ the width of the resonance. Close to the pole we can find a similar structure for the case of our decaying boson in Eq. (2.33). The cross section is given by

$$\sigma \sim \left| \frac{1}{l^2 - m^2 + iZ\mathrm{Im}\left(M^2\left(l^2\right)\right)} \right|^2, \tag{2.35}$$

where m is the particle mass in terms of the shifted propagator and Z a renormalization factor. Hence we can relate the imaginary part of the physical mass M^2 to the width of the particle described in Eq. (2.33).

2.5.3. Calculation of the Width

In this thesis we will calculate the width utilizing different methods to allow a consistency check. Since introduced in our theory by the cross section most calculations will be done in the picture introduced now. In general in quantum field theory it is rather difficult to embrace unstable particles in the usual way as they are not allowed in asymptotic states and all results for scattering processes are based on asymptotic states [35]. However, the decay rate for an particle A at rest can be expressed in terms of the reduced matrix element $\mathcal{M}$ by

$$\mathrm{d}\Gamma = \frac{1}{2M_A}\left(\prod_f \frac{\mathrm{d}^3 p_f}{(2\pi)^3}\frac{1}{2E_f}\right)\left|\mathcal{M}\left(M_A \mapsto \{p_f\}\right)\right|^2 (2\pi)^4\,\delta^{(4)}\left(p_A - \sum_f p_f\right) \tag{2.36}$$

as for example derived in Ref. [2] in a relativistic framework. The part in front of $\mathcal{M}$, denoting the decay transition matrix element, in Eq. (2.36) describes the phase space and the incoming flux. The the δ function behind $\mathcal{M}$ ensures that energy and momentum are conserved. In this work, however, we need to adjust this expression to a non-relativistic treatment for some of the particles, Hence we drop the relativistic normalization factors for all non-relativistic particles. Hence the decay rate for a non-relativistic decaying particle A reads

$$\mathrm{d}\Gamma = \prod_{f\in\mathrm{rel}} \frac{\mathrm{d}^3 p}{(2\pi)^3}\frac{1}{2E_f}\prod_{f\in\mathrm{nrel}}\frac{\mathrm{d}^3 p}{(2\pi)^3}\left|\mathcal{M}\left(M_A \mapsto \{p_f\}\right)\right|^2 (2\pi)^4\,\delta^{(4)}\left(p_A - \sum_f p_f\right). \tag{2.37}$$

In order to obtain the total width Γ we must finally integrate over all outgoing momenta.

2.5.4. Optical Theorem and Cutting Rules

The optical theorem relates the forward scattering amplitude to the cross section. This can be expressed diagrammatically, see Fig. 2.7.

We can relate the imaginary part of a diagram directly to the width of the decaying particle. This therefore offers us another way to calculate the width. In practice, however, it might be difficult to calculate the imaginary part of any given diagram directly. However, we can simplify such an evaluation by realizing that the imaginary parts of Feynman diagrams arise when particles allowed to go on-shell. A contribution to the imaginary part of a diagram is directly connected to parts of the diagram exhibiting a $i\epsilon$ prescription. Indeed we used this theorem without mentioning it already in Ch. 2.5.2. Cutkosky developed powerful cutting rules to calculate the imaginary parts of diagrams [36]. The main idea is that only the discontinuities contribute to imaginary parts and it is therefore sufficient to calculate those. These are connected to the imaginary part of the amplitude $\mathcal{A}$ by Disc $(\mathcal{A}) = 2i\,\mathrm{Im}\,(\mathcal{A})$ Hence we need to:[3]

---

[3] These rules for a relativistic theory can for example be found in Ref. [2]

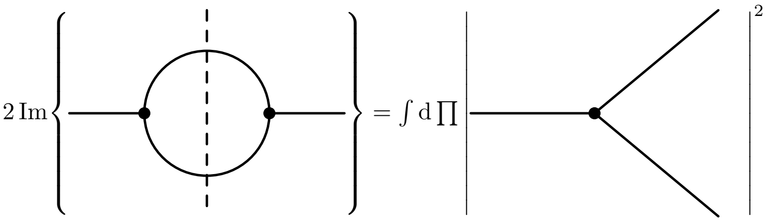

Figure 2.7.: Diagrammatic relation between the imaginary part of a diagram with the cross section.

1. Cut through a diagram in all ways, so that the cut propagators can go simultaneously on shell.
2. Replace these propagators S_i with $-1^{\text{sgn}(\pm i\epsilon)}\,(2\pi i)\,\delta\,(\text{Den}\,(S_i))$, with Den (S_i), the denominator of the cut propagator.
3. Sum the contribution of all cuts.

The sign of the $i\epsilon$ prescription determines the sign in front of the δ function of the denominator of the cut propagator. however these rules are in general only defined for Feynman diagrams [36]. Here we therefore present a method to cut through certain types of amplitudes. Let us consider two-to-two particle scattering of non-relativistic

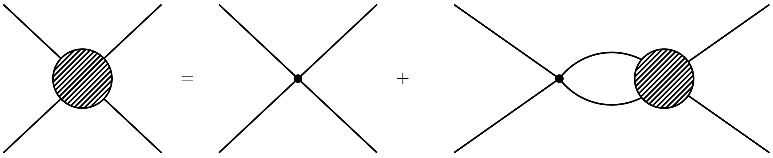

Figure 2.8.: Equation for two-to-two particle scattering of two distinguishable bosons

distinguishable bosons 1 and 2. The propagators are then given by

$$iS_i\left(P_0, \boldsymbol{p}\right) = \frac{i}{P_0 - \frac{\boldsymbol{p}^2}{2m_i} + i\epsilon} \tag{2.38}$$

and the coupling constant is g. We can then calculate the two-body scattering amplitude $\mathcal{A}$ as depicted in Fig. 2.8 to be

$$\mathcal{A} = \frac{1}{-\frac{1}{g} - i\mathcal{I}} \tag{2.39}$$

with $\mathcal{I} = (i\mu)/(2\pi)\sqrt{-2\mu E - i\epsilon} \in \mathbb{R}$ the loop integral with $E > 0$ the energy of the system and μ the reduced mass[4]. Calculating the imaginary part yields

$$2i\,\mathrm{Im}\left(\mathcal{A}\right) = \frac{2i\mathcal{I}}{\frac{1}{g^2} + \mathcal{I}^2} = \mathcal{A}^* 2i\mathcal{I}\mathcal{A} \tag{2.40}$$

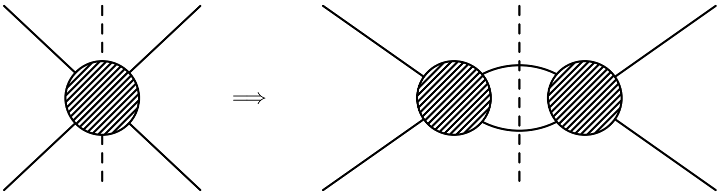

Figure 2.9.: Graphical cutting through a two-body scattering amplitude, yields the imaginary part of the amplitude $\mathcal{A}$

In order to reproduce this result now by applying cutting rules, we first need to identify the parts of the diagram that are relevant for cutting, we therefore rewrite $\mathcal{A}$ in such a way that the imaginary part stands in the numerator. Therefore we find that the $\mathrm{Disc}\left(\mathcal{A}\right) = \mathcal{A}^* \cancel{i\mathcal{I}} \mathcal{A}$, where $\cancel{i\mathcal{I}}$ stands for the cut through the loop integral $\mathcal{I}$. When drawing the cut expression diagrammatically, as depicted in Fig. 2.9, at first glance it seems rather unintuative that a cut through the amplitude should scale like the amplitude squared, but the result for the imaginary part of $\mathcal{A}$, Eq. (2.40), already

---

[4] We only take energies under consideration where $\mathcal{I}$ is indeed real.

indicates that this might be correct taking in consideration the scaling behavior of $\mathcal{I} \sim 1/\mathcal{A}$. Further, this reflects the fact that the amplitude is indeed a sum of infinitely many bubbles. Now evaluating $\cancel{i\mathcal{I}}$ by applying the three steps described before we obtain

$$\cancel{i\mathcal{I}} = \frac{i}{\pi} \int_0^\infty \mathrm{d}q \, \frac{\mu}{\sqrt{2\mu E}} \delta\left(q - \sqrt{2\mu E}\right) = 2i\mathcal{I} \tag{2.41}$$

returning the desired result $\mathrm{Disc}\left(\mathcal{A}\right) = \mathcal{A}^* 2i\mathcal{I}\mathcal{A}$ yielding a graphical prescription how to cut through amplitudes that are created by an infinite loop of bubble diagrams. Further details on the calculation are given in App. A.3.

3. Hypernuclear Physics

In this chapter we address the properties and specialties of hypernuclear physics before going into the details of our three-body hypernuclei calculations. We concentrate on the relevant particles and properties only.

3.1. Historical Overview and Introduction

After the introduction of strangeness back in 1953, the first observation of a hypernucleus, formed by a Λ and nucleons, in an emulsion experiment [37] followed shortly. Ever since then hypernuclei have been studied in emulsion experiment and accelerator facility in the more recent years. Drastically increasing the amount of accessible events. A hypernucleus is in general formed out of normal nucleus containing protons and neutrons, by adding hyperons such as the Λ, Σ or Ξ particle. Those hyperons are typically part of the $SU(3)$-octet, as shown in Fig. 3.1. We can see that the atomic number Z is for hyperons not only covered by the number of protons but, in principle, also includes the number of charged hyperons.

For the remainder of this thesis only two hyperons, the Λ and Σ^0[1], will be relevant. The mass of both particles is in the order of magnitude of the nucleon masses $M_\Lambda = 1115.683 \pm 0.006$ MeV and $M_\Sigma = 1192.642 \pm 0.024$ MeV. In addition both particles have spin$^{\text{parity}}$ $S^P = 1/2^+$. With a quark content of one up, one down and one strange quark each, both have the same quark content and isospin $I = 0$ and $I = 1$ respectively [7].

The Λ decays mostly in hadronic channels. The most important decays are the ones in one nucleon and a pion. All other, especially leptonic decays, are suppressed by at least

---

[1] Since the Σ^+ and Σ^- are not relevant for the remainder of this thesis, we will from now on omit the superscript 0 for the Σ^0.

Figure 3.1: The $SU(3)$-octet. The "normal" matter ($S = 0$), neutron and proton is depicted in gray. The $S = -1$ hyperons in green, including the for our case relevant Λ and Σ^0 baryon (depicted in one picture). The $S = -2$ Ξ baryons are depicted in orange. The quark content is given in brackets below.

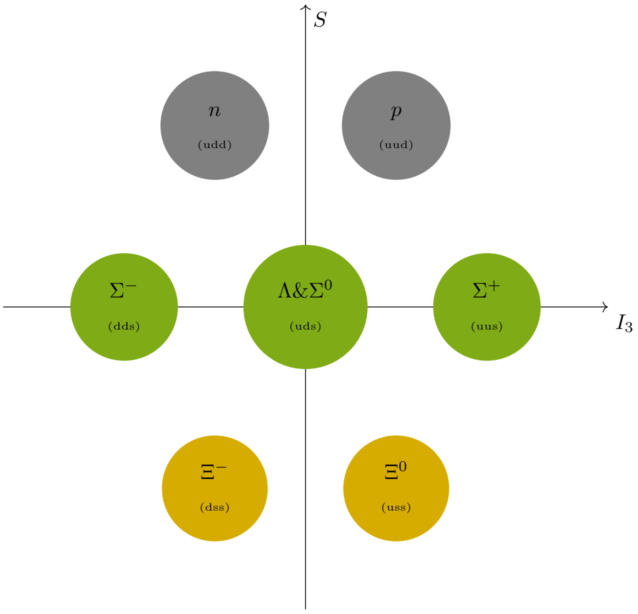

5 orders of magnitude. The mean average for the lifetime is 263.2 ± 2.0 ps. The Σ on the other side decays to nearly 100% through emission of a photon in a Λ-particle [7].

Therefore so-called $\Lambda \Leftrightarrow \Sigma$ conversion may occur which is a particular feature of three-body systems and the three-body force entering the description of such systems with three or more particles. These will be described in Ch. 4.3.

Most hypernuclei contain only one hyperon, a Λ, and can be found over the whole nuclear chart, an extract for a low number of protons and neutrons is shown in Fig. 3.2 in the lower layer. The "classical" nuclear chart only consists of protons and neutrons. With the inclusions of hyperons, such as the Λ, it needs to be extended to a third dimension representing the amount of strange particles within a nucleus. This is depicted in the upper layer of Fig. 3.2. In principle this figure can be easily extended with a third layer containing a fair amount of double Λ nuclei and hypernuclei containing a cascade particle. At this point it is worth mentioning that the Σ-N interaction is found to be strongly repulsive, hence except from pseudo-bound particles, no bound Σ hypernucleus is known.

Furthermore, hyperons offer ideal conditions to test our understanding of the nuclear force beyond the up and down quark sector. Additionally hyperons allow us to probe

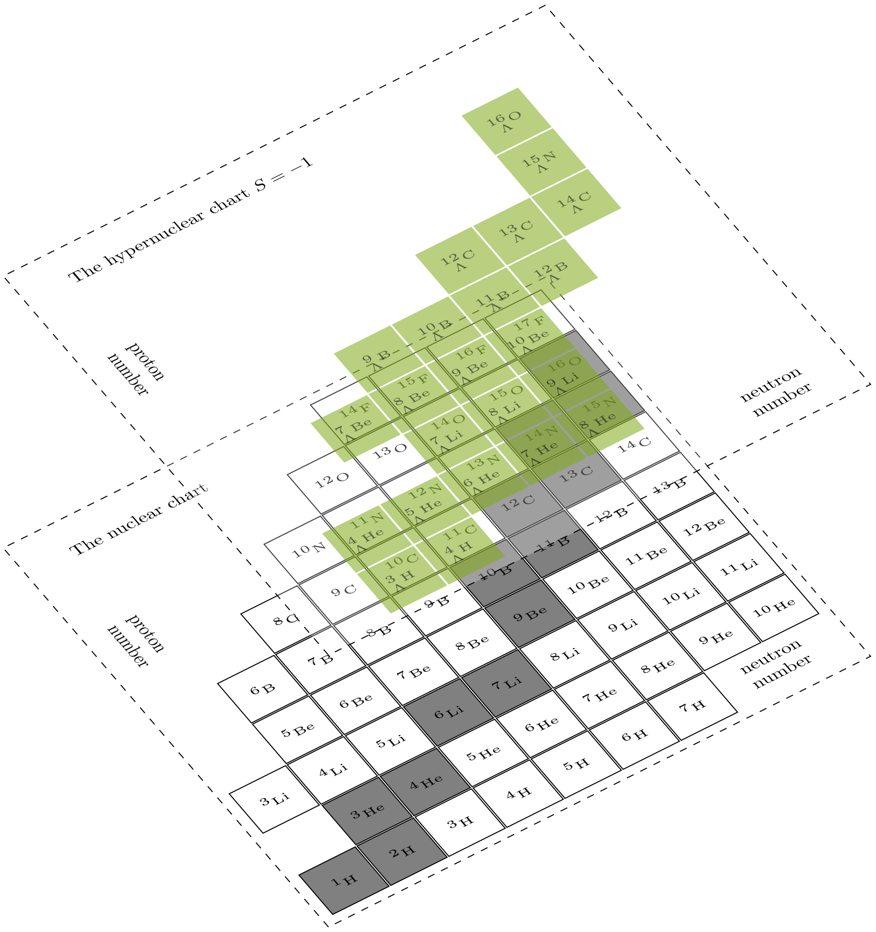

Figure 3.2.: Excerpt of the nuclear chart as given by Ref. [38] extended to a third dimension determined by the Λ hyperon. The existent hyperons are taken from Ref. [4]. Note that we neglected pseudo-bound Σ-hypernuclear states. In principle we could extend the chart to a third layer containing hypernuclei with multiple hyperons with strangeness ($S = -1$) or hyperons with more strange content, see also Fig. 3.1.

the nuclear interior in a unique way without being affected by the Pauli principle. Ever since their discovery hypernuclei have been studied theoretically in various approaches. For an extended discussion about those efforts see for example Ref. [4].

Light hypernuclei can be studied ab initio using hyperon-nucleon interactions derived from chiral EFT [39, 40]. These interactions are based on an extension of chiral EFT to $SU(3)$ in an attempt to incorporate kaon and eta exchange by counting M_K and M_η as low-energy scales. The two-baryon potential has been derived up to next-to-leading order (NLO) in the chiral counting [17, 41–43]. Within the Weinberg scheme, a description of hyperon-nucleon data of a quality comparable to the most advanced phenomenological models is obtained. The leading order three-baryon forces have also been written down [44]. Finally, first lattice QCD calculations of light hypernuclei at unphysical pion masses have also become available [45].

3.2. Weak Decay of Hyperons

Hyperons and for our purposes most importantly Λ particles decay, as mentioned before, mainly through non-leptonic decays. In the following we will describe the theoretical foundations for those leptonic decays following closely the introduction presented in Refs. [46, 47]. However, we will adapt and extent their presentation to our framework and conventions used later. A hyperon (H) can in principle decay into a baryon B and a pion π. We are therefore interested in the matrix elements of the following type

$$\mathcal{M}\left(H \mapsto B\pi\right) = iG_f M_\pi^2 \bar{u}\left(\boldsymbol{p}'\right)\left[A_\pi + B_\pi \gamma_5\right] u\left(\boldsymbol{p}\right) \tag{3.1}$$

with γ_5 the usual Dirac matrix and $u, \bar{u}$ are defined in standard sense of relativistic quantum field theory. Note that we made the coupling $G_f M_\pi^2$, with G_f the Fermi-interaction constant and M_π the mass of the pion here explicit. But in principle it can be absorbed in the two amplitudes A_π and B_π, which encode the parity violating and parity conserving part of the interaction. Due to the parity of the pion, the parity conserving amplitude comes with γ_5. The phase of these amplitudes, however, is given by the strong $B\pi$ scattering phase shift, which is known for the for us relevant Nπ systems. We can express A_π and B_π then by the corresponding S- and P-wave phase shifts. We obtain

$$A_\pi = A_0 e^{i\delta^S_{B\pi}} \quad \text{and} \quad B_\pi = B_0 e^{i\delta^P_{B\pi}} \tag{3.2}$$

with A_0 and B_0 real numbers, if CP (Charge-conjugation Parity) is conserved. The decay rate can then be calculated to be

$$\Gamma_{\mathrm{H}} = G_f^2 M_\pi^4 \frac{|\boldsymbol{q}|\left(E' - M_H\right)}{4\pi M_B}\left(|A_\pi|^2 + |B|^2\right) \tag{3.3}$$

with $|\boldsymbol{q}|$ the pion momentum in the rest frame and $B \equiv \sqrt{\left(E' - M_B\right)\left(E' + M_B\right)} B_\pi$. The energy of the outgoing baryon is denoted by E'. The hyperon (baryon) mass is given by $M_H (M_B)$. Further observables are the angular decay distribution $W\left(\theta\right)$,

$$W\left(\theta\right) = 1 + \alpha \boldsymbol{P}_B \hat{\boldsymbol{p}}_B \quad \text{with} \quad \alpha = \frac{2\,\mathrm{Re}\left(A_\pi B\right)}{|A_\pi|^2 + |B|^2} \tag{3.4}$$

and $\boldsymbol{P}_B$ the polarization of the outgoing baryon. The unit vector in direction of the outgoing baryon is denoted by $\hat{\boldsymbol{p}}_B$. Studies of these observables, either by obtaining them from theoretical approaches or experiment then show that the decay into a charged baryon (and therefore charged pion) is not independent from a decay into an uncharged one. Indeed they are related by the so-called isospin $\Delta I = 1/2$ rule, which is empirical and also found for example for kaon decays [47]. Typically this relation is set to a ratio of $2/(-1)$. In order to obtain only one value for A_π and B_π it is adroit to factorize them out of A_π and B_π. For possible sets of those amplitudes see for example Ref. [46], which are, however, dependent on the experimental value α. We will therefore not use them but instead fix our interactions directly to the polarization of the outgoing proton. Further on we will reduce the vertex for our purposes to a non-relativistic one, since as we will see later non-relativistic baryons are indeed sufficient for our purposes.

4. Three-Body S=-1 Hypernuclei

In this thesis we focus our studies on three-body hypernuclei with strangeness $S = -1$. This limits the nuclei we consider to contain only one hyperon and ordinary nucleons. We concentrate our efforts on the Λ baryon at this point. Utilizing the structure of the two-nucleon interaction depicted in Fig. 2.1 we expect that the hypernucleus combining a deuteron and a Λ baryon is most likely to exist, especially due to the negative scattering lengths for the Λ-nucleon interactions. This state is similar to the triton, replacing a neutron with the slightly more heavy Λ particle.

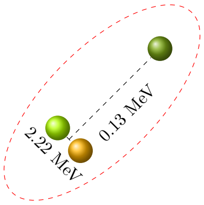

Figure 4.1.: Illustration of the hypertriton as two-body bound state with a deuteron as a core and a shallowly attached Λ (green ball) with a binding energy of only $B_\Lambda = 0.13$ MeV.

4.1. The Hypertriton

Apparently this state in the $I = 0$ channel exists (see also Fig. 3.2) the so-called hypertriton is bound with a binding energy that is typically considered to be 2.35 ± 0.05 MeV with a separation energy of the Λ by only 0.13 ± 0.05 MeV. As discussed in the general introduction early experimental results are from emulsion experiment. In the more recent years the hypertriton has also been found in accelerator facilities in heavy-ion experiments such as the LHC [48, 49], see also Fig. 4.2 for an example result obtained in Pb-Pb collisions at $\sqrt{s} = 2.76$ TeV [48].

Naturally the picture of a bound two-body system of a deuteron with a binding energy of 2.22 MeV and a shallow Λ arises. This structure of the hypertriton is depicted in Fig. 4.1. The quantum numbers of the hypertriton are $J^P = 1/2^+$. For a discussion of the hypertriton in this "picture" see for example Ref. [50]. Note that although the deuteron core is bound tightly compared to the Λ particle, the binding energy is small compared to the typical nuclear binding energies of $B/A \sim 8$ MeV [51]. This is stressed by the fact that the deuteron emerges as shallow bound state in pionless EFT, see also Ch. 2.4.1. Remember that low binding energies correspond to a large mean separation in the two-body sector as indicated by Eq. (2.24) and Eq. (5.47). More recent measurements of the STAR collaboration suggest a slightly higher binding energy of the Λ particle with $B^\star_\Lambda = 0.41 \pm 0.12(\text{stat.}) \pm 0.11(\text{syst.})$ MeV [8].

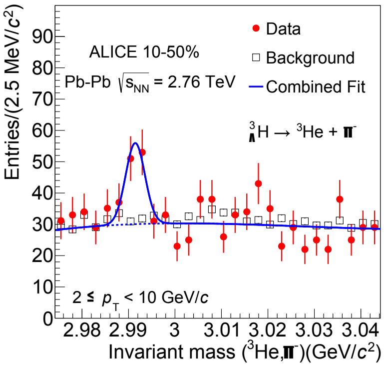

Figure 4.2.: Result of the Alice collaboration [48] for the invariant mass distribution for the hypertriton for events with $10 - 5\%$ centrality in the pair $2 \leq p_T < 10$ GeV/c interval. For further details see Ref. [48].

Since the deuteron is stable we expect that the lifetime of the hypertriton is mainly determined by the lifetime of the Λ particle and therefore is given at first approximation by the free Λ-lifetime. Measurements of the hypertriton lifetime show a different picture. The lifetime of the hypertriton is in some experiments significantly shorter than the lifetime of the free Λ. However, the main decay channels are driven by the decay of the

Λ and therefore are hadronic. The main decays are

$$\begin{aligned} {}^3_\Lambda\mathrm{H} &\mapsto \pi^- + {}^3\mathrm{He}, & {}^3_\Lambda\mathrm{H} &\mapsto \pi^0 + {}^3\mathrm{H}, \\ {}^3_\Lambda\mathrm{H} &\mapsto \pi^- + d + p, & {}^3_\Lambda\mathrm{H} &\mapsto \pi^0 + d + n, \\ {}^3_\Lambda\mathrm{H} &\mapsto \pi^- + p + n + p, & {}^3_\Lambda\mathrm{H} &\mapsto \pi^0 + p + n + n. \end{aligned} \tag{4.1}$$

In the first channels of Eq. (4.1) no break up of the three-body nucleus appears. Going down from top to bottom more and more break ups are taken into consideration. While in heavier hypernuclei these decays are often Pauli blocked and therefore not accessible, these channels are open for the three-body case and are the main decays [52]. Note that like for the case of the free Λ decay leptonic processes are suppressed. Theoretical analyses predict that they make up for roughly 1.5% of the total free Λ decay rate [53]. Experimentally these decay rates cannot be separated. An overview of the experimental results for the hypertriton lifetime is given in Fig. 4.3. The free Λ lifetime as given by the PDG [7] is marked as red straight line. Bubble chamber experiments up to the year 1973 are depicted in black and accumulate around the free lifetime, with two results significantly lower. In the more recent years the hypertriton lifetime has been measured in relativistic heavy-ion experiments (blue points) from different collaborations like STAR [54, 55], ALICE [48, 56] or HypHI [57], whose central values tend to lie below the non-accelerator accumulation point. Note that the x-axis has a break in Fig. 4.3.

The general principle of those bubble chamber experiments is a recoil technique. If the velocity of a hypernucleus is known at the creation point, it is possible to reconstruct the lifetime of such a particle by the distance it travels before decaying into the particles given in Eq. (4.1). However in emulsion experiments hypernuclei are typically generated at low momenta and therefore traveling only short distances within the chambers. This induces large error bars as depicted in Fig. 4.3. While the first results back in 1963 only accounted four events [58], the statistics and yet the precision became better in the succeeding experiments [59–61], reaching thousands of events. However the lifetimes obtained from helium bubble chamber were significantly longer $\tau = 246^{+62}_{-41}$ ps and hence closer to the free Λ lifetime [61].

4.2. The Λnn

In 2013 the HypHI collaboration found evidence that the Λnn-system might be bound by observing the reaction products of ^{6}Li on a ^{12}C target [9]. The analysis of the invariant mass distribution of two final states $d + \pi^-$ and $t + \pi^-$ yield evidence a Λnn state might

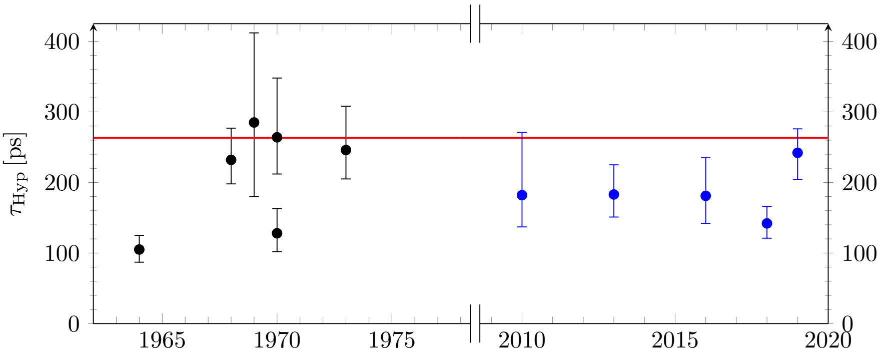

Figure 4.3.: Compilation of lifetime measurements for the hypertriton. In blue, results obtained in accelerators by different collaborations [48, 54–57]. Earlier results from emulsion experiments are depicted in black [59–64]. PDG value for the free Λ as in Ref. [7].

exist. A hint that strangeness content might be involved is the associated lifetime for both channels which is in order of hundreds of ps which is typical for decays involving strangeness. One possible explanation of those final states are therefore decays of the Λnn system

$$\begin{aligned} {}^3_\Lambda n &\mapsto t + \pi^-, \\ {}^3_\Lambda n &\mapsto t^* + \pi^- \mapsto d + n + \pi^-. \end{aligned} \tag{4.2}$$

with the respective invariant masses of $2059.3 \pm 1.3 \pm 1.7$ MeV and $2993.7 \pm 1.3 \pm 0.6$ MeV respectively suggesting a binding energy about ~ 1 MeV for the Λnn. If this is correct, this state is expected to be observable in other experiments, such as ALICE [65]. The associated lifetimes are given by $181^{+30}_{-24} \pm 25$ ps and $190^{+47}_{-35} \pm 36$ ps, respectively. As expected the quantum numbers are again $J = 1/2^+$ but the Isospin channel is $I = 1$ according to Fig. 2.1 [9].

In this sense the structure of the Λnn is similar to the hypertriton (see Fig.4.1) when exchanging a proton with a neutron, but without the bound two-body subsystem, since the di-neutron is considered to be unbound. At this point we would also not expect that the wave function of the Λnn does not extend as far as indicated by Fig. 4.1 for the hypertriton. Since the di-neutron is unbound the Λnn, if bound, would be the first nucleus that does not contain at least one proton. Furthermore, the introduction of a di-neutron leads to a dependence of the neutron-neutron scattering length, the exact value of this property is highly discussed within the community.

The existence of a bound Λnn system is a matter of current debate. Since the first evidence appeared the existence of a bound Λnn system as well as its implications on nuclear physics have been investigated in many different approaches. Most of these studies reject the existence of such a bound state due to constraints from other nuclear and hypernuclear observables [66–70]. A resonance above the three-body threshold was also considered as a possible explanation [71–73]. The pionless EFT investigation by Ando et al. precluded a definitive conclusion [74].

4.3. Lambda-Sigma Conversions

Shortly above the nucleons proton and neutron ($M \approx 1$ GeV) we find the Δ-Baryons with an mass of $M_\Delta \approx 1.2$ GeV. If the energy of the scattering process of two nucleons is high enough, it is possible to generate such particles. Even if the outgoing particles are nucleons, such particles can be generated in intermediate states. The inclusion of such state in nuclear forces is known most prominent in three-body forces as for example described by Ref. [75, 76], but is also known in Born-Oppenheimer potentials [77]. The first guess at which scale these conversions between nucleon and Δ particles become important is the mass difference and therefore given by

$$N \Leftrightarrow \Delta \sim \sqrt{M\left(M_\Delta - M\right)} \approx 523\,\mathrm{MeV} \tag{4.3}$$

Such an intermediate state, for example a Δ state, is typically introduced in a theory including pions since the expected scale Eq. (4.3) is much larger than the pion mass. Therefore we can for example include such an intermediate state as illustrated in Fig. 4.4 in our theory.

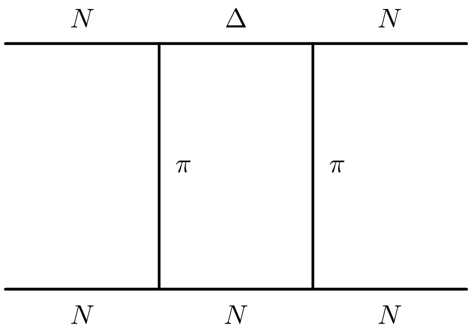

Figure 4.4.: Typical intermediate state generated by the exchange of pions.

Since for the lightest hyperon, the Λ, a similar state with a relative small mass difference, the Σ, exists, the question arises how important similar conversion of a Λ into a Σ and vice versa are for hypernuclear physics. Indeed are $\Lambda \Leftrightarrow \Sigma$ conversions considered to be of uttermost importance for the binding of the lightest hypernuclei such as the just introduced hypertriton as well as nuclei in the $A = 4$ sector [78, 79]. The mass difference of the Σ and Λ particle is given by $\Delta_{\Sigma\Lambda} = 70$ MeV. In similar fashion as done by Savage [80] for the nucleon $\Leftrightarrow$ Δ conversions we now estimate the typical scale for $\Lambda \Leftrightarrow \Sigma$ conversion. Therefore we consider explicit $\Lambda \Leftrightarrow \Sigma$ conversions in the ΛN interaction as illustrated in Fig. 4.5. We obtain for the amplitudes

$$\begin{aligned} iA_1 &= -ig_\Lambda + ig_\Lambda I_{\Lambda \mathrm{N}} A_1 + ig_\Sigma I_{\Sigma \mathrm{N}} A_2 \\ iA_2 &= -ig_\Sigma + ig_\Sigma I_{\Lambda \mathrm{N}} A_1 + i\tilde{g}_\Sigma I_{\Sigma \mathrm{N}} A_2 \end{aligned} \tag{4.4}$$

where we labeled the loop integrals I_{ab} according to the involved particles a and b. Solving the second equation in Eq. (4.4) respect to A_2 we obtain for A_1 the following expression

$$iA_1 = \frac{-ig_\Lambda + ig_\Lambda \tilde{g}_\Sigma I_{\Sigma \mathrm{N}} - ig_\Sigma^2 I_{\Sigma \mathrm{N}}}{1 - \tilde{g}_\Sigma I_{\Sigma \mathrm{N}} - g_\Lambda I_{\Lambda \mathrm{N}} + g_\Lambda \tilde{g}_\Sigma I_{\Lambda \mathrm{N}} I_{\Sigma \mathrm{N}} - g_\Sigma^2 I_{\Lambda \mathrm{N}} I_{\Sigma \mathrm{N}}}. \tag{4.5}$$

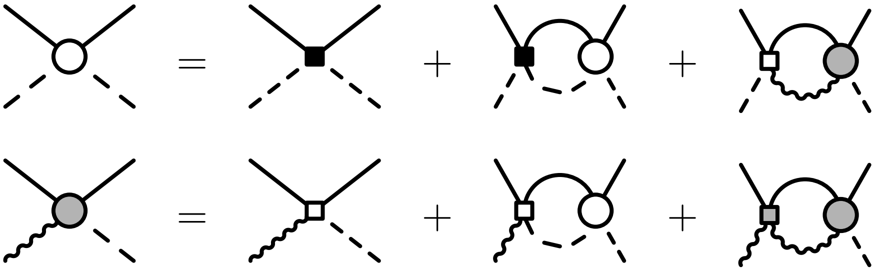

Figure 4.5.: ΛN interaction with the amplitudes A_1 and A_2 (circles). Nucleons are depicted as plain line. Λ and Σ baryons are dashed and wiggly lines, respectively. The coupling constants are given by squares (black= g_Λ, white= g_Σ and gray= $\tilde{g}_\Sigma$).

Choosing the non-relativistic single particle propagators to be

$$iS_\mathrm{N}\left(P_0, \boldsymbol{p}\right) = \frac{i}{P_0 - \frac{\boldsymbol{p}^2}{2M_N} + i\epsilon}, \tag{4.6}$$

$$iS_\Lambda\left(P_0, \boldsymbol{p}\right) = \frac{i}{P_0 - \frac{\boldsymbol{p}^2}{M_\Lambda} + i\epsilon}, \tag{4.7}$$

$$iS_\Sigma\left(P_0, \boldsymbol{p}\right) = \frac{i}{P_0 - \frac{\boldsymbol{p}^2}{2M_\Lambda} - \Delta_{\Sigma\Lambda} + i\epsilon}, \tag{4.8}$$

we can evaluate the integrals directly and obtain

$$iI_{\Lambda\mathrm{N}} = i\frac{\mu}{2\pi}\sqrt{-2\mu\left(E_{cm} + i\epsilon\right)} + \mathcal{O}\left(d-3\right) \tag{4.9}$$

$$iI_{\Sigma\mathrm{N}} = i\frac{\mu}{2\pi}\sqrt{-2\mu\left(E_{cm} + i\epsilon - \Delta_{\Sigma\Lambda}\right)} + \mathcal{O}\left(d-3\right) \tag{4.10}$$

using dimensional regularization and with $\mu = \left(M_\mathrm{N}M_\Lambda\right)/\left(M_\mathrm{N}+M_\Lambda\right)$ the reduced mass of the nucleon Λ system and E_{cm} the center of mass energy. Note that the additional shift we obtain due to a wrong propagating mass is small since the mass difference is small compared to the total mass. At this point we recall the effective range expansion Eq. (2.8) and that the S-wave phase shift is defined as $p\cot\left(\delta_0\right) = \frac{2\pi}{\mu}\mathrm{Re}\left(1/A\right)$. Therefore we can express the typical scale of a $\Lambda \Leftrightarrow \Sigma$ conversion through the scattering length a

in the limit $E_{cm} \mapsto 0$. Exploiting the fact that $I_{\Lambda\text{N}}^{E_{cm}=0} = \lim\limits_{E_{cm}\mapsto 0} I_{\Lambda\text{N}} = 0$ we obtain

$$A_1 = \frac{-g_\Lambda + g_\Lambda \tilde{g}_\Sigma I_{\Sigma\text{N}}^{E_{cm}=0} - g_\Sigma^2 I_{\Sigma\text{N}}^{E_{cm}=0}}{1 - \tilde{g}_\Sigma I_{\Sigma\text{N}}^{E_{cm}=0}}. \tag{4.11}$$

We then are able to express the amplitude through the scattering length and obtain for a:

$$a = \frac{\mu}{2\pi} \frac{g_\Lambda + \left(g_\Sigma^2 - g_\Lambda \tilde{g}_\Sigma\right) I_{\Sigma\text{N}}^{E_{cm}=0}}{1 - \tilde{g}_\Sigma I_{\Sigma\text{N}}^{E_{cm}=0}} \tag{4.12}$$

Inspired by the discussion of $NN \Leftrightarrow \Delta\Delta$ by Savage [80] we set all couplings equal $g_\Lambda = g_\Sigma = \tilde{g}_\Sigma = g$. Note that at this point in principle we could use $SU(3)$ symmetry to connect the different coupling constants with each other. However, these coupling constant are related to each other by Clebsch-Gordon coefficients of the order 1, hence are of the same order of magnitude. The scattering length and therefore the coupling constant are then given by

$$a = \frac{\mu}{2\pi} \frac{g}{1 - g I_{\Sigma\text{N}}^{E_{cm}=0}} \quad \text{and} \quad g = \frac{2\pi}{\mu} \frac{1}{\frac{2\pi}{\mu} I_{\Sigma\text{N}}^{E_{cm}=0} + \frac{1}{a}}. \tag{4.13}$$

Implementing now $I_{\Sigma n}^{E_{cm}=0} = \frac{\mu}{2\pi}\sqrt{2\mu\Delta_{\Sigma\Lambda}}$ yields

$$g = \frac{2\pi}{\mu} \frac{1}{\sqrt{2\mu\Delta_{\Sigma\Lambda}} + \frac{1}{a}} \tag{4.14}$$

and therefore sets an intrinsic momentum scale for a $\Lambda \Leftrightarrow \Sigma$ conversion to $\sqrt{2\mu\Delta_{\Sigma\Lambda}} \approx 280$ MeV. For further calculation details see also App. C.1.

In a less sophisticated way it is also possible to estimate the typical scale of a $\Lambda \Leftrightarrow \Sigma$ conversion as depicted in Fig. 4.6 by the excitation energy of a Λ to form a Σ

$$\Lambda \Leftrightarrow \Sigma \sim \sqrt{M_\Lambda \left(M_\Sigma - M_\Lambda\right)} \approx 290\text{MeV}. \tag{4.15}$$

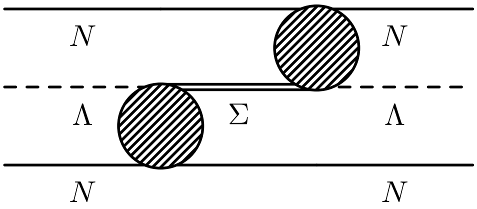

Figure 4.6.: Typical intermediate state for the Λ particle, contributing in a three-body system corresponding to an effective three-body force. The hatched amplitudes are two body potentials.

Typical momentum scales in the $I = 1$ as well as in the $I = 0$ channel are now set by the expected binding energies of both systems. For the hypertriton this energy is well known to be $B = 2.35$ MeV, in case of the Λnn we can estimate from Ref. [9] that B does not exceed 1.1 MeV. The total energy of one system is given by

$$E = \frac{3k^2}{4M} - \frac{\gamma_{\text{NN}}^2}{M} \tag{4.16}$$

with γ_{NN} the nucleon-nucleon binding momentum if the nucleons are bound. Setting $E = -B$ while B being positive we obtain with $k \mapsto i\gamma_3^\Lambda$ that

$$\gamma_3^\Lambda = 2\sqrt{\frac{MB - \gamma_{\text{NN}}^2}{3}} \tag{4.17}$$

sets the typical momentum scale for the hypertriton as well as the Λnn. Inserting the binding energy and the deuteron binding momentum for the hypertriton, we obtain as the typical scale ${}^{\text{Hyp}}\gamma_3^\Lambda = 12.27$ MeV. For the Λnn system we set $\gamma_{\text{NN}} = 0$ since the di-neutron is unbound. This results in a typical scale of ${}^{\Lambda\text{nn}}\gamma_3^\Lambda = 37.12$ MeV.

Summarizing the previous analysis both scales, the one for the hypertriton and the one for the Λnn system, are small compared to the typical scale for the conversions of Λs into Σs and vice versa. Since a bound di-neutron would decrease the typical momentum scale of the problem, this analysis would still hold if the di-neutron would be indeed bound.

5. Three-Body Hypernuclei in Pionless EFT

Parts of this chapter have been published in this or similar form in Phys. Rev. C, 2019, 100, 034002 [81].

5.1. Introduction

Certain hypernuclei with weak binding are also accessible by pionless and/or halo EFT where the Goldstone boson exchanges are not explicitly resolved [23,82]. Using pionless EFT, the process of Λd scattering and the properties of the hypertriton ${}^{3}_{\Lambda}\mathrm{H}$ were studied in [83]. The viability of the Λnn bound state suggested by the experiment of the HypHI collaboration at GSI [9] was investigated in [74]. If M_K or M_η are assumed to be large scales, the onset of η-nuclear binding can be considered in a pionless EFT approach in order to derive constraints on the ηN scattering length [84, 85]. A solution to the overbinding problem for ${}^{5}_{\Lambda}\mathrm{He}$ was presented in Ref. [86]. In addition, some hypernuclei, such as ${}^{4}_{\Lambda\Lambda}\mathrm{H}$ [87] and ${}^{6}_{\Lambda\Lambda}\mathrm{He}$ [88], have been studied in halo EFT. (See [89] for a review of these efforts.)

In this chapter, we study the structure of strangeness $S = -1$ hypernuclei in pionless EFT at leading order in the large scattering lengths, focusing on the hypertriton and the Λnn system. We will sequentially use the concepts and physics introduced in the chapters before. The pionless EFT framework provides a controlled, model-independent description of weakly-bound nuclei based on an expansion in the ratio of short- and long-distance scales, as introduced Ch. 2.3. The typical momentum scale for the hypertriton can be estimated from the energy required for breakup into a Λ and a deuteron as $\gamma_3^\Lambda \sim 2\sqrt{\left(MB_\Lambda^3 - \gamma_d^2\right)/3} \approx 0.3\gamma_d$ with $\gamma_d = 45.68$ MeV the deuteron binding momentum and M the nucleon mass as shown in the previous section. The momentum scale for the full three-body breakup is of order γ_d. As shown before in the case of the Λnn system, the invariant mass distribution from possible decays shown in

Ref. [9] suggests a binding energy of order 1 MeV which implies a binding momentum slightly smaller than γ_d. Because these typical momentum scales set the scale of relevant physics and are small compared to the pion mass, one expects that all meson exchanges can be integrated out and pionless EFT is applicable to these states. This allows us to construct an effective Lagrangian only containing contact interactions. A second important scale is given by the conversion of a Λ into a Σ and back in intermediate states. However, in the previous chapter we explored that this scale is much larger than the typical momentum scales of our theory $\gamma_3^\Lambda, \gamma_d \ll \sqrt{M_\Lambda\left(M_\Sigma - M_\Lambda\right)} \approx 290$ MeV. As a consequence $\Lambda - \Sigma$ conversion is not resolved explicitly in the hypertriton and the Λnn system, and the Σ degrees of freedom can be integrated out of the EFT, similar to the pions. The physics of $\Lambda - \Sigma$ conversion, however, are not neglected but will appear in a ΛNN three-body force [79, 83], which we will find necessary to renormalize the system at leading order.

5.2. Two-Body System

For convenience, we consider the Λnn system and the hypertriton using the isospin formalism. However, we note in passing that a calculation in the particle basis leads to the same results since we do not use isospin symmetry to relate the properties of the three $I = 1$ states. The three-body hypernuclei split up into an isospin triplet and singlet:

$$I = 1 \quad : \quad \begin{cases} pp\Lambda \\ \frac{1}{\sqrt{2}}\left(np + pn\right)\Lambda \\ nn\Lambda \end{cases} \quad , \qquad I = 0 \quad : \quad \frac{1}{\sqrt{2}}\left(pn - np\right)\Lambda\,, \tag{5.1}$$

where the hypertriton is the $I = 0$ state and the Λnn state has $I = 1$ and $I_3 = -1$. The according modified picture is shown in Fig. 5.1. This reflects the isospin channels introduced for the $N - N$ interaction. While the deuteron is part of the singlet, all other combinations of nucleons live within the triplet, the $n - n$ interaction thereby has projection $I_3 = -1$. As mentioned in the introduction of interactions the $N - N$ scattering parameters are taken from experiment. For the ΛN interaction, we use the chiral EFT predictions from Ref. [17] as input for our calculations. Since the $\Lambda - N$ mass difference is so small, $y = \left(M_\Lambda - M\right) / \left(M_\Lambda + M\right) \approx 0.086$, we consider the equal mass case $y = 0$ first and later extend our calculation to finite y.

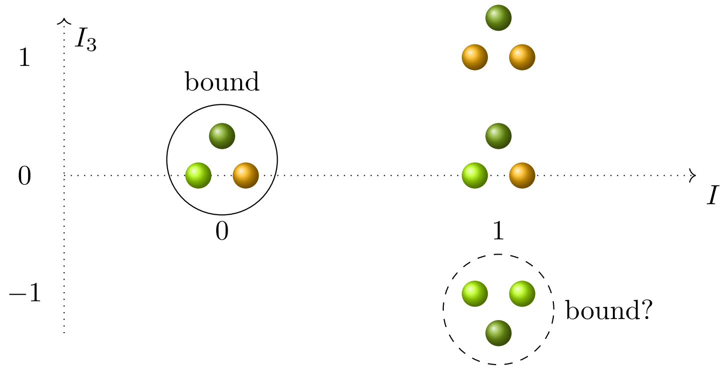

Figure 5.1.: Modified nuclear isospin channels with the addition of a Λ particle (darker green). The studied systems are circled with respect to their research status.

As discussed above, all interactions are considered to be contact interactions. For the NN system, the standard pionless EFT power counting for large scattering length is used [90,91]. We take the typical momentum $p \sim 1/a \sim Q$ where a denotes the S-wave scattering length. Depending on the channel the pole momentum of the bound/virtual states is

$$\gamma = 1/a + \mathcal{O}\left(R_{NN}/a^2\right) \ , \tag{5.2}$$

with $R_{NN} \sim 1/m_\pi \approx 1.4$ fm the range of the NN interaction. The expansion of the EFT is then done in powers of $QR_{NN} \approx \gamma r$. The scattering lengths predictions for the ΛN systems, on the contrary, are only of order $2-3$ fm [17]. Thus they are not large compared to the inverse pion mass used as expansion parameter before. However, since the one-pion exchange is forbidden between a Λ particle and a nucleon due to isospin symmetry, the range of the ΛN interaction is set by two-pion exchange: $R_{\Lambda N} \sim 1/(2m_\pi) \approx 0.7$ fm [79], which is small compared to $2-3$ fm. As a consequence, the standard pionless EFT counting can be applied for the ΛN interactions as well. In the following calculations we will stay at leading order in this counting. Up to this order only S-Wave contact interactions without derivatives contribute. However, we note that the effective range corrections in the ΛN sector are potentially large and may need to be resummed at NLO.

For the description of the two-body interactions, we use the dibaryon formalism introduced in Ch. 2.3.2. In order to describe the hypertriton ($I = 0$) and the Λnn system ($I = 1$) four auxiliary fields representing the possible interactions, three for each system, are needed. The two nucleons can be combined into either a ${}^3S_1$ (NN) partial wave denoted by d (deuteron) or a ${}^1S_0$ (NN) partial wave labeled s. The ΛN channels yield a ${}^3S_1$ and a ${}^1S_0$ partial wave denoted with a u^3 and u^1 respectively. The effective Lagrangian for S-wave scattering of a Λ's and nucleons is then given by [83]

$$\begin{aligned} \mathcal{L} =& N^\dagger \left(i\partial_t + \frac{\nabla^2}{2M}\right) N + \Lambda^\dagger \left(i\partial_t + \frac{\nabla^2}{2M_\Lambda}\right) \Lambda \\ &+ \Delta_d d_l^\dagger d_l - \frac{g_d}{2} \left[d_l^\dagger N^T (i\tau_2)(i\sigma_l\sigma_2) N + \text{H.c.}\right] \\ &+ \Delta_s s_j^\dagger s_j - \frac{g_s}{2} \left[s_j^\dagger N^T (i\tau_j\tau_2)(i\sigma_2) N + \text{H.c.}\right] \\ &+ \Delta_3 \left(u_l^3\right)^\dagger u_l^3 - g_3 \left[i \left(u_l^3\right)^\dagger \Lambda^T (i\sigma_l\sigma_2) N + \text{H.c.}\right] \\ &+ \Delta_1 \left(u^1\right)^\dagger u^1 - g_1 \left[i \left(u^1\right)^\dagger \Lambda^T (i\sigma_2) N + \text{H.c.}\right] + \dots \, , \end{aligned} \tag{5.3}$$

where H.c. denotes the Hermitian conjugate and the dots represent terms with more fields and (or) derivatives. As stated before at leading order, however, these will not contribute, since contributions with more derivatives are suppressed at low energy. Furthermore we added a channel for the ${}^1S_0$ (NN) partial wave. The d field will only contribute in the hypertriton case, while the s field will only contribute to the Λnn system. This represents the splitting into the two different isospin channels introduced before. The Pauli matrices are denoted by σ_j and τ_j acting in spin or isospin space respectively. The parameters Δ and g in each partial wave are not independent from each other at this order and therefore only the combination g^2/Δ enters in physical quantities. Hence at a two body level one input parameter is sufficient to renormalize the system. The Lagrangian is equivalent to one without auxiliary fields [92, 93] but more convenient to use for three-body calculations (see also Ch. 2.3.2). For a graphical visualization of this Lagrangian in terms of Feynman diagrams see also Fig.5.2. Parts that contribute only in the hypertriton calculation are depicted in red. The ones only contributing to the Λnn system are depicted in blue. Similar to the NN case where the tensor force only appears at N^3LO and can be treated in perturbation theory, a possible tensor force in the ΛN interactions would appear in higher orders of the EFT.

Since the theory is non-relativistic, the propagators for the Λ and the nucleons N is

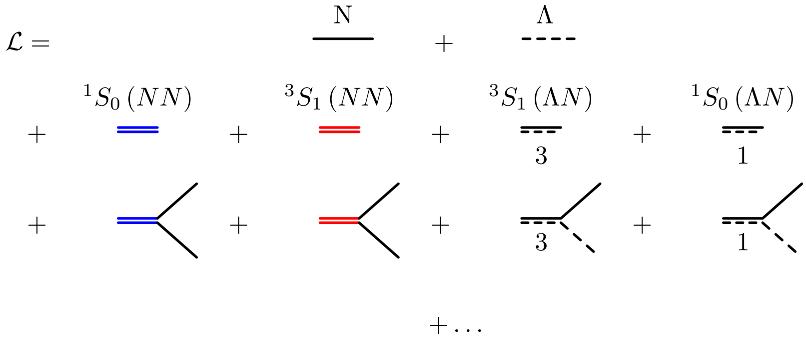

Figure 5.2.: Graphical representation of the Lagrangian Eq. (5.3), the color scheme indicates parts that are only relevant for one system (hypertriton=red, Λnn=blue).

given by

$$iS\,(p_0, \mathbf{p}) = \frac{i}{p_0 - \frac{\mathbf{p}^2}{2m} + i\epsilon}, \tag{5.4}$$

as already used to estimate the $\Lambda \Leftrightarrow \Sigma$ conversions where m denotes either M or M_Λ depending on the particle.

The bare dibaryon propagator is given by a constant i/Δ. In order to obtain the full dibaryon propagators for each partial wave, one has to dress the bare propagator with baryon loops to all orders [92]. This leads to a geometric series shown in Fig. 5.3 for the ΛN case. An alternative approach to obtain the corresponding dimer fields in given is Ch.2.3.2. Summing the geometric series leads to

$$iD_j\,(p_0, \mathbf{p}) = \frac{\pi}{\mu g_j^2} \frac{-i}{-\gamma_j + \sqrt{-2\mu\left(p_0 - \frac{\mathbf{p}^2}{2(M_\Lambda + M)} + i\epsilon\right)}}, \tag{5.5}$$

where $\mu = M_\Lambda M/\left(M_\Lambda + M\right)$ is the reduced mass of the ΛN system. The corresponding pole momentum for one subsystem is given by γ_j, $j \in \{1, 3\}$. Divergent loop integrals are regulated using dimensional regularization. Note the factor two missing compared to the propagators presented in Ref. [83]. The pole momenta are determined from

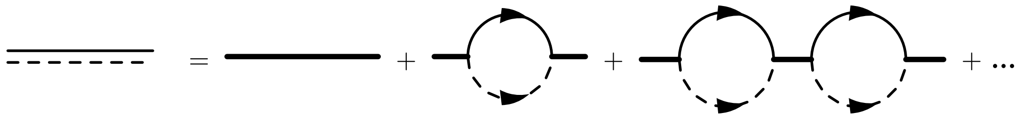

Figure 5.3.: Dibaryon propagator for the ΛN channel. Nucleons are given by solid lines, while Λ particles are given by dashed lines. The constant bare propagator, i/Δ, is denoted by a thick solid line.

the chiral EFT prediction for the ΛN scattering length at NLO using Eq. (5.2). The respective values for the different channels are given by $a_1^{\Lambda p} = (-2.90 \ldots - 2.91)$ fm and $a_3^{\Lambda p} = (-1.48 \ldots - 1.70)$ fm [17] depending on the cutoff and assuming isospin symmetry. For an explicit calculation of those propagators see also App. D.1.

The full propagators for the NN partial waves are given by [93, 94]

$$iD_{d/s}\left(p_0, \mathbf{p}\right) = \frac{2\pi}{M g_{d/s}^2} \frac{-i}{-\gamma_{d/s} + \sqrt{-M\left(p_0 - \frac{\mathbf{p}^2}{4M} + i\epsilon\right)}}, \tag{5.6}$$

where γ_d is the deuteron pole momentum and γ_s the momentum of the virtual state pole in the NN singlet partial wave. In order to obtain the full two-body scattering amplitude, external baryon lines are attached to the full dibaryon propagators [93]. Dependencies on the bare coupling constants cancel for all physical quantities.

5.3. Three-Body System

We now derive the integral equations for the hypertriton ($I = 0$) and the Λnn system ($I = 1$). In both cases we have to project onto total angular momentum $J = 1/2$. As a consequence, the integral equations have three coupled channels. Both systems can be constructed by combining a ${}^3S_1$ (ΛN) or a ${}^1S_0$ (ΛN) partial wave with another nucleon in a relative S-wave. In addition, the ${}^1S_0$ (NN) partial plus a spectator Λ particle in a relative S-wave contributes to the Λnn system, while a ${}^3S_1$ (NN) partial wave plus a Λ particle contributes to the hypertriton due to isospin symmetry. As a consequence, three three-body amplitudes T_A^I, T_B^I, T_C^I, where I denotes the respective isospin channel, are needed to describe each system. We choose $T_A^{I=0/1}$ to describe the $\Lambda - d$ / $\Lambda - nn$

channels. The amplitudes $T^I_{B/C}$ describe the ${}^3S_1/{}^1S_0\,(\Lambda N) - N$ channel for isospin I. The integral equations are shown pictorially in Fig. 5.4. Note that there is no tree level

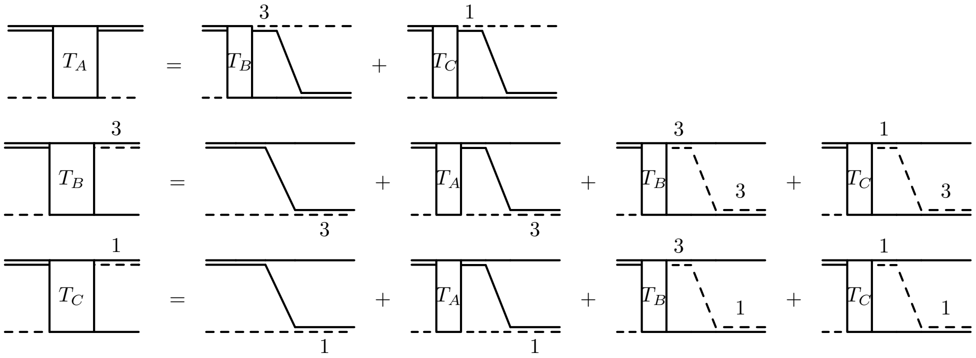

Figure 5.4.: Integral equations for the Λnn system ($I = 1$) and the hypertriton ($I = 0$). The solid double line corresponds to a ${}^1S_0\ (NN)$ dibaryon (Λnn case) or a ${}^3S_1\ (NN)$ dibaryon (hypertriton case). The dashed-solid double lines with index 1/3 correspond to ΛN dibaryons in the singlet/triplet channel. Single lines are as in Fig. 5.3.

and no loop diagram with T_A in the first equation, since the outgoing states would not correspond to the ones of T_A. The amplitudes are taken semi-offshell as depicted in Fig. 5.5. The energy E can be set as the sum on the NN momenta and the Λ particle momentum and a binding momentum term $\left(-\gamma^2/M\right)$ if needed (hypertriton channel). The offshellness $h = k^2/(2m) - p^2/(2m)$ can be determined by evaluating the loop diagrams explicitly.

$I = 0$ Channel

In case of the hypertriton, we correct the integral equations obtained in Ref. [83] for the case $y = 0$ by a factor of $1/2$ in front of the loop diagrams containing $T_C^{I=0}$ and $T_B^{I=0}$. For the case of an arbitrary y, see Eq. (D.19) in App. D.3. This factor results from the corrected dimer propagator for the ΛN partial waves, Eq. (5.5). We obtain

$$T_A^{I=0}(k,p) = -\frac{1}{2\pi}\int_0^{\Lambda_c} dq q^2 \left[L_B(p,q,E)\,T_B^{I=0}(k,q) - 3L_C(p,q,E)\,T_C^{I=0}(k,q)\right]$$

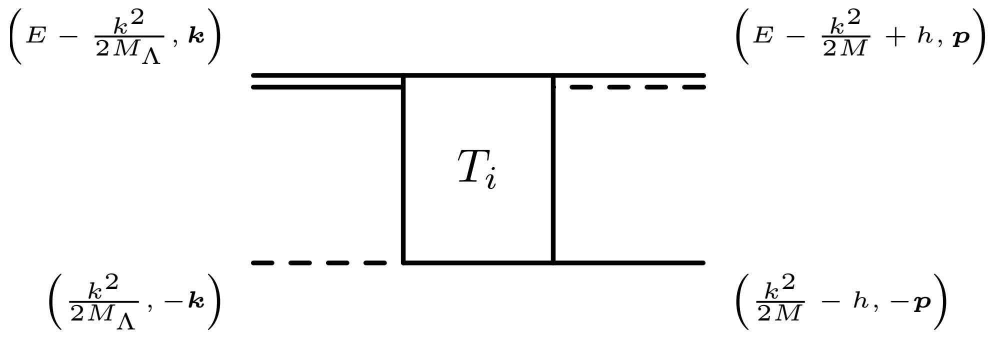

Figure 5.5.: Kinematics of NN-Λ scattering with the offshell parameter h.

$$\begin{aligned} T_B^{I=0}(k,p) =& -\frac{4\pi\gamma_d}{M} L_I(p,k,E) - \frac{1}{\pi}\int_0^{\Lambda_c} dq q^2 L_A(p,q,E)\, T_A^{I=0}(k,q) \\ & - \frac{1}{2\pi}\int_0^{\Lambda_c} dq q^2 \left[L_B(p,q,E)\, T_B^{I=0}(k,q) + 3L_C(p,q,E)\, T_C^{I=0}(k,q)\right] \end{aligned} \tag{5.7}$$

$$\begin{aligned} T_C^{I=0}(k,p) =& \frac{4\pi\gamma_d}{M} L_I(p,k,E) + \frac{1}{\pi}\int_0^{\Lambda_c} dq q^2 L_A(p,q,E)\, T_A^{I=0}(k,q) \\ & - \frac{1}{2\pi}\int_0^{\Lambda_c} dq q^2 \left[L_B(p,q,E)\, T_B^{I=0}(k,q) - L_C(p,q,E)\, T_C^{I=0}(k,q)\right] , \end{aligned}$$

where k (p) denotes the incoming (outgoing) momenta in the center-of-mass frame. Note that we suppressed the dependence of the amplitudes on the total energy $E = 3k^2\,(4M) - \gamma_d^2/M$ for convenience. A cutoff Λ_c is introduced in order to regulate the integral equations. The function L_I is given by

$$L_I(p,k,E) = \frac{1}{pk}\log\left(\frac{k^2+p^2+pk-ME}{k^2+p^2-pk-ME}\right) , \tag{5.8}$$

while the functions $L_{A/B/C}$ are

$$L_{A/B/C}(p,q,E) = \frac{1}{pq}\log\left(\frac{q^2+p^2+pq-ME}{q^2+p^2-pq-ME}\right)\left[-\gamma_{d/3/1} + \sqrt{\frac{3}{4}q^2 - ME - i\epsilon}\right]^{-1} . \tag{5.9}$$

The amplitude is normalized in such a way that

$$T_A^{I=0}(k,k) = \frac{3\pi}{M}\frac{1}{k\cot\delta - ik} \tag{5.10}$$

with δ the elastic scattering phase shift for Λd scattering. For further details of the calculation and the partial wave projection, see App. D.4 and Ref. [83].

$I = 1$ Channel

In the $I = 1$ channel, the integral equations have a similar structure, exchanging only the nucleon-nucleon dimer fields. For vanishing mass difference $y = 0$, we obtain

$$\begin{aligned}
T_A^{I=1}(k,p) =& \frac{1}{2\pi}\int \mathrm{d}q\, q^2 \left[3\tilde{L}_B(p,q,E)\, T_B^{I=1}(k,q) + \tilde{L}_C(p,q,E)\, T_C^{I=1}(k,q)\right] \\
T_B^{I=1}(k,p) =& + \frac{4\pi\gamma_{nn}}{M} L_I(p,q,E) + \frac{1}{\pi}\int \mathrm{d}q\, q^2 L_A(q,p,E)\, T_A^{I=1}(k,q) \\
&+ \frac{1}{2\pi}\int \mathrm{d}q \left[L_B(p,q,E)\, T_B^{I=1}(k,q) + L_C(p,q,E)\, T_C^{I=1}(k,q)\right] \\
T_C^{I=1}(k,p) =& \frac{4\pi\gamma_{nn}}{M} L_I(p,q,E) + \frac{1}{\pi}\int \mathrm{d}q\, q^2 L_A(q,p,E)\, T_A^{I=1}(k,q) \\
&+ \frac{1}{2\pi}\int \mathrm{d}q \left[3L_B(p,q,E)\, T_B^{I=1}(k,q) - L_C(p,q,E)\, T_C^{I=1}(k,q)\right] ,
\end{aligned} \tag{5.11}$$

where $\gamma_s \equiv \gamma_{nn}$ is the di-neutron pole momentum, which also replaces the deuteron pole momentum in the definition of L_A in Eq. (5.9). In this case there are no bound two-body subsystems. However, we have chosen the normalization in such a way that the scattering phase shift for scattering of a Λ and a hypothetical bound di-neutron can be obtained from $T_A^{I=1}$ as in Eq. (5.10) for the bound case. We can use this as an opportunity to study hypothetical neutron-neutron bound states. In addition; due to the interchange of the role of the isospin and spin part for the nucleon-nucleon interaction, the roles of T_B and T_C seem to switch as well. To be precise, the roles in the spin and isospin space of the ${}^1S_0\,(NN)$ partial wave are directly inverted to the ${}^3S_1\,(NN)$ which can be seen convincingly in the Lagrangian Eq. (5.3). For further details of the calculation and the partial wave projection, see App. D.4.

5.4. Asymptotic Analysis

In order to assess the need for a ΛNN three-body force for proper renormalization we perform an asymptotic analysis of the three-body equations [92,93]. We expect this to be needed and include the contributions from $\Lambda \Leftrightarrow \Sigma$ conversions [79,83]. In the asymptotic limit $\Lambda_c \gg q, p \gg \gamma_d, \gamma_{nn}, \gamma_1, \gamma_3 \sim k$ the integral equations can be solved analytically. We do this in two steps. First, we neglect the Λ-nucleon mass difference and set $y = 0$. In a second step, we relax this simplification.

5.4.1. $I = 0$ Channel

In the limit $\Lambda_c \gg q, p \gg \gamma_d, \gamma_{nn}, \gamma_1, \gamma_3 \sim k$, we can neglect the inhomogeneous terms in the equations and the k-dependence of the amplitudes $T^{I=0}_{A/B/C}$. Setting $y = 0$, the logarithmic dependencies of the kernel are the same for each amplitude (see also Eq. (5.9)). The equations can be rewritten in a compact form as

$$\begin{pmatrix} \tilde{T}^{I=0}_A(p) \\ \tilde{T}^{I=0}_B(p) \\ \tilde{T}^{I=0}_C(p) \end{pmatrix} = \frac{1}{2\pi}\frac{2}{\sqrt{3}} \int dq \frac{1}{q} \ln\left(\frac{p^2+q^2+pq}{p^2+q^2-pq}\right) \begin{pmatrix} 0 & -1 & 3 \\ -2 & -1 & -3 \\ 2 & -1 & 1 \end{pmatrix} \begin{pmatrix} \tilde{T}^{I=0}_A(q) \\ \tilde{T}^{I=0}_B(q) \\ \tilde{T}^{I=0}_C(q) \end{pmatrix}, \tag{5.12}$$

where we have defined $\tilde{T}^{I=0}_j(p) = pT^{I=0}_j(k \sim \gamma_d, p)$ for $j \in \{A, B, C\}$ absorbing part of the p dependence within the amplitudes. It is possible to decouple this set of integral equations[1], we obtain

$$\begin{pmatrix} T^{I=0}_1 \\ T^{I=0}_2 \\ T^{I=0}_3 \end{pmatrix} = \frac{1}{2\pi}\frac{2}{\sqrt{3}} \int dq \frac{1}{q} \ln\left(\frac{p^2+q^2+pq}{p^2+q^2-pq}\right) \begin{pmatrix} -2 & 0 & 0 \\ 0 & -2 & 0 \\ 0 & 0 & 4 \end{pmatrix} \begin{pmatrix} T^{I=0}_1 \\ T^{I=0}_2 \\ T^{I=0}_3 \end{pmatrix}, \tag{5.13}$$

where

$$\begin{pmatrix} \tilde{T}^{I=0}_A \\ \tilde{T}^{I=0}_B \\ \tilde{T}^{I=0}_C \end{pmatrix} = \frac{1}{12} \begin{pmatrix} -2 & 1 & 3 \\ 2 & 5 & 3 \\ 4 & -2 & 6 \end{pmatrix} \begin{pmatrix} T^{I=0}_1 \\ T^{I=0}_2 \\ T^{I=0}_3 \end{pmatrix}. \tag{5.14}$$

Danilov showed that an equation of the the form [26]

$$f(p) = \frac{4\lambda}{\sqrt{3}\pi} \int \frac{\mathrm{d}q}{q} \ln\left(\frac{p^2+q^2+pq}{p^2+q^2-pq}\right) f(q), \tag{5.15}$$

---

[1] This is expected at this point since otherwise one of the channels would be redundant.

the type of equations we obtained, is invariant under scale transformations and under the inversion $q \to 1/q$. Utilizing the Mellin-transformation, we find the solution has the form of a power law $p^{\pm is_0}$. If $\lambda < \lambda_c = 3\sqrt{3}/(4\pi) \approx 0.4135$, the exponent is_0 of the power law is real. On the one hand this is obviously fulfilled for the amplitudes $T_1^{I=0}$ and $T_2^{I=0}$. On the other hand for $T_3^{I=0}$ we find $\lambda = 1$ and there are two linearly independent solutions with complex exponents, $T_3^{I=0}(k,p) = p^{\pm is_0}$. The parameter s_0 is given by the transcendental equation [26]

$$1 = \frac{8\lambda}{\sqrt{3}s} \frac{\sin\frac{\pi s}{6}}{\cos\frac{\pi s}{2}}\,, \tag{5.16}$$

leading to the expected result for three distinguishable particles of $s_0 = 1.00624$ for the equal mass considered here [11]. This corrects the result $s_0 = 1.35322$ found in Ref. [83] due to the missing factors in Eq. (5.7).

The phase between the two solutions $T_3^{I=0}(k,p) = p^{\pm is_0}$, however, is not fixed. Instead it depends strongly on the cutoff Λ_c of the integral equations. This cutoff dependence can be absorbed by adding a one-parameter three-body force $H(\Lambda_c)$ in the equation for $T_3^{I=0}$ [83]

$$T_3^{I=0}(p) = \frac{4}{\sqrt{3}\pi}\int_0^{\Lambda_c} \frac{\mathrm{d}q}{q}\left[\ln\left(\frac{p^2+q^2+pq}{p^2+q^2-pq}\right) + 2H^{I=0}(\Lambda_c)\frac{pq}{\Lambda_c^2}\right] T_3^{I=0}(q)\,. \tag{5.17}$$

This three-body force $H^{I=0}(\Lambda_c)$ runs with the cutoff as [92]

$$H^{I=0}(\Lambda_c) = -\frac{\sin\left(s_0\ln\left(\frac{\Lambda_c}{\Lambda_*^{I=0}}\right) - \arctan\left(\frac{1}{s_0}\right)\right)}{\sin\left(s_0\ln\left(\frac{\Lambda_c}{\Lambda_*^{I=0}}\right) + \arctan\left(\frac{1}{s_0}\right)\right)}\,, \tag{5.18}$$

and ensures that all low-energy three-body observables are independent of Λ_c. Thus the RG evolution is covered by a limit cycle as in the triton case [93]. Due to the periodicity the value of the function $H^{I=0}(\Lambda_c)$ returns to its original value if the cutoff is increased by a factor $\exp(\pi/s_0) \approx 22.7$. The three-body-parameter $\Lambda_*^{I=0}$ must be fixed from a three-body input, for example in our case the binding energy. As a consequence, there is an Efimov effect in the hypertriton channel but the spectrum is cut off in the infrared by the finite scattering length and only the shallowest state is physical. This be can easily visualized by going back to the Efimov plot in Ch. 2.4.2 following the deepest trimer state. Since the plot is the inverse scattering length the cut is at the origin. Due to the transformation given in equation Eq. (5.14) the three-body force introduced in $T_3^{I=0}$

enters in all amplitudes of the full problem. We use a similar backwards transition as given in App. D.5 to construct the full problem.

At first glance one might think that this also fixes the three-body force in the Λnn system but this is not the case due to the two different isospin channels of the hypertriton and the Λnn. This three-body force can also be implemented by constructing the effective three-body Lagrangian and matching the coefficients in order to achieve the behavior given by equation Eq. (5.17). An explicit form of the three-body term of the effective Lagrangian is shown in App. D.5.

5.4.2. $I = 1$ Channel

We carry out a similar analysis for the Λnn system. With the same assumptions, $\Lambda_c \gg q, p \gg \gamma_d, \gamma_{nn}, \gamma_1, \gamma_3 \sim k$, as for the hypertriton case, we obtain

$$\begin{pmatrix} \tilde{T}_A^{I=1}(p) \\ \tilde{T}_B^{I=1}(p) \\ \tilde{T}_C^{I=1}(p) \end{pmatrix} = \frac{1}{2\pi}\frac{2}{\sqrt{3}} \int dq \frac{1}{q} \ln\left(\frac{p^2+q^2+pq}{p^2+q^2-pq}\right) \begin{pmatrix} 0 & 3 & 1 \\ 2 & 1 & 1 \\ 2 & 3 & -1 \end{pmatrix} \begin{pmatrix} \tilde{T}_A^{I=1}(q) \\ \tilde{T}_B^{I=1}(q) \\ \tilde{T}_C^{I=1}(q) \end{pmatrix} . \tag{5.19}$$

Using the transformation constructed in similar fashion as before

$$\begin{pmatrix} \tilde{T}_A^{I=1} \\ \tilde{T}_B^{I=1} \\ \tilde{T}_C^{I=1} \end{pmatrix} = \frac{1}{12} \begin{pmatrix} -2 & 3 & 5 \\ -2 & 3 & -1 \\ 4 & 6 & 2 \end{pmatrix} \begin{pmatrix} T_1^{I=1} \\ T_2^{I=1} \\ T_3^{I=1} \end{pmatrix} , \tag{5.20}$$

we obtain the same set of equations as for the hypertriton:

$$\begin{pmatrix} T_1^{I=1} \\ T_2^{I=1} \\ T_3^{I=1} \end{pmatrix} = \frac{1}{2\pi}\frac{2}{\sqrt{3}\pi} \int dq \frac{1}{q} \ln\left(\frac{p^2+q^2+pq}{p^2+q^2-pq}\right) \begin{pmatrix} 4 & 0 & 0 \\ 0 & -2 & 0 \\ 0 & 0 & -2 \end{pmatrix} \begin{pmatrix} T_1^{I=1} \\ T_2^{I=1} \\ T_3^{I=1} \end{pmatrix} , \tag{5.21}$$

where we once more absorbed part of the p dependence in the amplitudes. As a consequence, the structure of the solutions is the same and the same scaling exponent $s_0 = 1.00624$ emerges. This is the well-known result for three distinguishable particles with equal masses, for the hypertriton one proton, one neutron and a Λ. In this case one neutron with spin up and down each and a Λ [11]. In passing, we note that this result for s_0 disagrees with the value $s_0 = 0.803$ found in Ref. [74].

The three-body force of this channel $H^{I=1}$ has the same structure as $H^{I=0}$ in the hypertriton channel, Eq. (5.18), but the three-body parameter $\Lambda_*^{I=1}$ is not related to $\Lambda_*^{I=0}$ at the resolution level of pionless EFT. An explicit form of the three-body term of the effective Lagrangian constructed in a similar fashion to the hypertriton one is shown again in App. D.5.

5.4.3. Asymptotic Analysis with Different Masses

Next we relax our assumption of equal masses and include the Λ-nucleon mass difference, hence looking at the physical case, and repeat the analysis for finite non-vanishing y. The integral equations for this case are given in App. D.3 and App. D.4. Since the logarithm in Eq. (D.20) depends on y, it can no longer be factorized out of the matrix describing the coupling between the channels as done before. In the limit $y \to 0$, however, the result from the analysis above must be reproduced. Thus we assume that the T_i^I can be written as a linear combination of three new amplitudes, which each behave as a power law

$$T_i^I = \alpha_i T_1^I + \beta_i T_2^I + \gamma_i T_3^I \,, \quad i \in \{A, B, C\} \,. \tag{5.22}$$

Integrating term by term and utilizing the Mellin-transform on the y dependent L_i leads to two different y dependent functions,

$$F(s) = \frac{\cos(\phi^+ s) - \cos(\phi^- s)}{\sin(\pi s)} \,, \quad \text{with} \quad \phi^\pm = \arccos\left(\pm\frac{\sqrt{1+y}}{2}\right) \,, \tag{5.23}$$

$$G(s) = \frac{\cos(\phi^+ s) - \cos(\phi^- s)}{\sin(\pi s)} \,, \quad \text{with} \quad \phi^\pm = \arccos\left(\pm\frac{1-y}{2}\right) \,, \tag{5.24}$$

with s the exponent of the of the power law ansatz. Since none of the three new amplitudes is preferred by construction, the transformed integral equations decouple into three times the same subset of equations for α_i, β_i and γ_i. Without loss of generality, we choose the subset γ_i to contain the complex exponent. For the $I = 1$ channel, we obtain the equation

$$\begin{pmatrix} \gamma_A^{I=1} \\ \gamma_B^{I=1} \\ \gamma_C^{I=1} \end{pmatrix} = \frac{1}{s}\frac{1}{\sqrt{3-y}} \begin{pmatrix} 0 & 6(y+1)^{-\frac{s+3}{2}}F & 2(y+1)^{-\frac{s+3}{2}}F \\ 4(y+1)^{\frac{s+1}{2}} & \frac{2G}{\sqrt{y+1}(1-y)} & \frac{2G}{\sqrt{y+1}(1-y)} \\ 4(y+1)^{\frac{s+1}{2}} & \frac{6G}{\sqrt{y+1}(1-y)} & -\frac{2G}{\sqrt{y+1}(1-y)} \end{pmatrix} \begin{pmatrix} \gamma_A^{I=1} \\ \gamma_B^{I=1} \\ \gamma_C^{I=1} \end{pmatrix} , \tag{5.25}$$

where the s dependence of the functions G and F has been suppressed. This equation has only non-trivial solutions if the determinant of the matrix on its right-hand side vanishes. This leads to the following governing equation for s

$$16 \cdot \frac{s(3-y)(y+1)\left(2F^2(y-1)^2+G^2\right)+8F^2G(1-y)\sqrt{(3-y)(y+1)}}{s^3(y-3)^2(y-1)^2(y+1)^2}=1\,. \quad (5.26)$$

In the case of the hypertriton ($I=0$), one obtains the same equation for s. This was expected due to the similar structures of the integral equations. As expected, for vanishing mass difference the result $s_0=1.00624$ is reproduced, which can be also seen by taking the limits of F and G directly. The result for the scaling $\exp(\pi/s_0)$ as a function of $M/M_\Lambda=(1-y)\,/\,(1+y)$ is shown in Fig. 5.6. For the physical value of $y=0.086$ corresponding to $M/M_\Lambda=0.84$ we obtain $s_0=1.00760$ for both cases, the Λnn one and the hypertriton one. Our result for arbitrary non equal masses is in good agreement with the results obtained in Ref. [11] utilizing a different method.

5.4.4. Renormalization

In order to check the validity of our asymptotic analysis and the proper renormalization of the three-body equations, we calculate the three-body force for the hypertriton and the Λnn system numerically. The results are shown in Fig. 5.7. The points represent our numerical results while the straight lines are fitting curves to the theoretical expression, Eq. (5.18). We use the binding energy as three-body input. The respective results for the three-body parameter Λ_* are

$$\begin{aligned} \text{hypertriton:} \quad & B_3^\Lambda = 2.35\ \ \text{MeV}\,, \quad \Lambda_*^{I=0} = (6.372\pm0.008)\,\text{MeV}\,,\\ \Lambda nn: \quad & B_{\Lambda nn} = 1.1\ \text{MeV}\,, \quad \Lambda_*^{I=1} = (13.95\pm0.02)\ \ \text{MeV}\,. \end{aligned} \quad (5.27)$$

The three-body force H is then determined numerically in a way that the binding energy remains fixed as the cutoff Λ_c is varied. In both cases, the three-body force shows the expected limit cycle behavior. Therefore three-body states generated by the Efimov effect can be expected for $I=0$ and $I=1$. At this point the $\Lambda \Leftrightarrow \Sigma$ conversions enter the theory since this three-body force will fix our theory to a certain binding energy.

For inclusion of the three-body force in leading-order numerical calculations it is convenient to choose cutoff values at which the three-body force vanishes [95], see also App. D.2 for further details:

$$\Lambda_n = \Lambda_* \exp\left[\frac{1}{s_0}\left(n\pi + \arctan\left(\frac{1}{s_0}\right)\right)\right]\,, \quad (5.28)$$

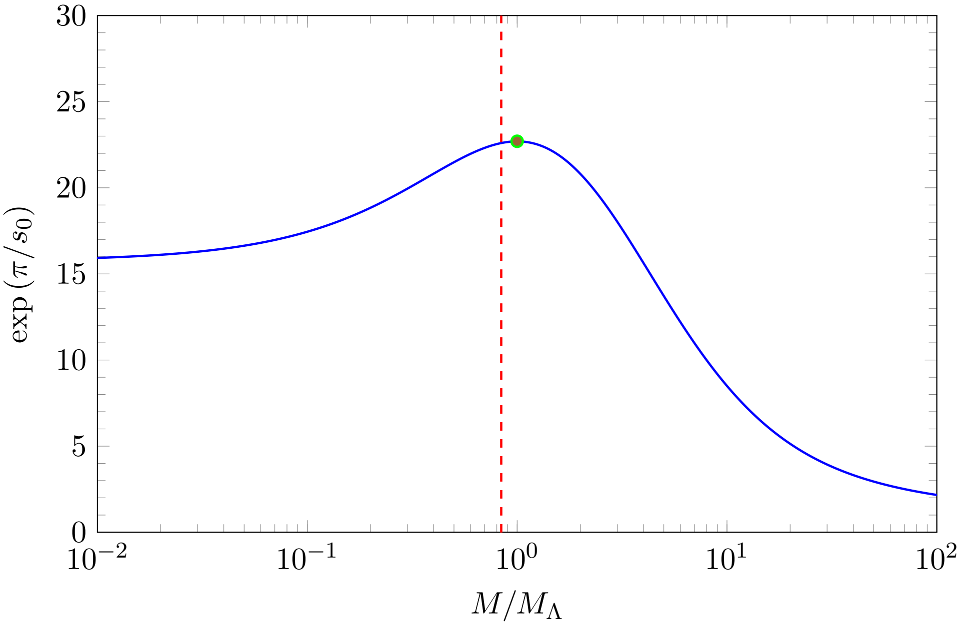

Figure 5.6.: Scaling factor $\exp\left(\pi/s_0\right)$ determined by Eq. (5.26) as function of the mass ratio $M/M_\Lambda = (1-y)/(1+y)$. The physical value is indicated by the dashed red line. The value for $y = 0$ is given by the green dot.

with $n > 0$ an integer. In the following part, equation Eq. (5.28) with $n = 1$ is used as the cutoff for all numerical calculations.

5.5. Numerical Implementation

In order to calculate the amplitude of this three-body problems we need to solve coupled integral equations of the following type

$$a\left(p\right) = h\left(p\right) + \int_0^{\Lambda_c} \mathrm{d}q\, \frac{K\left(p,q\right)}{q-k-i\epsilon} a\left(q\right), \tag{5.29}$$

where $K\left(p,q\right)$ is singularity-free. In order to do so we need to deal with the singularities generated by the $1/\left(q-k-i\epsilon\right)$ structure which is typical for such a calculation. The

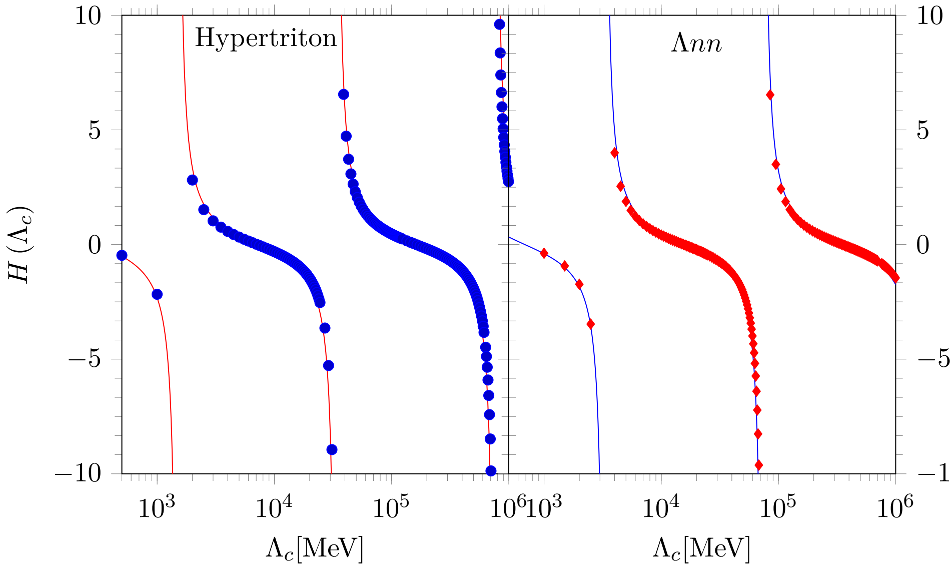

Figure 5.7.: Three-body force $H(\Lambda_c)$ for the hypertriton (left panel) and the Λnn system (right panel) as a function of the cutoff Λ_c. The points are numerical determinations obtained from taking the three-body binding energy as input (cf. Eq. (5.27)), while the solid lines are fitting curves to Eq. (5.18).

method of choice is to treat this by utilizing the so-called principal value, see also App. B.2.

$$a\left(p\right)=h\left(p\right)+\int_0^{\Lambda_c}\mathrm{d}q\,\mathcal{P}\frac{K\left(p,q\right)}{q-k}a\left(q\right)+i\pi K\left(p,k\right)a\left(k\right) \tag{5.30}$$

Rewriting the integration by adding and subtracting suitable terms simplifies the calculation and makes it numerically accessible

$$\begin{aligned}a\left(p\right)=&h\left(p\right)+\int_0^{\Lambda_c}\mathrm{d}q\,\frac{K\left(p,q\right)a\left(q\right)-K\left(k,q\right)a\left(k\right)}{q-k}a\left(q\right)+i\pi K\left(p,k\right)a\left(k\right)\\&+\int_0^{\Lambda_c}\mathrm{d}q\,\frac{\mathcal{P}}{q-k}K\left(p,k\right)a\left(k\right),\end{aligned} \tag{5.31}$$

where the integral in the second line can now be directly evaluated. We set

$$\phi\left(k\right)=\int_0^{\Lambda_c}\mathrm{d}q\,\frac{\mathcal{P}}{q-k}=\ln\left(\frac{\Lambda_c-k}{k}\right). \tag{5.32}$$

We can therefore now implement Eq. (5.31) by choosing a Gaussian grid with N number of points q_i and weights w_i with $i=1,2,\ldots N$. Setting $q_{N+1}=k$, we obtain the discrete version of Eq. (5.31)

$$a_i=h_i+\sum_{j=1}^{N}\frac{w_jK_{ij}}{q_j-q_{N+1}}a_j+K_{i,N+1}a_{N+1}\left(\phi_{N+1}-\sum_{j=1}^{N}\frac{w_j}{q_j-q_{N+1}}+i\pi\right), \tag{5.33}$$

with $i,1,2\ldots N+1$. Further on we have used the short notation $f\left(q_i\right)\equiv f_i$ in Eq. (5.33). Important here is that we rewrote the original problem in such fashion that the sums do not depend on i and hence do not hit the singularity and can therefore be directly evaluated. A second method, that we have not used in this work, is to rewrite the problem into one only for the real part since the imaginary part of such an amplitude is known by construction, see also Ch.2.

5.6. Numerical Results

In order to solve the integral equations for the Λnn system or the hypertriton we need to set the interaction parameters. For the spin-triplet nucleon-nucleon interaction, which contributes in the $I=0$ channel, we take the deuteron binding momentum $\gamma_d=45.68$ MeV as input. For the spin-singlet interaction we take the value for neutron-neutron scattering length, $a_{nn}=-18.63\pm 0.10\,\text{(stat.)}\pm 0.44\,\text{(syst.)}\pm 0.30\,\text{(theo.)}$ fm [15] since we focus explicitly on the Λnn system in this channel. The values for the ΛN S-wave interaction cannot be extracted from phase shift analyses of the limited scattering data. Instead, we use the NLO chiral EFT values [17] for all calculations in this work, i.e. $a_1^{\Lambda p}=-2.91$ fm and $a_3^{\Lambda p}=-1.61$ fm for the spin-singlet and spin-triplet channels respectively.

5.6.1. $I=0$ Channel

The Λd scattering phase is shown in Fig. 5.8. The dark blue/red band is a variation of the chiral EFT scattering lengths $a_1^{\Lambda p}=-2.91$ fm and $a_3^{\Lambda p}=-1.61$ fm. We used a variation around these input parameters by 15 percent, which covers the entire predicted range. Therefore the scattering phase shifts seems to be independent from the exact values of the low ΛN scattering lengths for small momenta. Small deviations occur closer to the deuteron breakup threshold. The hatched bands give an estimate of the pionless EFT error at leading order.

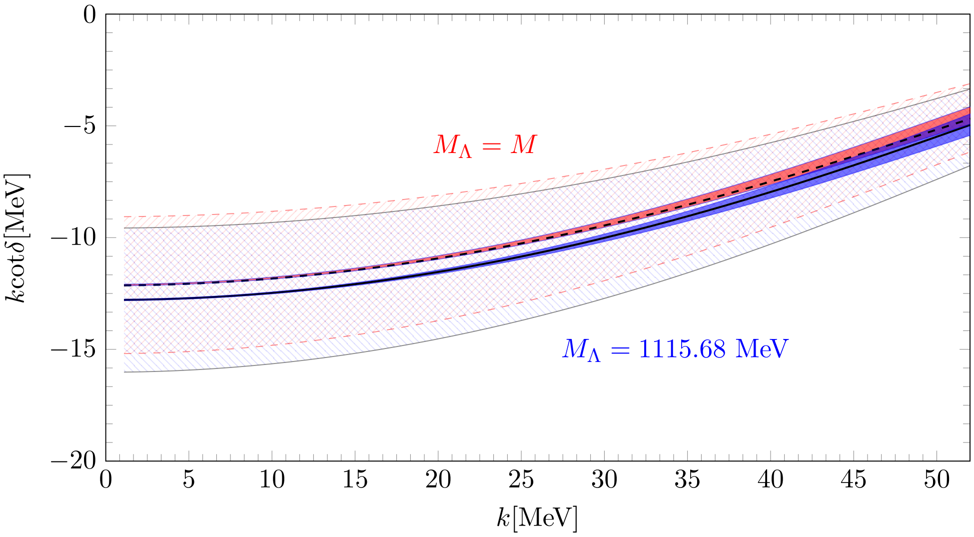

Figure 5.8.: $\Lambda - d$ scattering phase shifts for $y = 0$ (dashed black line) and physical value of the Λ mass (black solid line). The dark blue/red bands represent the sensitivity to a variation of the chiral EFT input scattering lengths by 15%, while the blue/red hatched bands give an estimate of the EFT error.

The large scattering lengths induce universal correlation between different observables. One prominent example is the Phillips line, which was first observed in deuteron-neutron system [96]. The Phillips line is a correlation between the nd S-wave scattering length and the triton binding energy. A similar correlation occurs in the hypertriton channel, where the Λ takes the role of the neutron [83]. The Phillips line for the hypertriton is shown in Fig. 5.9 for both the equal mass case (green dashed line) and for the physical Λ ($y = 0.084$) mass (blue solid line). The correlation shows the expected behavior with $a_{\Lambda d}$ going to infinity as B_3^Λ approaches the deuteron binding energy. The EFT is expected to break down when the three-body binding momentum is of the order of the pion mass, corresponding to $B_3^\Lambda \gtrsim 8\gamma_d^2/M \approx 18$ MeV (grey shaded area). The Phillips line correlation is not very sensitive to the precise values of the the ΛN scattering lengths. This is illustrated by the different black symbols in Fig. 5.9 showing the sensitivity to changes in $\gamma_i = 1/a_i$, where $i = 1, 3$ with the range of applicability of the theory. Such a behavior is not completely unexpected since the Λd separation energy is very small. This is also indicated in the plot of the Λ-d scattering phase shift. The correction to the variation of the input parameters vanishes as $k \mapsto 0$.

From the hypertriton binding energy we predict the Λd scattering length to be

$$a_{\Lambda d}^{y=0} = 16.25^{+4.45}_{-2.40}\,\text{fm}\,, \qquad a_{\Lambda d}^{y=0.086} = 15.4^{+4.3}_{-2.3}\,\text{fm} \tag{5.34}$$

where the error is determined by the uncertainty in the hypertriton binding energy. The change from finite y is of order 15% which is within errors of this LO calculation. The value for the equal mass case, $y = 0$, is in good agreement with the previous work in Refs. [83, 97]. The value of the effective range ,however, changes to $r_{\Lambda d}^{y=0.086} \approx 1.4$ fm. As mentioned before the values for the Λ-N interaction have been constructed in such a way to reproduce a specific binding energy of B_Λ. However, the scattering length is very insensitive to the exact value of the Λ-N scattering length. Hence the errors induced by the Λ-N scattering length arising from corrections to the binding energy are negligible.

5.6.2. $I = 1$ Channel

The question of whether the Λnn system is bound or not has not been answered conclusively. After regularization pionless EFT always produces one (or more) bound states in the Λnn system for a sufficiently large value of the cutoff Λ. Yet such bound states are only physically relevant if they are below the breakdown scale of the EFT. The general idea of this argument is depicted in Fig. 5.10. Following the blue trimer state in this plot allows us to find a bound state outside of the area in which the EFT is valid. Since we do not have any three-body information besides the HypHI experiment, we cannot make a conclusive statement about the existence of such a state. Assuming a flat probability distribution for possible values of the three-body parameter $\Lambda_*^{I=1}$ generated by QCD and deformations of QCD in the relevant parameter window (one cycle) we can make a statistical estimate. Taking the relevant thresholds into account, we estimate the probability P of finding a bound Λnn from the ratio of the allowed values for $\Lambda_*^{I=1}$ for a Λnn state below the breakdown scale and a whole cycle

$$P = \frac{\Lambda_*^{I=1,\text{breakdown}} - \Lambda_*^{I=1,\text{threshold}}}{(e^{\pi/s_0} - 1)\Lambda_*^{I=1,\text{threshold}}}\,. \tag{5.35}$$

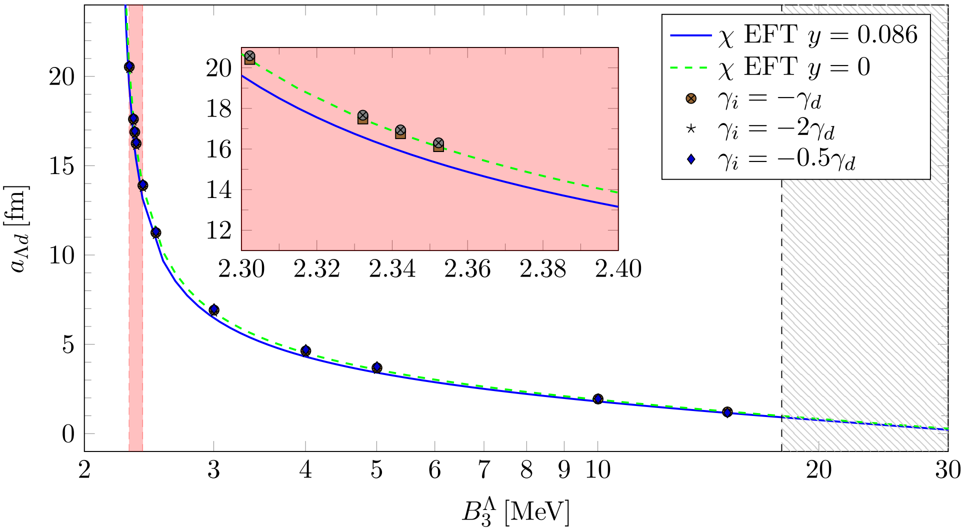

Figure 5.9.: Phillips line for the hypertriton for $y = 0$ (dashed green line) and physical Λ mass (solid blue line). In the gray shaded area the EFT description breaks down, while the red shaded area represents the physical binding energy region and is enhanced in the inset. The different black symbols illustrate the sensitivity to changes in $\gamma_i = 1/a_i$, where $i = 1, 3$ in the case $y = 0$.

We estimate that there is a 6% chance to find a Λnn bound state within the range of pionless EFT, which breaks down for typical momenta of the order of the pion mass. We note that this simple estimate does not take into account any constraints from other nuclear and hypernuclear observables and/or theory assumptions beyond pionless EFT. In the case of the hypertriton we would estimate a probability of order 20% using the same method.

For illustrative purposes, we also discuss the Phillips line correlation for a hypothetical bound di-neutron (^2n) [98] since a scattering length is only defined meaningful between two bound systems. The accepted value for the neutron-neutron scattering length is $a_{nn} = -18.63$ fm [15] but experiments are primarily sensitive to the absolute value of the scattering length. Therefore the sign is mainly determined by the non-observation of a bound di-neutron and theoretical considerations about charge symmetry breaking [99]. The corresponding Phillips line correlation for the Λ-di-neutron system is shown in

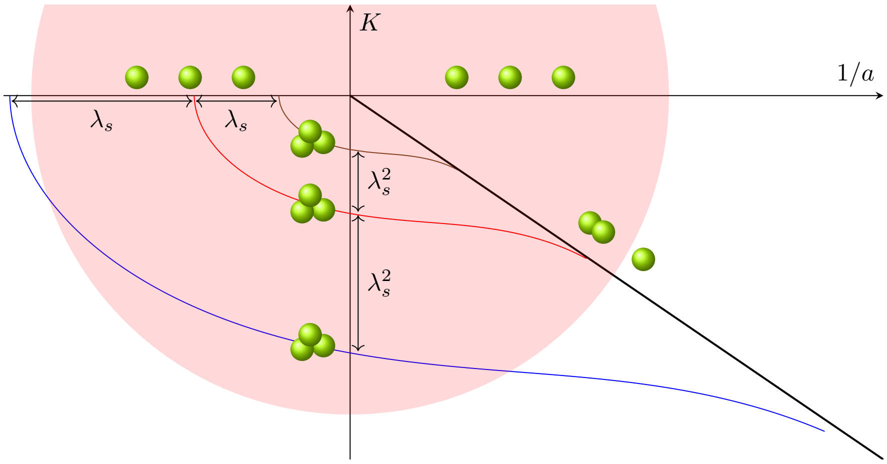

Figure 5.10.: Schematic Efimov plot, as described in 2.4.2. The red area is the parameter range for which the EFT is valid. Parts of the bottom blue trimer line is now outside of the EFT validity range.

Fig. 5.11. The correlation again shows the expected behavior for low binding momenta and the Λ-di-neutron scattering length diverges as the di-neutron binding energy is approached. The scattering length associated with the extracted value of the Λnn binding energy $B_{\Lambda nn} = 1.1$ MeV [9] for the hypothetical value $a_{nn} = 18.63$ fm=-a_{nn}^{physical} is very low. This is expected since the binding of the Λ-dineutron system must be very tight. (The di-neutron binding energy $B_{nn} = 1/(Ma_{nn}^2) \approx 0.12$ MeV is very small for this example, hence the di-neutron is shallowly bound.) The point of expected theory breakdown is far away from the displayed area in Fig. 5.11.

5.7. Wave Functions and Matter Radii

In this section we discuss the structure of the hypertriton and Λnn states and calculate their wave functions and matter radii. A discussion of hypertriton structure as a loosely bound object of a Λ and a deuteron in the context of heavy ion collisions at the LHC can be found in [100, 101].

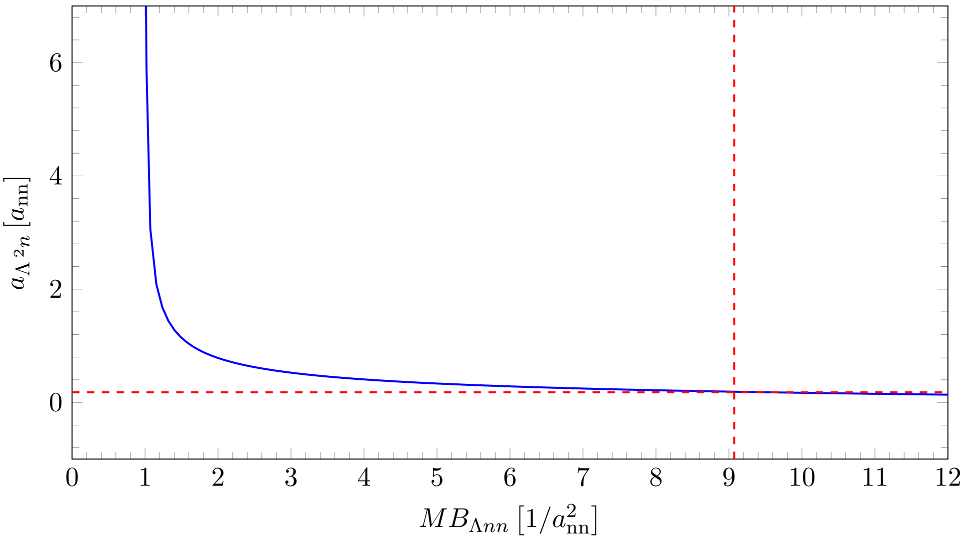

Figure 5.11.: Phillips line for the Λnn system in the case of a hypothetical bound di-neutron for arbitrary positive values of a_{nn}. The extracted mass of the Λnn system by the HypHI collaboration [9] and the corresponding Λ-di-neutron scattering length for a hypothetical value $a_{nn} = 18.63$ fm are marked by dashed lines.

5.7.1. $I = 0$ Channel

Using the integral equations for scattering in the hypertriton channel, we can obtain the bound state equation by dropping the inhomogeneous terms and the k-dependence of the amplitudes. For further calculations it is useful to use Jacobi coordinates in momentum space. Hence we use momentum plane-wave states $|p,q\rangle_i$. These plane-wave state momenta are defined in the two-body fragmentation channel (i,jk). The particle i is the spectator while the particles j and k are interacting with each other [20, 102, 103]. Therefore the momentum $\mathbf{p}$ describes the relative momentum between the interacting pair while $\boldsymbol{q}$ is the relative momentum between the spectator and the interacting-pair center of mass. The projection between the different spectators (nucleons (N) and

Lambda-particle (Λ)) must obey

$$
{}_N\left\langle \mathbf{p},\mathbf{q}\middle|\mathbf{p}',\mathbf{q}'\right\rangle_\Lambda = (2\pi)\,\delta^{(3)}\left(\mathbf{p}+\boldsymbol{\pi}_1\left(\mathbf{q}',\mathbf{q}\right)\right)\delta^{(3)}\left(\mathbf{p}'-\boldsymbol{\pi}_2\left(\mathbf{q},\mathbf{q}'\right)\right)\ , \tag{5.36}
$$

$$
{}_N\left\langle \mathbf{p},\mathbf{q}\middle|\mathcal{P}\middle|\mathbf{p}',\mathbf{q}'\right\rangle_N = (2\pi)\,\delta^{(3)}\left(\mathbf{p}+\boldsymbol{\pi}_3\left(\mathbf{q}',\mathbf{q}\right)\right)\delta^{(3)}\left(\mathbf{p}'-\boldsymbol{\pi}_3\left(\mathbf{q},\mathbf{q}'\right)\right)\ . \tag{5.37}
$$

The operator $\mathcal{P}$ denotes the permutation of the two nucleons. The momentum functions are

$$
\begin{aligned}
\boldsymbol{\pi}_1\left(\mathbf{q},\mathbf{q}'\right) &= \mathbf{q}+\frac{1+y}{2}\mathbf{q}'\ , \\
\boldsymbol{\pi}_2\left(\mathbf{q},\mathbf{q}'\right) &= \mathbf{q}+\frac{1}{2}\mathbf{q}'\ , \\
\boldsymbol{\pi}_3\left(\mathbf{q},\mathbf{q}'\right) &= \mathbf{q}+\frac{1-y}{2}\mathbf{q}'\ ,
\end{aligned} \tag{5.38}
$$

where y is again the mass parameter. Starting from the hypertriton bound state equations, we obtain the wave functions for different spectators by adding dimer and one-particle propagators to the transition amplitudes. This prescription is visualized in Fig. 5.11.

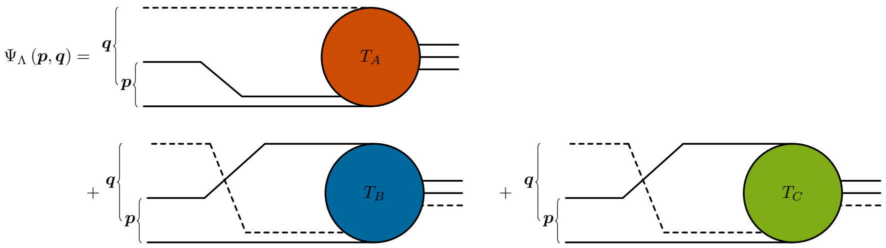

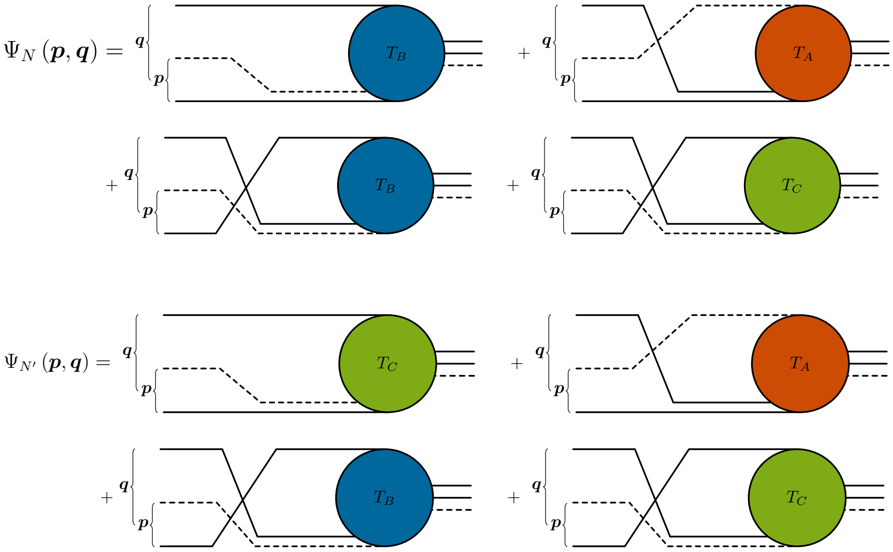

Figure 5.11.: Visualization of the construction of wave functions out of the bound state equations for the hypertriton.

This leads to the wave function given in Eq. (5.39) [23, 104, 105]. The cosine of the angle between the two momenta $\mathbf{p}$ and $\mathbf{q}$ is given by x. In principle, higher partial waves arise at this point due to recoupling between different spectators, however, in the case of pure S-wave interactions discussed here they are negligibly small [106]. Indeed we find that their contribution is of the order 10^{-8} to the wave function normalization. However their contribution might be important for example when considering P-waves. The prefactors result from projecting onto spin $S = 1/2$. The structure reassembles the structure of the integral equations Eq. (5.7):

$$\begin{aligned}\Psi_\Lambda(p,q) =& G_\Lambda(p,q,B)\left[D_D(q,B)\,T_A(q)\right.\\ &-\frac{1}{2}\int_{-1}^{1}\mathrm{d}x\,D_3(\pi_2(\mathbf{p},-\mathbf{q}),B)\,T_B(\pi_2(\mathbf{p},-\mathbf{q}))\\ &\left.+\frac{3}{2}\int_{-1}^{1}\mathrm{d}x\,D_1(\pi_2(\mathbf{p},-\mathbf{q}),B)\,T_C(\pi_2(\mathbf{p},-\mathbf{q}))\right],\end{aligned}$$

$$
\begin{aligned}
\Psi_N(p,q) = & G_n(p,q,B)\left[D_3(q,B)\,T_B(q)\right. \\
& -\frac{1}{2}\int_{-1}^{1}\mathrm{d}x\,D_D(\pi_1(\mathbf{p},-\mathbf{q}),B)\,T_A(\pi_1(\mathbf{p},-\mathbf{q})) \\
& -\frac{1}{2}\int_{-1}^{1}\mathrm{d}x\,D_3(\pi_3(\mathbf{p},-\mathbf{q}),B)\,T_B(\pi_3(\mathbf{p},-\mathbf{q})) \\
& \left.-\frac{3}{2}\int_{-1}^{1}\mathrm{d}x\,D_1(\pi_3(\mathbf{p},-\mathbf{q}),B)\,T_C(\pi_3(\mathbf{p},-\mathbf{q}))\right],
\end{aligned}
\tag{5.39}
$$

$$
\begin{aligned}
\Psi_{N'}(p,q) = & G_n(p,q,B)\left[D_1(q,B)\,T_B(q)\right. \\
& +\frac{1}{2}\int_{-1}^{1}\mathrm{d}x\,D_D(\pi_1(\mathbf{p},-\mathbf{q}),B)\,T_A(\pi_1(\mathbf{p},-\mathbf{q})) \\
& -\frac{1}{2}\int_{-1}^{1}\mathrm{d}x\,D_3(\pi_3(\mathbf{p},-\mathbf{q}),B)\,T_B(\pi_3(\mathbf{p},-\mathbf{q})) \\
& \left.+\frac{1}{2}\int_{-1}^{1}\mathrm{d}x\,D_1(\pi_3(\mathbf{p},-\mathbf{q}),B)\,T_C(\pi_3(\mathbf{p},-\mathbf{q}))\right].
\end{aligned}
$$

The free Green's functions $G_i^0(p,q,B)$ are given by

$$
\begin{aligned}
G_\Lambda(p,q,B) &= \left[mB + p^2 + \frac{3-y}{(1+y)\,4}q^2\right]^{-1}, \\
G_n(p,q,B) &= \left[mB\,(1+y) + p^2 + \frac{3-y}{4}q^2\right]^{-1}.
\end{aligned}
\tag{5.40}
$$

The absolute square of the spectator wave functions is shown on a logarithmic scale in Fig. 5.12. Starting from there we can calculate one-body matter-density form factors

$$
F_i\left(\mathbf{k}^2\right) = \int \mathrm{d}^3p \int \mathrm{d}^3q\,\Psi_i(p,q)\,\Psi_i(p,|\mathbf{q}-\mathbf{k}|)\,, \tag{5.41}
$$

where i is again the spectator. Matter radii then can be extracted by expanding the form factors in terms of $\mathbf{k^2}$ leading to the relation

$$
F_i\left(\mathbf{k}^2\right) = 1 - \frac{1}{6}\mathbf{k}^2\langle r_{i-jk}^2\rangle + \dots\ , \tag{5.42}
$$

where $\langle r_{i-jk}^2\rangle$ denotes the mean square distance between the spectator center of mass of the interacting pair [23]. An overview over the different radii corresponding to different

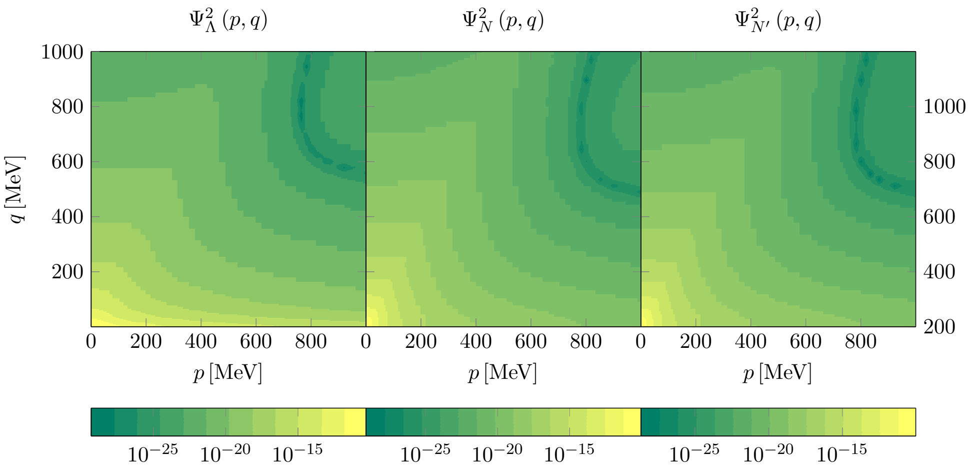

Figure 5.12.: The absolute square of the wave functions $\Psi^2_\Lambda\,(p,q)$, $\Psi^2_N\,(p,q)$ and $\Psi^2_{N'}\,(p,q)$ (normalized to one). The z axis is logarithmic; p describes the momentum between the interacting pair while q describes the momentum between the spectator and the interacting pair.

form factors is shown in Fig. 5.13. In contrast to two-body systems, in which only one meaningful matter radius exists, in a three-body system one can define a large set of radii with a meaningful interpretation. The form factor $F_{jk}\left(\mathbf{k}^2\right)$ is given by

$$F_{jk}\left(\mathbf{k}^2\right) = \int \mathrm{d}^3p \int \mathrm{d}^3q\, \Psi_i\,(p,q)\, \Psi_i\,(|\mathbf{p}-\mathbf{k}|, q)\,. \tag{5.43}$$

Since we consider a tightly bound proton-neutron pair compared to the binding energy of the Λ particle to the pair, we expect the results to be close to treating the system as a two-body state. A first estimate is given by considering a shallow S-wave two-body bound state resulting in

$$B_2 = \frac{1}{2\mu a^2} \quad \text{and} \quad \langle r^2 \rangle = \frac{a^2}{2}\,, \tag{5.44}$$

where μ is the two-body reduced mass [11]. Using these two equations, we can get an estimate for the two radii

$$\sqrt{\langle r^2_{NN'}\rangle} \approx 3.04\,\mathrm{fm} \quad \text{and} \quad \sqrt{\langle r^2_{\Lambda-NN'}\rangle} \approx 10.34\,\mathrm{fm}\,. \tag{5.45}$$

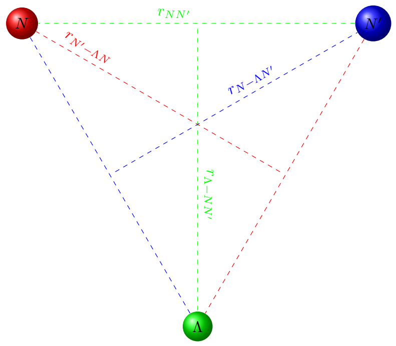

radius	corresponding F
$\langle r^2_{\Lambda-NN'}\rangle$	$F_\Lambda\left(\mathbf{k}^2\right)$
$\langle r^2_{N-\Lambda N'}\rangle$	$F_N\left(\mathbf{k}^2\right)$
$\langle r^2_{N'-\Lambda N}\rangle$	$F_{N'}\left(\mathbf{k}^2\right)$
$\langle r^2_{NN'}\rangle$	$F_{NN'}\left(\mathbf{k}^2\right)$

Figure 5.13.: Different matter radii for the ΛNN systems and the corresponding form factors.

The results for the different form factors are shown in Fig. 5.14. It is also possible to combine those radii to a geometric matter radius given by

$$\langle r^2_{geo}\rangle = \frac{(A+1)^2}{(A+2)^3}\langle r^2_{N'-\Lambda N}\rangle + \frac{(A+1)^2}{(A+2)^3}\langle r^2_{N-\Lambda N'}\rangle + \frac{4A}{(A+2)^3}\langle r^2_{\Lambda-NN'}\rangle\ , \tag{5.46}$$

where $A = M_\Lambda/M$ is the Λ-nucleon mass ratio. This radius averages radii by the mass of the constituents. The results are shown in Table 5.1. We have fitted the linear part of the form factors shown in Fig. 5.14 close to $k^2 = 0$. The errors are mainly given by the uncertainties of the binding energy of the system rather than the uncertainties of the ΛN scattering lengths. Comparing the three-body results for $\sqrt{\langle r^2_{NN'}\rangle}$ and $\sqrt{\langle r^2_{\Lambda-NN'}\rangle}$ given in Table 5.1 with the two-body ones in Eq. (5.45) confirms that the "picture" as a two-body system consisting of a deuteron and a Λ is a good approximation.

The recent result of the STAR collaboration suggests a different value of $B_\Lambda = 0.41$ MeV for the binding of the Λ particle to the deuteron [8]. We therefore analyze the impact of this new result on the structure of the hypertriton. The Phillips line depicted in Fig. 5.9 already indicates that the resulting Λd scattering length is reduced by about 40%. To sharpen our analysis, we calculate the Λd scattering length for the central value and upper/lower bound of the uncertainty estimate of the STAR collaboration measurement of the hypertriton binding energy $B_\Lambda = 0.41 \pm 0.12 \pm 0.11$ MeV [8]. The last two columns in Tab. 5.2 estimate the impact of the Λd effective range. We compare the zero-range

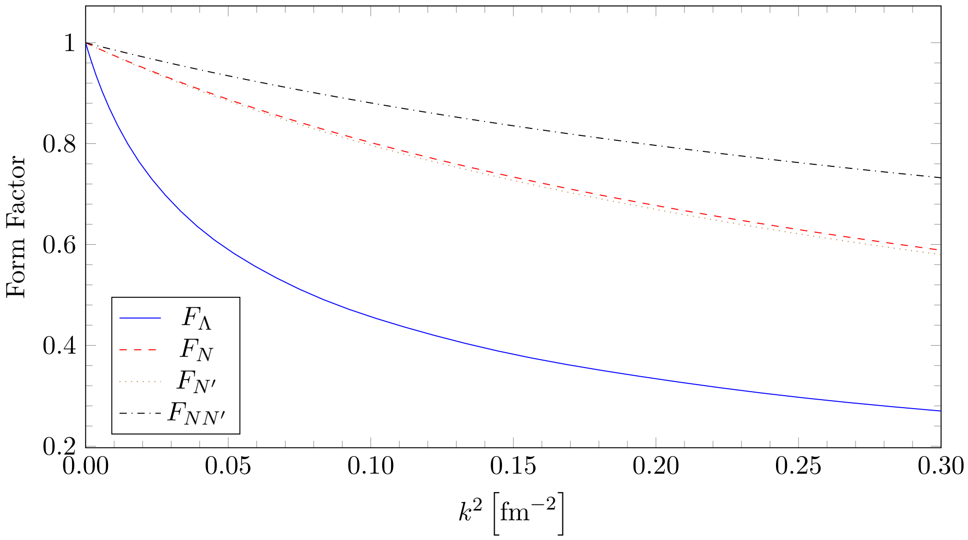

Figure 5.14.: The formfactors F_i and $F_{NN'}$ as a function of k^2. The lines for F_N and $F_{N'}$ are close to each other. For identical spin-triplet and spin-singlet scattering lengths F_N and $F_{N'}$ would fall on top of each other

approximation B_0 of the hypertriton as a Λd bound state with the exact value (taken as input to determine the Λd scattering length). For a vanishing Λd effective range we have $B_\Lambda = B_0$. We obtain the following values for $a_{\Lambda d}$: While $a_{\Lambda d}$ varies from 6 to 14 fm over the 1σ error band for the new value, the estimate of effective range corrections due to $r_{\Lambda d}$ to the hypertriton binding energy varies from 11 to 15%. This indicates that effective range corrections are very small and the convergence behavior of the effective range expansion is unchanged.

The matter radii using the new binding energy confirm this conclusion. Using Eq. (5.44) we obtain for the Λd two-body approximation:

$$\sqrt{\langle r^2_{NN'}\rangle} \approx 3.04\,\text{fm} \quad \text{and} \quad \sqrt{\langle r^2_{\Lambda-NN'}\rangle} \approx 5.82\,\text{fm}\,, \tag{5.47}$$

for $B_\Lambda = 0.41$ MeV. From the full three-body calculation, we obtain the matter radii shown in Table 5.3. The relative deviation of $\sqrt{\langle r^2_{\Lambda-NN'}\rangle}$ for $B_\Lambda = 0.41$ MeV from the two-body approximation is about 2%. We therefore conclude that the two-body picture

Table 5.1.: Different matter radii for the hypertriton in fm. The first row is for the binding energy of 2.35 MeV with the chiral EFT predictions for the ΛN interactions. Further rows are corrections to this value given by variations in the binding energy and ΛN interactions.

$\sqrt{\langle r^2_{\Lambda-NN'}\rangle}$ [fm]	$\sqrt{\langle r^2_{N'-\Lambda N}\rangle}$ [fm]	$\sqrt{\langle r^2_{N-N'\Lambda}\rangle}$ [fm]	$\sqrt{\langle r^2_{NN'}\rangle}$ [fm]	$\sqrt{\langle r^2_{geo}\rangle}$ [fm]
10.79	3.96	4.02	2.96	4.66
$+3.04/-1.53$	$+0.40/-0.25$	$+0.41/-0.25$	$+0.06/-0.05$	$+1.19/-0.54$
$+0.03/-0.02$	$+0.03/-0.03$	$+0.03/-0.03$	$+0.03/-0.04$	$+0.01/-0.01$

Table 5.2.: The $a_{\Lambda d}$ scattering length for different values of B_Λ for the uncertainty estimates and the central value of the STAR Collaboration. In addition we perform an analysis how good our estimation is based on neglecting effective range utilizing the shallow dimer approximation in the third and fourth column. See also Ch. 2.4.1 .

comment	B_Λ [MeV]	$a_{\Lambda d}$ [fm]	$B_0 = \frac{1}{2\mu_{\Lambda d} a^2_{\Lambda d}}$ [MeV]	$\frac{B_\Lambda - B_0}{B_\Lambda}$
Eq. (5.34)	0.13	15.40	0.11	0.15
lower bound	0.18	13.06	0.16	0.11
central value	0.41	8.77	0.35	0.14
upper bound	0.64	7.08	0.55	0.14

is still justified despite the slightly larger value of B_Λ measured by STAR.

5.7.2. $I = 1$ Channel

Utilizing the same procedure as before, we obtain equations for the wave functions and matter radii for the Λnn system. The respective diagrammatic equations for the Λnn system look similar to the ones depicted in Fig. 5.11 due to the similarity of the integral equations before. Therefore we only need to change the prefactors accordingly. We obtain the following set of equations for the Λnn case. The structure is of course in

Table 5.3.: Different matter radii for the hypertriton for different binding energies in fm. The chosen values reflect the results obtained by the STAR collaboration [8]. The procedure used is the same as in Fig. 5.13

B_Λ[MeV]	$\sqrt{\langle r^2_{\Lambda-NN'}\rangle}$	$\sqrt{\langle r^2_{N'-\Lambda N}\rangle}$	$\sqrt{\langle r^2_{N-N'\Lambda}\rangle}$	$\sqrt{\langle r^2_{NN'}\rangle}$	$\sqrt{\langle r^2_{geo}\rangle}$
0.18	9.26	3.71	3.77	2.91	4.12
0.41	5.92	2.95	2.99	2.60	2.85
0.64	4.57	2.53	2.56	2.35	2.32

alignment with the structure of the integral equations for the scattering properties.

$$
\begin{aligned}
\Psi_\Lambda(p,q) =& G_\Lambda(p,q,B)\left[D_D(q,B)\,T_A(q)\right.\\
&+\frac{3}{2}\int_{-1}^{1}\mathrm{d}x\,D_3\left(\pi_2(\mathbf{p},-\mathbf{q}),B\right)T_B\left(\pi_2(\mathbf{p},-\mathbf{q})\right)\\
&\left.+\frac{1}{2}\int_{-1}^{1}\mathrm{d}x\,D_1\left(\pi_2(\mathbf{p},-\mathbf{q}),B\right)T_C\left(\pi_2(\mathbf{p},-\mathbf{q})\right)\right],\\
\\
\Psi_n(p,q) =& G_n(p,q,B)\left[D_3(q,B)\,T_B(q)\right.\\
&+\frac{1}{2}\int_{-1}^{1}\mathrm{d}x\,D_D\left(\pi_1(\boldsymbol{p},-\mathbf{q}),B\right)T_A\left(\pi_1(\mathbf{p},-\mathbf{q})\right)\\
&+\frac{1}{2}\int_{-1}^{1}\mathrm{d}x\,D_3\left(\pi_3(\mathbf{p},-\mathbf{q}),B\right)T_B\left(\pi_3(\mathbf{p},-\mathbf{q})\right)\\
&\left.+\frac{1}{2}\int_{-1}^{1}\mathrm{d}x\,D_1\left(\pi_3(\mathbf{p},-\mathbf{q}),B\right)T_C\left(\pi_3(\mathbf{p},-\mathbf{q})\right)\right],\\
\\
\Psi_{n'}(p,q) =& G_n(p,q,B)\left[D_1(q,B)\,T_B(q)\right.\\
&+\frac{1}{2}\int_{-1}^{1}\mathrm{d}x\,D_D\left(\pi_1(\mathbf{p},-\mathbf{q}),B\right)T_A\left(\pi_1(\mathbf{p},-\mathbf{q})\right)\\
&+\frac{3}{2}\int_{-1}^{1}\mathrm{d}x\,D_3\left(\pi_3(\mathbf{p},-\mathbf{q}),B\right)T_B\left(\pi_3(\mathbf{p},-\mathbf{q})\right)\\
&\left.-\frac{1}{2}\int_{-1}^{1}\mathrm{d}x\,D_1\left(\pi_3(\mathbf{p},-\mathbf{q}),B\right)T_C\left(\pi_3(\mathbf{p},-\mathbf{q})\right)\right].
\end{aligned}
\tag{5.48}
$$

The binding energy of the Λnn system is not known, but the invariant mass distributions suggest a separation energy of $B_{\Lambda nn} = 1.1$ MeV [9]. This is much larger compared to the Λ-deuteron separation energy of only 0.13 ± 0.05 MeV. This implies that the radii of the Λnn should be smaller. We therefore calculate the matter form factors for the Λnn system for this value of $B_{\Lambda nn}$. Our results for the wave functions and form factors are shown in Figs. 5.15 and 5.16, respectively.

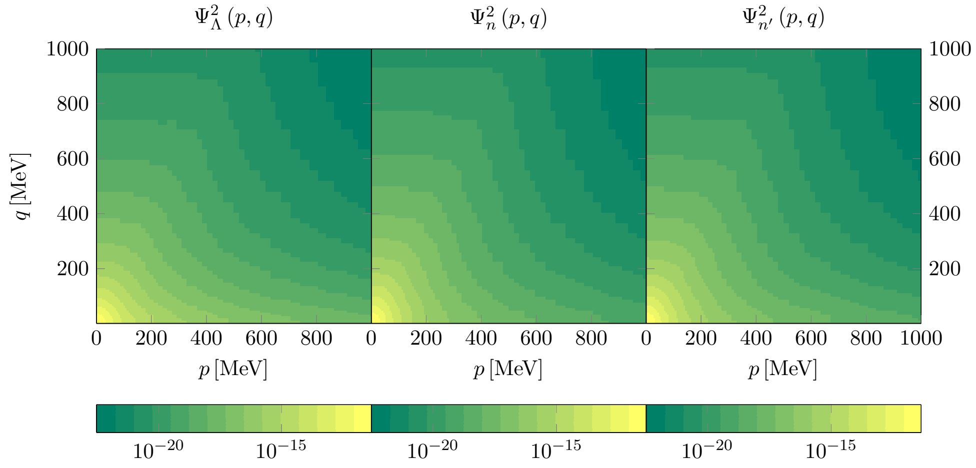

Figure 5.15.: The absolute square of the wave functions $\Psi^2_\Lambda(p,q)$, $\Psi^2_n(p,q)$ and $\Psi^2_{n'}(p,q)$ for the Λnn bound with a binding energy $B_{\Lambda nn} = 1.1$ MeV. The z axis is logarithmic; p describes the momentum between the interacting pair while q describes the momentum between the spectator and the interacting pair.

As expected the Λnn system does not show the two-body halo character of the hypertriton since it does not have a bound two-body subsystem. Moreover, all matter radii are of comparable size.

Since the value of the Λnn binding energy is uncertain, we calculate the matter radii as a function of $B_{\Lambda nn}$. The results for the different radii as a function of the Λnn binding energy (but keeping the NN and ΛN interaction fixed) are shown in Fig. 5.17. The bands represent a variation of the chiral EFT ΛN scattering length values by 15% around the central value. The general observation that all matter radii are of comparable size continues to hold if $B_{\Lambda nn}$ is varied.

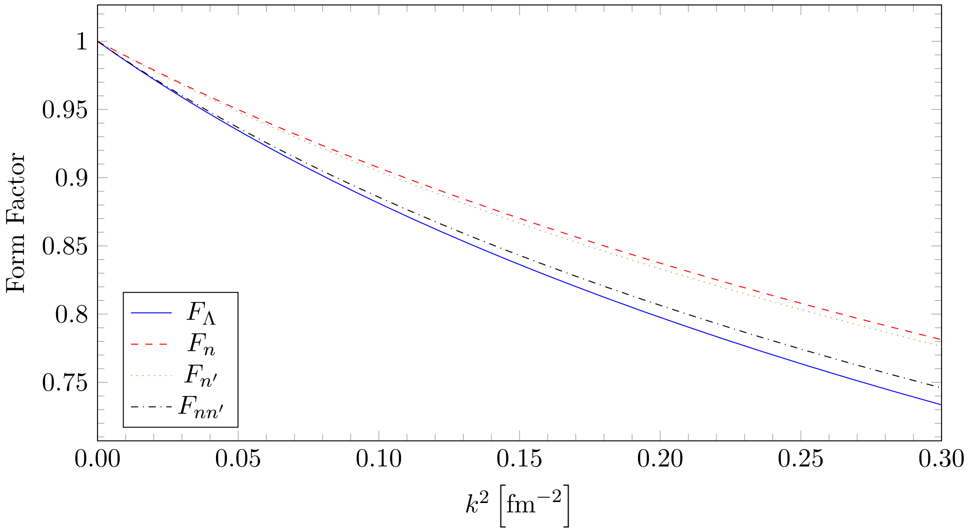

Figure 5.16.: The formfactors F_i and F_{nn} as a function of k^2 for the Λnn system. The form factors of F_n and $F_{n'}$ are again close to each other. For identical spin-triplet and spin-singlet scattering lengths F_n and $F_{n'}$ would fall on top of each other.

.

5.8. Possibility of a Hypertriton with $J = 3/2$

In this section we discuss briefly the possibility of a hypertriton with a total $J = 3/2$, which can be found in some lattice QCD calculations at non-physical pion masses and is also discussed at an exited state [107]. In contrast to the system considered before all spins are now aligned. It is known from other systems in nuclear physics that a bound state of maximum aligned spin might be forbidden. However, this is here allowed. In this case we still have three distinguishable particles. So within our framework we still expect that this system will show the Efimov effect and therefore we will be able to acquire a bound state. We will show that this will be indeed the case. We start our analysis with the Lagrangian from before given in Eq. (5.3). It becomes immediately clear that the ${}^1S_0\,(\Lambda N)$ partial wave is not allowed to contribute in order to obtain a $J = 3/2$ hypertriton due to the alignment of the spins. The amplitude T_C of the $J = 1/2$ hypertriton therefore vanishes. For the $J = 3/2$ hypertriton with only S-wave

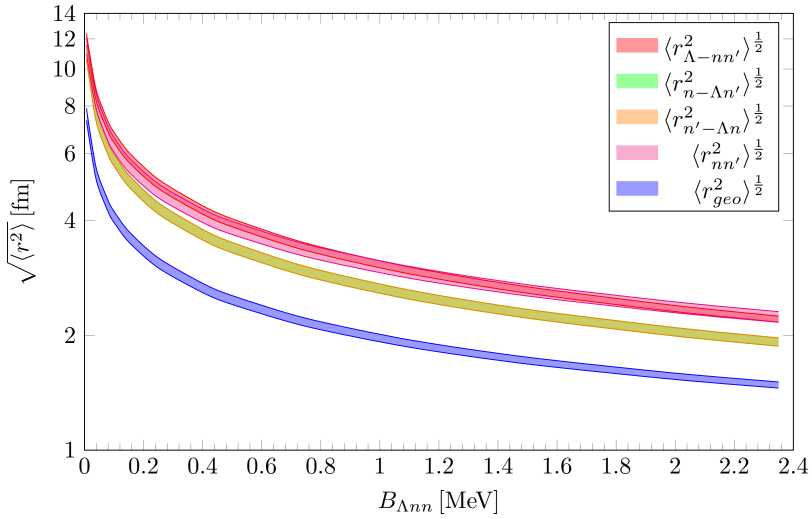

Figure 5.17.: Matter radii for the Λnn system as function of the binding energy $B_{\Lambda nn}$ for a neutron-neutron scattering length of -18.63 fm and chiral EFT values for the Λn scattering lengths $\pm 15\%$. The band for the radii with the two nucleons as spectator lie on top of each other.

interactions we obtain only two coupled integral equations

$$t_A^{ij}\left(\boldsymbol{k},\boldsymbol{p}\right)_{\alpha\beta} = g_d g_3 \int \frac{\mathrm{d}^3 q}{\left(2\pi\right)^3} t_B^{ik}\left(\boldsymbol{p},\boldsymbol{q}\right)_{\alpha\gamma} \frac{\left(\sigma_j\sigma_k\right)_{\gamma\beta} D_3\left(E-q^2/\left(2M\right),\boldsymbol{q}\right)}{E-\frac{p^2}{2M_\Lambda}-\frac{q^2}{2M}-\frac{\left(\boldsymbol{q}+\boldsymbol{p}\right)^2}{2M}+i\epsilon}, \tag{5.49}$$

$$\begin{aligned} t_B^{ij}\left(\boldsymbol{k},\boldsymbol{p}\right)_{\alpha\beta} = & -2g_d g_3 \frac{\left(\sigma_j\sigma_i\right)_{\alpha\beta}}{E-\frac{k^2}{2M_\Lambda}-\frac{p^2}{2M}-\frac{\left(\boldsymbol{k}+\boldsymbol{p}\right)^2}{2M}+i\epsilon} \\ & + 2g_d g_3 \int \frac{\mathrm{d}^3 q}{\left(2\pi\right)^3} t_A^{ik}\left(\boldsymbol{p},\boldsymbol{q}\right)_{\alpha\gamma} \frac{\left(\sigma_j\sigma_k\right)_{\gamma\beta} D_d\left(E-q^2/\left(2M_\Lambda\right),\boldsymbol{q}\right)}{E-\frac{p^2}{2M}-\frac{q^2}{2M_\Lambda}-\frac{\left(\boldsymbol{q}+\boldsymbol{p}\right)^2}{2M}+i\epsilon} \\ & + g_3^2 \int \frac{\mathrm{d}^3 q}{\left(2\pi\right)^3} t_B^{ik}\left(\boldsymbol{p},\boldsymbol{q}\right)_{\alpha\gamma} \frac{\left(\sigma_j\sigma_k\right)_{\gamma\beta} D_3\left(E-q^2/\left(2M\right),\boldsymbol{q}\right)}{E-\frac{p^2+q^2}{2M}-\frac{\left(\boldsymbol{q}+\boldsymbol{p}\right)^2}{2M}+i\epsilon}, \end{aligned} \tag{5.50}$$

where everything is defined as in the $J = 1/2$ case. In contrast to before we now need to project onto the quartet part by choosing $\alpha = \beta = 1$ and $i = (i + 2i)/\sqrt{2}$,$i = (i - 2i)/\sqrt{2}$. This leads to

$$\sigma^j \sigma^i = 2 \begin{pmatrix} 0 & 0 \\ 0 & 1 \end{pmatrix} . \tag{5.51}$$

Since spins are not allowed to change their alignment, this is the only channel that contributes. This leads to

$$\begin{aligned} T_A(\boldsymbol{k}, \boldsymbol{p}) =& 2 g_d g_3 \int \frac{\mathrm{d}^3 q}{(2\pi)^3} T_B(\boldsymbol{p}, \boldsymbol{q}) \frac{D_3\left(E - q^2/(2M), \boldsymbol{q}\right)}{E - \frac{p^2}{2M_\Lambda} - \frac{q^2}{2M} - \frac{(\boldsymbol{q}+\boldsymbol{p})^2}{2M} + i\epsilon} \\ T_B(\boldsymbol{k}, \boldsymbol{p}) =& -4 g_d g_3 \frac{1}{E - \frac{k^2}{2M_\Lambda} - \frac{p^2}{2M} - \frac{(\boldsymbol{k}+\boldsymbol{p})^2}{2M} + i\epsilon} \\ & + 4 g_d g_3 \int \frac{\mathrm{d}^3 q}{(2\pi)^3} T_A(\boldsymbol{p}, \boldsymbol{q}) \frac{D_d\left(E - q^2/(2M_\Lambda), \boldsymbol{q}\right)}{E - \frac{p^2}{2M} - \frac{q^2}{2M_\Lambda} - \frac{(\boldsymbol{q}+\boldsymbol{p})^2}{2M} + i\epsilon} \\ & + 2 g_3^2 \int \frac{\mathrm{d}^3 q}{(2\pi)^3} T_B(\boldsymbol{p}, \boldsymbol{q}) \frac{D_3\left(E - q^2/(2M), \boldsymbol{q}\right)}{E - \frac{p^2+q^2}{2M} - \frac{(\boldsymbol{q}+\boldsymbol{p})^2}{2M} + i\epsilon} . \end{aligned} \tag{5.52}$$

Now projecting onto relative S-waves and neglecting the inhomogeneous term since we are looking for bound states yields

$$\begin{aligned} T_A(k, p) =& g_d g_3 M \int \frac{\mathrm{d}^3 q}{(2\pi)^3} T_B(p, q) D_3\left(E - q^2/(2M), q\right) \\ & \times \frac{1}{pq} \log\left(\frac{q^2 + pq + p^2/(1+y) - ME}{q^2 - pq + p^2/(1+y) - ME}\right) \\ T_B(k, p) =& 2 g_d g_3 M \int \frac{\mathrm{d}^3 q}{(2\pi)^3} T_A(p, q) D_d\left(E - q^2/(2M_\Lambda), q\right) \\ & \times \frac{1}{pq} \log\left(\frac{q^2/(1+y) + pq + p^2 - ME}{q^2/(1+y) - pq + p^2 - ME}\right) \\ & + g_3^2 M_\Lambda \int \frac{\mathrm{d}^3 q}{(2\pi)^3} T_B(p, q) D_3\left(E - q^2/(2M), q\right) \\ & \times \frac{1}{pq} \log\left(\frac{q^2 + pq + p^2(1-y) - ME(1+y)}{q^2 - pq(1-y) + p^2 - ME(1+y)}\right) . \end{aligned} \tag{5.53}$$

Implementing an wave function renormalization so that we have a pole in the deuteron propagator in similar fashion as before results in:

$$\begin{aligned} T_A(k,p) =& \frac{1}{\pi(1+y)} \int \mathrm{d}q\, q^2 T_B(k,q)\, \tilde{L}(p,q,E) \\ T_B(k,p) =& \frac{2}{\pi} \int \mathrm{d}q\, q^2 T_A(p,q)\, L_A(p,q,E) + \frac{1}{\pi(1-y)} \int \mathrm{d}q\, q^2 T_B(p,q)\, L_B(p,q,E)\,. \end{aligned} \tag{5.54}$$

To check whether we need a one-parameter three-body force as for the $J = 1/2$ hypertriton, we do an asymptotic analysis in the same fashion as before. As system to solve we obtain:

$$\begin{pmatrix} T_1 \\ T_2 \end{pmatrix} = \frac{1}{2\pi} \frac{2}{\sqrt{3}} \int \mathrm{d}q\, \frac{1}{q} \ln\left(\frac{p^2+q^2+pq}{p^2+q^2-pq}\right) \begin{pmatrix} 4 & 0 \\ 0 & -2 \end{pmatrix} \begin{pmatrix} T_1 \\ T_2 \end{pmatrix} \tag{5.55}$$

Utilizing again the result of Danilov for equations of the type Eq. (5.15), we find once more a scaling parameter of $\lambda_s \exp(\pi/s_0) \approx 22.6$ and need indeed a one parameter three-body-force to renormalize the system. This is exactly the result we expect for three-distinguishable particles. Alternatively we could also solve the integral equations directly. The resulting binding energy B as a function of the cutoff Λ_c depicted in Fig. 5.18 shows the typical discrete scaling with the scaling parameter λ_s as the bound states arise form the deuteron threshold.

5.9. Chapter Summary

In this chapter we have discussed the structure of three-body $S = -1$ hypernuclei in pionless EFT with a focus on the hypertriton ($I = 0$) and the hypothetical Λnn bound state in the $I = 1$ channel. Both systems show the Efimov effect and have the same scaling factor, therefore the occurrence of bound states is natural within pionless EFT. However, the three-body parameters need not to be the same for both cases. This is in contrast to other approaches which implicitly make assumptions about the relation between the two-channels [66, 66–70]. However, due to the finite scattering lengths, a physical state will only appear in the $I = 1$ channel if it is within the range of validity of the pionless EFT description, i.e. if it is shallow enough. Based on our leading order analysis, we cannot rule out a Λnn bound state. From a simple statistical argument we estimate that there is a 6% chance to find a Λnn bound state within in the range of pionless EFT.

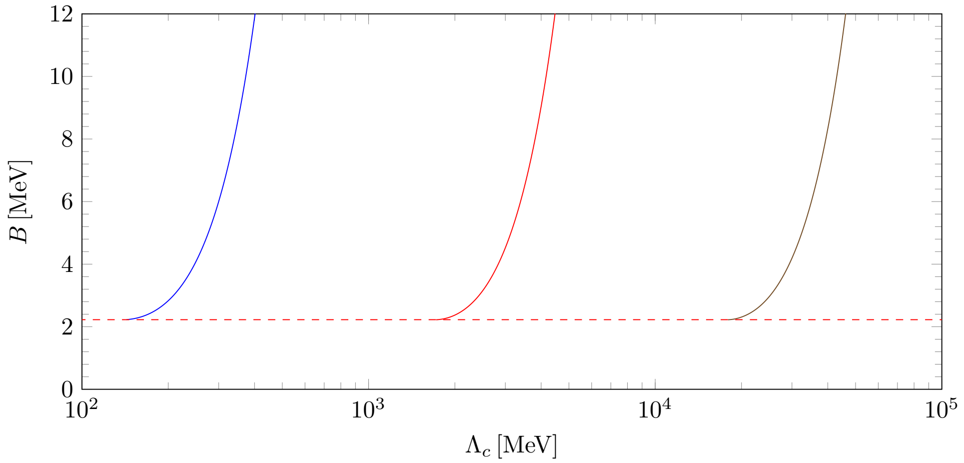

Figure 5.18.: Binding energy as a function of the cutoff Λ_c for a $J = 3/2$ hypertriton. Bound states arise from the deuteron threshold at 2.225 MeV.

In addition, we perform a detailed analysis of the structure of the hypertriton and the hypothetical Λnn bound state and related scattering processes. While the NN interaction parameters are well known, the ΛN parameters are taken from a chiral EFT analysis at NLO [17]. For Λd scattering system we predict a scattering length of $a^{0.086}_{\Lambda d} = 13.4^{+4.3}_{-2.3}$ fm. This result is insensitive to the details of the ΛN interaction and mainly driven by the value of the hypertriton binding energy [83].

Moreover, we have performed calculations of matter radii and wave functions in both isospin channels. For the hypertriton, the calculation shows a large separation between the Λ and the "deuteron" core of $10.79^{+3.04}_{-1.53}$ fm, which is also reflected in the Λ-deuteron separation energy of only 0.13 ± 0.05 MeV. This separation is comparable to the one obtained in a straight two-body calculation with Λ and deuteron degrees of freedom, which lends further credibility to an effective two-body description in the case of the hypertriton [50]. Again these results are insensitive to the exact values of the ΛN scattering lengths. Since the Λnn system lacks a bound two-body subsystem, this behavior is not observable for a hypothetical bound state in the $I = 1$ channel. Although the question whether the Λnn system is bound cannot be answered definitely, we are able to predict matter radii and wave functions for this system as a function of its binding energy.

Further on we discussed the existence of a $J = 3/2$ hypertriton within pionless EFT, since the three particles are still distinguishable, the Efimov effect allows this bound state by construction. However so far such a state has not been observed. Further on a recent analysis with the complex scaling method predicts a virtual state [107]. In the future it would be beneficial to include effective range corrections. In addition, an impact analysis of the two-body scattering lengths and three-body binding energies in four-body hyper-nuclei similar to Ref. [108] would be worthwhile. Moreover, it would be interesting to include the full three-body structure of the hypertriton wave function in coalescence models for production in heavy ion collisions [100, 109]. Finally, one could combine pionless EFT with input from lattice QCD calculations in the $S = -1$ sector [45] to elucidate the structure of hypernuclei at unphysical pion masses [110].

6. The Hypertriton Width

In this chapter we want to focus on the second open question of the hypertriton lifetime. In contrast to the calculation done before, we now include the weak interaction in our systems [1]. This allows decays of the before against the strong interaction stable Λ. In light of the new result of the STAR Collaboration for the binding energy of the hypertriton [8], we attempt to study this highly discussed property of the lifetime of the hypertriton as a function of the binding energy, yet allowing to study possible impacts of a higher binding energy compared to the often used value of $B_\Lambda = 0.13 \pm 0.05$ MeV [5].

In the previous chapter only the breakup into two nucleons and the Λ as well as the deuteron-Λ thresholds were relevant. Allowing the decay of the Λ opens a wide range of relevant thresholds. While the hypertriton is stable against a breakup by strong interaction, the Λ and therefore the hypertriton is unstable against weak interaction with an energy release of about $\Delta - M_\pi \approx 38$ MeV. An overview over the most relevant thresholds is given in Fig. 6.1. We depict the Λ green, the proton red and the neutron blue. The in a Λ weak decay generated pion is depicted yellowish. The pictograms indicate which systems are (still) bound, due to the reference point of a breakup into a Λ, a proton and a neutron. The hypertriton (third pictogram from the right) in this figure is bound according to the binding energy obtained by Juric et al. [5]. Note that the binding energies of the triton and helium are taken with respect to the deuteron threshold. Due to nucleon and pion isospin breaking in the masses, the thresholds involving charged pions and uncharged ones might differ. As already introduced in Ch. 4.1 experimentally the results for the lifetime remain a puzzle. Old emulsion experiments give a very broad range of values for the lifetime [59–64]. Newer heavy ion experiments tended to lie significantly below the free Λ width [48, 54, 55, 57]. Recent results from ALICE yield a lifetime closer to the free Λ width [56].

Theoretical evaluation of the hypertriton started parallel with the experimental results [112, 113]. An intuitive picture is due to the small binding energy of the Λ to the

---

[1] Parts of this chapter are about to be published in the near future. [111]

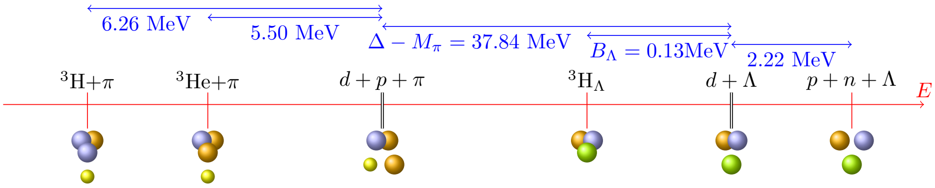

Figure 6.1.: Most relevant thresholds for the hypertriton relative to the deuteron - Λ threshold. The Λ is depicted green, the proton red and the neutron blue. The pion is drawn yellowish. All energies are given in MeV, the figure is not up to scale.

deuteron one of a quasie free Λ. Therefore it is expected that the lifetime is driven by the free width. In the 1990s Congleton calculated the mesonic decays of the hypertriton in a deuteron closure approximation [50][2]. This calculation also hinted that the details of the hypertriton wave function do not seem to be utmost important. Also first Fadeev calculations using realistic potentials were available [114]. Newer approaches try to combine the assets of both calculations [6] discussing the impact of pionic final state interactions. Also the leptonic decays were studied for example in [53, 115], but were found to be suppressed compared to the mesonic ones. Hence the mesonic decays are the important ones to study, we do this in the following calculations taking the recent results on the weak Λ decay parameter α_- [116, 117], having an impact on all properties being evaluated in dependency of this quantity, into consideration.

6.1. Formalism

Since the deuteron is stable, we expect that the lifetime of the hypertriton is mainly determined by the lifetime of the Λ particle and therefore is driven by the free Λ-lifetime. Some measurements of the hypertriton lifetime show a different picture. The lifetime of the hypertriton is significantly shorter than the lifetime of the free Λ. The main decay

---

[2] This means the deutereon is considered to be a fundamental stable particle.

channels are then driven as well by the decay of the Λ and therefore are hadronic. The main decays are

$$\begin{aligned}
&{}^3_\Lambda\mathrm{H} \mapsto \pi^- + {}^3\,\mathrm{He}, &&{}^3_\Lambda\mathrm{H} \mapsto \pi^0 + {}^3\,\mathrm{H},\\
&{}^3_\Lambda\mathrm{H} \mapsto \pi^- + d + p, &&{}^3_\Lambda\mathrm{H} \mapsto \pi^0 + d + n,\\
&{}^3_\Lambda\mathrm{H} \mapsto \pi^- + p + n + p, &&{}^3_\Lambda\mathrm{H} \mapsto \pi^0 + p + n + n.
\end{aligned} \tag{6.1}$$

In the first channels of Eq. (6.1) no breakup of the three-body nucleus takes place. Going down from top to bottom more and more breakups are taken into consideration. Since the deuteron is stable, the deuteron breakup processes are suppressed compared to the other ones [114]. It is therefore reasonable to treat the deuteron as a stable particle, since it is unlikely to resolve this puzzle. As already discussed in the introduction about hyper nuclear physics in heavier hypernuclei these decays are often Pauli blocked and therefore not accessible, these channels are open for the three-body case and the main decays [52]. Note that like for the case of the free Λ decay leptonic processes are suppressed, theoretical analyses predict that they make up for roughly 1.5% of the total free Λ decay rate [53, 115]. Experimentally these decay rates cannot be separated. Note that the charged channels (π^- channels) and the neutral channels (π^0 channels) are not independent but connected via the empirical $\Delta I = 1/2$ rule as discussed in Ch. 3.2, setting the ratio of the channels in Eq. (6.1) line for line equal to 2. We construct the hypertriton in leading order S-Wave pionless EFT out of a deuteron propagator and a Λ particle. The typical momenta are small compared to the pion mass for the interaction of nucleons and the Λ [81]. The pion in the outgoing state is included with relativistic kinematics due to the high energy release at the weak vertex of $\frac{M_\Lambda - m - M_\pi}{M_\pi} \approx 26\%$ of the pion mass. Note that the prescription used here is different from the one used by Schmidt et al. [118] which was used to calculate a strong decay non-perturbatively. However, we treat the weak interaction in perturbative manner. Hence we include the weak breakup only once, instead of including infinite bubble sums.

6.1.1. Fixing the Weak Interaction

Since the main decay channels of the hypertriton are driven by the Λ decay, we use the free Λ to fix the weak interaction within our theory. From textbook physics it is known that the non-leptonic decay matrix element can be written as

$$\mathcal{M}_{\Lambda\mapsto N\pi} = i\sqrt{2} G_F M_\pi^2 \bar{u}\left(\boldsymbol{p}'\right)\left[\tilde{A}_\pi + \tilde{B}_\pi \gamma_5\right] u\left(\boldsymbol{p}\right), \tag{6.2}$$

where due to the parity of the pion $\tilde{A}_\pi$ is the parity violating (PV) amplitude while $\tilde{B}_\pi$ is the parity conserving (PC), see also Ch. 3.2. The factor $\sqrt{2}$ is an isospin factor selecting the proton channel. The respective factor for the neutron is -1. The coupling strength is encoded in the Fermi constant $G_F = 1.1664 \times 10^{-5}\mathrm{GeV}^{-2}$ [7]. Due to this correlation we will calculate only the charged width from now on and then relate via the isospin correlation to the uncharged one. For an analysis of this approximation see also Sec. 6.4. In case of the hypertriton, due to the small binding momentum, it is sufficient to treat the baryons non-relativistically. Therefore it is reasonable to reduce this matrix element, leading to

$$\mathcal{W}(\boldsymbol{k}) = \mathcal{M}^{\text{reduced}}_{\Lambda\mapsto N\pi} = i\sqrt{2}G_F M_\pi^2 \left(A_\pi + \frac{B_\pi}{M_\Lambda + m}\boldsymbol{\sigma}\cdot\boldsymbol{k}\right), \tag{6.3}$$

with $\boldsymbol{k}$ the momentum of the pion and $\boldsymbol{\sigma}$ the usual Pauli matrices, see also [53, 114]. We modified the amplitudes in such a way that they absorb normalization constants. It is now straight forward to calculate the free width of the Λ, according to the diagram given in Fig.6.2

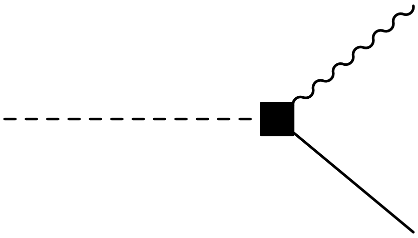

Figure 6.2.: Free decay of the Λ. The Λ is depicted dashed, the nucleon plain (momentum $\boldsymbol{p}$) and the pion by a wiggly line (momentum $\boldsymbol{k}$). The weak decay operator $\mathcal{W}$ is given by the black box.

$$\Gamma^{\mathrm{c}}_\Lambda = \int \frac{\mathrm{d}^3k}{(2\pi)^3}\frac{\mathrm{d}^3p}{(2\pi)^3}\frac{1}{2\omega(k)}(2\pi)^4\,\delta^{(3)}(\boldsymbol{p}+\boldsymbol{k})\,\delta\left(\Delta - \omega(k) - \frac{p^2}{2m}\right)\frac{1}{2}\sum_{m_\Lambda, m_p}|\mathcal{W}(k)|^2, \tag{6.4}$$

with $\omega = \sqrt{M_\pi + k^2}$ the relativistic energy of the pion and $\Delta = M_\Lambda - m$ the baryon mass difference, which is released at the weak vertex $\mathcal{W}(\boldsymbol{k})$ together with the energy of the pion. The upper index c denotes that we only give the width for the charged channel. The δ functions fix the momentum of the outgoing pion to be

$$k = \bar{k} = \sqrt{2}\sqrt{-\sqrt{m^2\left(m^2 + 2\Delta m + M_\pi^2\right)} + m^2 + \Delta m}. \tag{6.5}$$

At first glance, we would expect a possible mixing of the amplitudes A_π and B_π, however, the Pauli matrices are traceless, therefore we obtain for the sum

$$\sum_{m_\Lambda, m_p} |\mathcal{W}(k)|^2 = \sum_{m_\Lambda, m_p} \left| i\sqrt{2} G_F M_\pi^2 \left(A_\pi + \frac{B_\pi}{M_\Lambda + m} \boldsymbol{\sigma} \cdot \boldsymbol{k} \right)_{m_p, m_\Lambda} \right|^2 \tag{6.6}$$

$$= 4 G_f^2 m_\pi^4 \left(A_\pi^2 + \left(\frac{B_\pi}{M_\Lambda + m} \right)^2 k^2 \right), \tag{6.7}$$

where we used that the product $\sigma_i \sigma_j = \delta_{ij}\sigma_0 + i\varepsilon_{ijk}\sigma_k$ for $i, j, k \in \{1, 2, 3\}$. Hence the non-mixing is a direct result of the tracelessness of the Pauli matrix σ_k. The resulting width of the free Λ decay is therefore given by

$$\Gamma_\Lambda^p = \frac{G_F^2 M_\pi^4}{2\pi} \frac{m\bar{k}}{m + \omega\left(\bar{k}\right)} \left(A_\pi + \left(\frac{B_\pi}{M_\Lambda + m} \right)^2 \bar{k}^2 \right). \tag{6.8}$$

Like introduced in Ch.2, there is a second way to obtain the same result. We therefore

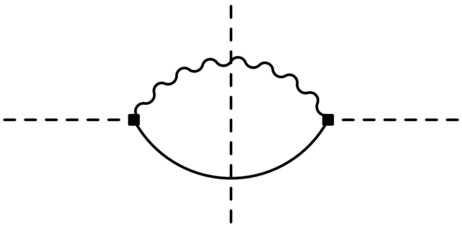

Figure 6.3.: Cut necessary to calculate the imaginary part for the free Λ decay, the optical theorem relates this diagram to the cross section.

need to calculate the cuts of the diagram depicted in Fig. 6.3. Applying the weak operator as introduced before, the diagram without the cut is given by the expression

$$D = \int \frac{\mathrm{d}^4 q}{(2\pi)^4} \frac{i}{\Delta - q_0 - \frac{q^2}{2m} + i\epsilon} \frac{i}{q_0^2 - q^2 - M_\pi^2 + i\epsilon} \mathcal{W}\left(q\right) \mathcal{W}^*\left(q\right), \tag{6.9}$$

where the pion is now explicitly included in the theory as a relativistic particle, since we expect it to obtain up to $\approx 26\%$ of its rest mass as energy when going on shell. The discontinuity Disc (D) of the diagram is given by the cut through the propagators within the loop. According to the cutting rules, see Ch. 2.5.3, we need to replace the propagators with the corresponding δ functions.

$$\begin{aligned} \text{Disc}\left(D\right) = &- \left(-2\pi i\right)^2 \int \frac{\mathrm{d}^4 q}{(2\pi)^4} \left(\Delta - q_0 - \frac{q^2}{2m}\right) \delta\left(q_0^2 - q^2 - M_\pi^2\right) \\ &\times \mathcal{W}\left(q\right) \mathcal{W}^*\left(q\right) \end{aligned} \tag{6.10}$$

Evaluating now the δ function resulting from the relativistic pion propagator and already neglecting terms that cannot contribute due to the second δ function yields

$$\not{D} = 2\pi \int \frac{\mathrm{d}^3 q}{(2\pi)^3} \left(\Delta - \omega\left(q\right) - \frac{q^2}{2m}\right) \frac{1}{2\omega\left(q\right)} \mathcal{W}\left(q\right) \mathcal{W}^*\left(q\right). \tag{6.11}$$

Averaging over the result, directly returns the result of Eq. (6.8) after performing the momentum δ function there. Note that the m_p sum is internal in the case here and therefore not explicitly written down. The δ function obtained by applying the cutting rules therefore reconstruct the energy conservation δ function of the phase space. The momentum δ function conveniently is automatically fulfilled due to the same outgoing states.

We can now use the empiric isospin rule to connect the charged channel to the total free width Γ_Λ. The to Γ_Λ associated lifetime $\tau_\Lambda = 263 \pm 2$ ps is established experimentally very well [7]. We use this observable together with the polarization of the Λ

$$P_\Lambda = \frac{\frac{A_\pi B_\pi}{M_\Lambda + m} \bar{k}}{A_\pi^2 + \left(\frac{B_\pi}{M_\Lambda + m}\right)^2 \bar{k}^2} = \frac{\alpha_-}{2}, \tag{6.12}$$

hence the Λ decay parameter α_- to fix the weak interaction strength. Up to 2018 the widely accepted value was $\alpha_-^{2018} = 0.642 \pm 0.013$, but new results from the BESIII Collaboration suggest a significantly higher value $\alpha_-^{\mathrm{BESIII}} = 0.750 \pm 0.009 \pm 0.004$ [116]. Also an independent estimation out of kaon-photo production suggests a value of $\alpha_-^{\mathrm{KP}} = 0.721 \pm 0.006 \pm 0.005$ [117] close to the results of BESIII. The results for the PC and PV amplitudes A_π and B_π are depicted in Fig. 6.4.

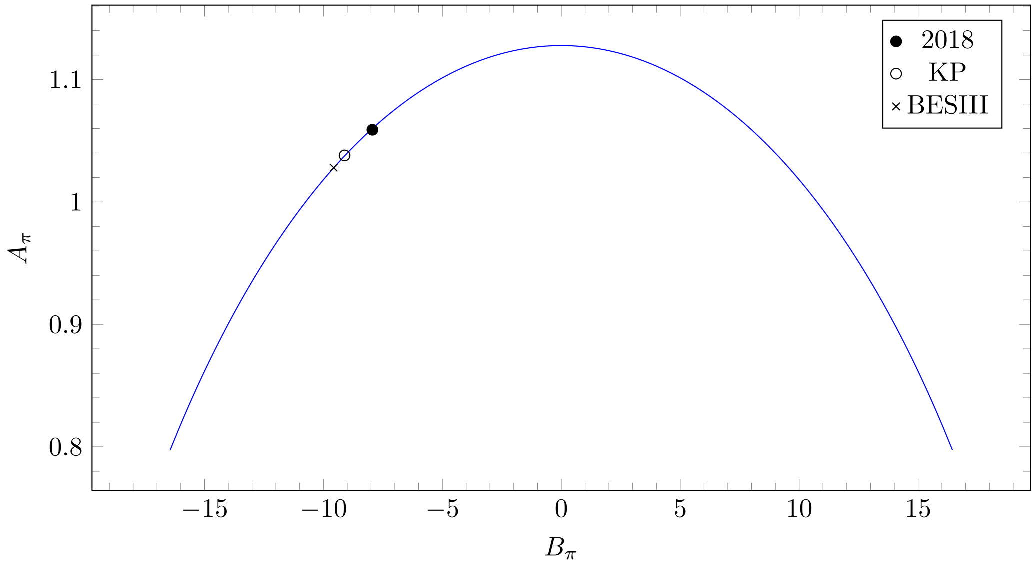

Figure 6.4.: Amplitudes A_π and B_π as a parameter plot of the Λ decay parameter $-1 \leq \alpha_- \leq 1$ as of Eq. (6.8) and Eq. (6.12). Different results for α_- given by singular markers.

6.1.2. Hypertriton as Two-Body System

Since we neglect the deuteron breakup into two singular nucleons, the hypertriton can be effectively described as a two-body bound state of a Λ and a deuteron. As shown previously, the typical momentum scale is low and therefore a non-relativistic treatment of all baryons is sufficient. Hence single particle propagators are given by

$$iS_{d,\Lambda,n}\left(p_0, \boldsymbol{p}\right) = \frac{i}{p_0 - \frac{\boldsymbol{p}^2}{2M_i} + i\epsilon}, \tag{6.13}$$

with M_i the respective particle masses of the deuteron and the Λ, and $M_N \equiv m$ the nucleon mass. Evaluating the typical geometric series depicted in Fig. 6.5 at the pole, we obtain the typical result for the effective field theory wave function renormalization $Z(B_\Lambda) = \frac{2\pi}{\mu_{\Lambda d} g^2}\sqrt{2\mu_{\Lambda d} B_\Lambda}$ with B_Λ the deuteron-Λ binding energy [11]. The full propagator of such a dimer field reads:

$$iD_{{}^3_\Lambda\text{H}}\left(p_0,\boldsymbol{p}\right) = \frac{2\pi}{\mu_{\Lambda d}g^2}\frac{-i}{-{}^3\gamma_\Lambda + \sqrt{-2\mu_{\Lambda d}\left(p_0 - \frac{\boldsymbol{p}^2}{2M_\Lambda+M_d} + i\epsilon\right)}}. \tag{6.14}$$

In the following sections we now calculate the decay of such a bound dimer.

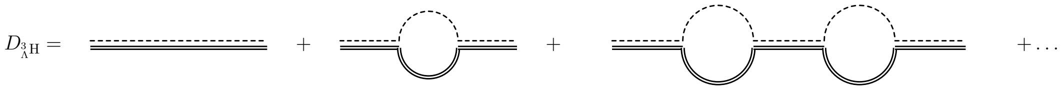

Figure 6.5.: Hypertriton dimer build as geometric series from the deuteron (double line) and the Λ

6.2. Nd Channels

The main contribution of the hypertriton binding energy for small binding energies is expected to come from the nucleon-deuteron channels, since in the limit of vanishing binding energy, we expect all other channels to close. To be precise, in the limit $\lim_{B_\Lambda\mapsto 0}\Gamma\left({}^3_\Lambda\text{H}\mapsto \cancel{\pi^{-/0}+N+d}\right)\mapsto 0$ because the outgoing states do not correspond to those of a free Λ. Therefore we need to retrieve the free Λ width for $B_\Lambda \mapsto 0$ from the Nd channels[3]. At leading order a diagram with and without a final state interaction between the decay nucleon and the deuteron contribute, see also Fig. 6.6. We neglect pionic final state interaction at leading order, since the energy of the decay pions is expected to be high. A recent calculation by Gal et al. shows that they may change the result by up to 6% of the free Λ width [6]. The final state interaction between the outgoing particles in the $S = 1/2$ channel is described by a standard two-body scattering amplitude

$$\mathcal{A}\left(E\right) = \frac{2\pi}{\mu_{\text{Nd}}}\left[-\frac{1}{a} + \sqrt{-2\mu_{\text{Nd}}E - i\epsilon}\right]^{-1}, \tag{6.15}$$

as for example introduced in [11]. We tuned the interaction strength in such a manner that the correct ^{3}He binding energy $B_{{}^3\text{He}}$ with respect to the $d{-}p$ threshold is reproduced.

---

[3] In the case of allowing the deuteron breakup, decays into three nucleons contribute at threshold as well.

To be more precise, the binding energy relative to the deuteron nucleon threshold is indicated as in Fig. 6.1. The resulting binding scattering length can then be calculated by the relations introduced in Ch. 2. We obtain

$$a = \frac{1}{\sqrt{2\mu_{\mathrm{Nd}} B_{^3\mathrm{He}}}} = 2.38\ \mathrm{fm}. \tag{6.16}$$

Utilizing the momentum δ function at once, the width Γ_{Nd} is given by

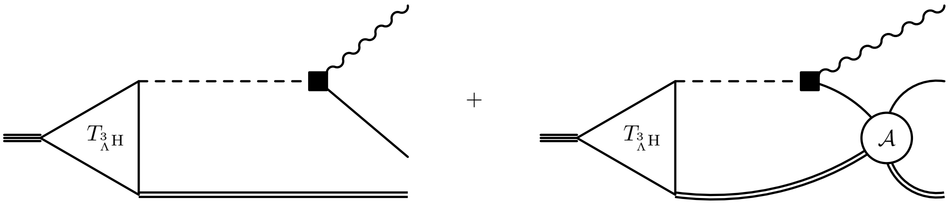

Figure 6.6.: Decaying hypertriton, the amplitude $\mathcal{A}$ depicts the final state interaction between the decay nucleon and the deuteron. The left diagram including no final state interaction is labeled $\mathcal{M}_{\mathrm{Nd}}$, the right one including final state interaction in the $S = 1/2$ channel $\mathcal{M}_{\mathrm{Nd}}^{\mathrm{FSI}}$

$$\begin{aligned}\Gamma_{\mathrm{Nd}} =& 2\pi \int\int \frac{\mathrm{d}^3 p}{(2\pi)^3} \frac{\mathrm{d}^3 k}{(2\pi)^3} \frac{1}{2\omega(k)} \frac{1}{2} \sum_{m_d, m_N, m_{^3_\Lambda\mathrm{H}}} \left|\mathcal{M}\left(^3_\Lambda\mathrm{H} \mapsto \pi\mathrm{Nd}\right)\right|^2 \\ & \times \delta\left(\Delta - B_\Lambda - \omega(k) - \frac{p^2}{2M_d} - \frac{(\boldsymbol{k}+\boldsymbol{p})^2}{2m}\right),\end{aligned} \tag{6.17}$$

with $\boldsymbol{k}$ the outgoing pion momentum and $\boldsymbol{p}$ the deuteron momentum. The matrix element is a sum of both diagrams from Fig 6.6 $\mathcal{M}\left(^3_\Lambda\mathrm{H} \mapsto \pi\mathrm{Nd}\right) = \mathcal{M}_{\mathrm{Nd}} + \mathcal{M}_{\mathrm{Nd}}^{\mathrm{FSI}}$.

6.2.1. The $B_\Lambda \mapsto 0$ Limit

Calculating the width in the limit $B_\Lambda \mapsto 0$ tends to be numerically difficult, since the propagator as well as the wave function normalization go to zero in this limit. Therefore the width itself becomes numerically unstable. However, we can evaluate this limit analytically. We will indeed show that the result is the one one would naively expect, the free Λ width. That the limit $B_\Lambda \mapsto 0$ is indeed fulfilled can be seen most easily by neglecting the final state interaction, the calculation including final state interactions is similar, but more oblong. The matrix element $\mathcal{M}_{\mathrm{Nd}}$ is then given by

$$\mathcal{M}_{\mathrm{Nd}}\left(\boldsymbol{k},\boldsymbol{p}\right) = g\sqrt{Z}S_\Lambda\left(-B_\Lambda - \frac{p^2}{2M_d}, -\boldsymbol{p}\right)\mathcal{W}\left(\boldsymbol{k}\right), \tag{6.18}$$

It is insightful to calculate the wave function normalization of the dimer, which we can write as

$$\begin{aligned} 1 =& \int \frac{\mathrm{d}^3 q}{(2\pi)^3}\left|g\sqrt{Z}\right|^2\left(\frac{1}{B_0 + \frac{q^2}{2\mu_{\Lambda d}}}\right)^2 \\ =& \frac{8\pi\mu_{\Lambda d}}{(2\pi)^3}\int \mathrm{d}q\left|g\sqrt{Z}\right|^2\left(\frac{q}{B_0 + \frac{q^2}{2\mu_{\Lambda d}}}\right)^2 \end{aligned} \tag{6.19}$$

Evaluating now the limit $\lim\limits_{B_\Lambda \mapsto 0}\Gamma_{\mathrm{Nd}}$ we obtain

$$\begin{aligned} \lim_{B_\Lambda \mapsto 0}\Gamma_{\mathrm{Nd}} = \lim_{B_\Lambda \mapsto 0} 2\pi \int\int \frac{\mathrm{d}^3 p}{(2\pi)^3}\frac{\mathrm{d}^3 k}{(2\pi)^3}\frac{1}{2\omega\left(k\right)}\left|\mathcal{M}_{\mathrm{Nd}}\right|^2 \\ \times\,\delta\left(\Delta - B_\Lambda - \omega\left(k\right) - \frac{p^2}{2M_d} - \frac{\left(\boldsymbol{k}+\boldsymbol{p}\right)^2}{2m}\right). \end{aligned} \tag{6.20}$$

Inserting now the Λ propagator S_Λ as matrix element yields

$$\begin{aligned} \lim_{B_\Lambda \mapsto 0}\Gamma_{\mathrm{Nd}} = \lim_{B_\Lambda \mapsto 0} 2\pi \int\int \frac{\mathrm{d}^3 p}{(2\pi)^3}\frac{\mathrm{d}^3 k}{(2\pi)^3}\frac{1}{2\omega\left(k\right)}\left|\frac{g\sqrt{Z\left(B_\Lambda\right)}}{-B_\Lambda - \frac{p^2}{2\mu}}\mathcal{W}\left(\boldsymbol{k}\right)\right|^2 \\ \times\,\delta\left(\Delta - B_\Lambda - \omega\left(k\right) - \frac{p^2}{2M_d} - \frac{\left(\boldsymbol{k}+\boldsymbol{p}\right)^2}{2m}\right). \end{aligned} \tag{6.21}$$

Swapping now the limit $B_\Lambda \mapsto 0$ with the integrations and utilizing the calculated waveform normalization we obtain a Dirac series, which reduces our expression to

$$\begin{aligned}\lim_{B_\Lambda \mapsto 0} \Gamma_{\text{Nd}} =& 2\pi \int\int \frac{\mathrm{d}^3 p}{(2\pi)^3} \frac{\mathrm{d}^3 k}{(2\pi)^3} \frac{(2\pi)^3 \delta(\boldsymbol{p})}{2\omega(k)} |\mathcal{W}(\boldsymbol{k})|^2 \\ & \times \delta\left(\Delta - \omega(k) - \frac{p^2}{2M_d} - \frac{(\boldsymbol{k}+\boldsymbol{p})^2}{2m}\right) \end{aligned} \tag{6.22}$$

$$=2\pi \int \frac{\mathrm{d}^3 k}{(2\pi)^3} |\mathcal{W}(\boldsymbol{k})|^2 \frac{1}{2\omega(k)} \delta\left(\Delta - \omega(k) - \frac{\boldsymbol{k}^2}{2m}\right), \tag{6.23}$$

which is the expression for $\Gamma_\Lambda^{\text{p}}$ given in Eq. (6.4) after evaluating the sum and the momentum delta function and hence $\lim\limits_{B_\Lambda \mapsto 0} \Gamma_{\text{Nd}} = \Gamma_\Lambda$. In principle we should also check that the other limit for a hypertriton bound deeper than Δ results in an infinite lifetime, however, this is trivial since the energy delta function would never be fulfilled and hence $\Gamma_{{}^3_\Lambda\text{H}} \mapsto 0$.

6.2.2. Arbitrary B_Λ

In the following part we move away from the limit $B_\Lambda \mapsto 0$ and start including final state interaction. We will therefore start with evaluating and analyzing the structure of the matrix element, before we will shift our focus on the evaluation of the phase space integral.

6.2.2.1. Structure of the Matrix Element

Including now final state interactions and moving away from the limit $B_\Lambda \mapsto 0$ the scalar part of the matrix element $\mathcal{M}_{\text{Nd}}^{\text{FSI}}$ reads

$$\begin{aligned} {}^S\mathcal{M}_{\text{Nd}}^{\text{FSI}} =& \underbrace{i \int \frac{\mathrm{d}^4 q}{(2\pi)^4} S_\Lambda(q_0, \boldsymbol{q}) S_d(-B_\Lambda - q_0, -\boldsymbol{q}) S_N(\Delta + q_0 - \omega(k), \boldsymbol{q} - \boldsymbol{k})}_{=I_q(k, B_\Lambda)} \\ & \times \mathcal{A}\left(\Delta - B_\Lambda - \omega(k) - \frac{k^2}{2M}\right) \sqrt{Z(B_\Lambda)} \mathcal{W}(\boldsymbol{k}). \end{aligned} \tag{6.24}$$

The energy shift in the amplitude $\mathcal{A}$ occurs due to the transformation of the center of mass frame of the nd system, which is shifted by the pion momentum compared to the incoming state. Therefore it is denoted by $-k^2/(2M)$ with M the total mass of the nd system.

Now we need to spend some time for evaluating the loop integral $I_q\left(k, B_\Lambda\right)$. Due to the energy release at the weak vertex the nucleon propagator S_N has now up to two poles in the $\boldsymbol{q}$ loop momentum integration depending on the angle between the outgoing pion momentum $\boldsymbol{k}$ and $\boldsymbol{q}$. We end up with the following expression

$$
\begin{aligned}
I_q\left(k, B_\Lambda\right) = & \frac{2}{(2\pi)^2} \int \mathrm{d}q \, \frac{m\mu_{d\Lambda} q}{k} \log\left[\frac{B_\Lambda + \frac{q^2}{2\mu_{d\Lambda}} - \frac{\mu_{\mathrm{Nd}} qk}{m\mu_{d\Lambda}} + \frac{\mu_{\mathrm{Nd}}^2}{2m^2\mu_{d\Lambda}^2} k^2}{B_\Lambda + \frac{q^2}{2\mu_{d\Lambda}} + \frac{\mu_{\mathrm{Nd}} qk}{m\mu_{d\Lambda}} + \frac{\mu_{\mathrm{Nd}}^2}{2m^2\mu_{d\Lambda}^2} k^2}\right] \\
& \times \frac{1}{q+\bar{q}} \frac{1}{q-\bar{q}}
\end{aligned}
\tag{6.25}
$$

with

$$
\bar{q} = \frac{1}{m}\sqrt{\mu_{dN}\left(-2m^2\left(B_\Lambda + \omega\left(k\right) - \Delta\right) + k^2\left(\mu_{dN} - m\right)\right)},
\tag{6.26}
$$

for more details see also App. E.2. This integral can then be evaluated by utilizing the principal value method, see also App. B.2. We obtain the following result

$$
\begin{aligned}
I_q\left(k, B_\Lambda\right) = & \frac{2}{(2\pi)^2} \int \mathrm{d}q \, \mathcal{P} \frac{m\mu_{d\Lambda} q}{k} \log\left[\frac{B_\Lambda + \frac{q^2}{2\mu_{d\Lambda}} - \frac{\mu_{nd} qk}{m\mu_{d\Lambda}} + \frac{\mu_{dn}^2}{2m^2\mu_{d\Lambda}^2} k^2}{B_\Lambda + \frac{q^2}{2\mu_{d\Lambda}} + \frac{\mu_{nd} qk}{m\mu_{d\Lambda}} + \frac{\mu_{dn}^2}{2m^2\mu_{d\Lambda}^2} k^2}\right] \frac{1}{q+\bar{q}} \frac{1}{q-\bar{q}} \\
& - \frac{2i\pi}{(2\pi)^2} \int \mathrm{d}q \, \frac{m\mu_{d\Lambda} q}{k} \log\left[\frac{B_\Lambda + \frac{q^2}{2\mu_{d\Lambda}} - \frac{\mu_{nd} qk}{m\mu_{d\Lambda}} + \frac{\mu_{dn}^2}{2m^2\mu_{d\Lambda}^2} k^2}{B_\Lambda + \frac{q^2}{2\mu_{d\Lambda}} + \frac{\mu_{nd} qk}{m\mu_{d\Lambda}} + \frac{\mu_{dn}^2}{2m^2\mu_{d\Lambda}^2} k^2}\right] \frac{\delta\left(q-\bar{q}\right)}{q+\bar{q}}.
\end{aligned}
\tag{6.27}
$$

The k dependent pole structure of this in principle leads to a kink in the partial decay with $\frac{\mathrm{d}\Gamma_{\mathrm{Nd}}}{\mathrm{d}k_\pi}$ at the point where $\bar{q}$ starts becoming imaginary and therefore the imaginary part vanishes, since there is no pole any longer in $I_q\left(k, B_\Lambda\right)$. Remarkably, since the integral is connected to the structure of the phase space, this point $k_{\bar{q}=0} = k_{max}$, the maximum value for k. We will derive this point in our phase space analysis in the next section. For an explicit value of k_{max} see also App. E.3. Since we are interested in the total cross section we need to evaluate the absolute value square of the diagrams depicted in Fig. 6.6. Hence the two diagrams $\mathcal{M}_{\mathrm{Nd}}^{\mathrm{FSI}}$ and $\mathcal{M}_{\mathrm{Nd}}$ show a rich interference pattern. This becomes imminently clear when evaluating the sum. For the averaged sum of all incoming states m_i and sum over all outgoing states m_f we obtain

$$\begin{aligned}
\frac{1}{2J+1}\sum_{m_{i,f}}\left|\mathcal{M}_{\mathrm{Nd}}^{\mathrm{tot}}\right|^2 =& \frac{1}{2J+1}\sum_{m_d,m_N,m_{{}^3_\Lambda\mathrm{H}}}\left|\mathcal{M}_{\mathrm{Nd}}^{\mathrm{FSI}}+\mathcal{M}_{\mathrm{Nd}}\right|^2 \\
=& \frac{A_\pi^2}{2}\left|{}^S\mathcal{M}_{\mathrm{Nd}}+{}^S\mathcal{M}_{\mathrm{Nd}}^{\mathrm{FSI}}\right|^2+\frac{1}{2}\frac{1}{9}\left(\frac{B_\pi k}{M_\Lambda+m}\right)^2 \\
&\times\left[9\left|{}^S\mathcal{M}_{\mathrm{Nd}}\right|^2+\left|{}^S\mathcal{M}_{\mathrm{Nd}}^{\mathrm{FSI}}\right|^2+2\,\mathrm{Re}\left\{{}^S\mathcal{M}_{\mathrm{Nd}}\left({}^S\mathcal{M}_{\mathrm{Nd}}^{\mathrm{FSI}}\right)^*\right\}\right],
\end{aligned} \tag{6.28}$$

where the left upper index S stands for the scalar part of the matrix element as for example given in Eq. (6.24). For further details see also App. E.1. We can observe that there is still no mixing between parity violating and parity conserving parts due to the structure of the weak vertex in terms of Pauli matrices.

6.2.2.2. Phase Space Evaluation

The evaluation of the phase space restricts the allowed momenta due the energy delta function in Eq. 6.17 depending on the angle between $\boldsymbol{k}$ and $\boldsymbol{p}$. Since the matrix element only depends on absolute values of the momenta $\boldsymbol{k}$ and $\boldsymbol{p}$, we can calculate this integral independently from the matrix element. We need to evaluate

$$\int_{-1}^{1}\mathrm{d}x\,\delta\left(\Delta-B_\Lambda-\omega\left(k\right)-\frac{p^2}{2M_d}-\frac{k^2}{2m}-\frac{p^2}{2m}-\frac{pkx}{m}\right). \tag{6.29}$$

Evaluating this angular integration between $\boldsymbol{k}$ and $\boldsymbol{p}$ leaves two heaviside step functions Θ behind, restricting the area of integration. The phase space reads

$$\rho\left(k,p\right)=\frac{mkp}{\omega\left(k\right)}\left[\Theta\left(\phi^+\left(k,p\right)\right)-\Theta\left(\phi^-\left(k,p\right)\right)\right] \quad \text{with} \tag{6.30}$$

$$\phi^\pm\left(k,p\right)=\frac{k^2}{m}\pm\frac{2kp}{m}+\frac{p^2}{\mu_{\mathrm{Nd}}}+2\left(B_\Lambda+\omega\left(k\right)-\Delta\right) \tag{6.31}$$

so that

$$\Gamma_{\mathrm{Nd}}=\frac{1}{\left(2\pi\right)^3}\int\!\!\int\mathrm{d}p\,\mathrm{d}k\,\rho\left(k,p\right)\frac{1}{2}\sum_{m_d,m_N,m_{{}^3_\Lambda\mathrm{H}}}\left|\mathcal{M}\left({}^3_\Lambda\mathrm{H}\mapsto\pi\mathrm{Nd}\right)\right|^2. \tag{6.32}$$

The structure of this phase space can be analyzed in the momentum as well as in the energy plane, while the first one is useful for calculations, the energy distribution gives us an easier understanding of the kinematics involved. Since we already eliminated the explicit dependence on the kinetic energy of the nucleon, which can be recovered out of the other two, we choose to plot this in the T_d-T_π plane with $T_d = p^2/(2M_d)$ and $T_\pi = \omega(k) - M_\pi = \sqrt{M_\pi + k^2} - M_\pi$, the result is depicted in Fig. 6.7. The allowed kinetic energies are within the blue circle. We can directly see that the kinetic energies of the pion are high compared to the rest mass of the particle. For the deuteron, however, this is not the case. This confirms that our treatment of the pion as an relativistic particle is reasonable, while a non-relativistic implementation for the baryons is sufficient. Therefore the favored momenta in the ellipse tends to lie at high pion momenta. We will see later that the main contribution to this channel is indeed coming from high pion momenta, which is not very surprising since the fixed pion momentum of the free decay is also high, and the hypertriton is only shallowly bound. Although it might be more direct and efficient to calculate the integral over the Heaviside function directly, it is quite insightful to study the momentum dependence in the right plot of Fig.6.7. Not only does it give a very good overview over the actual limits of integration for a numeric

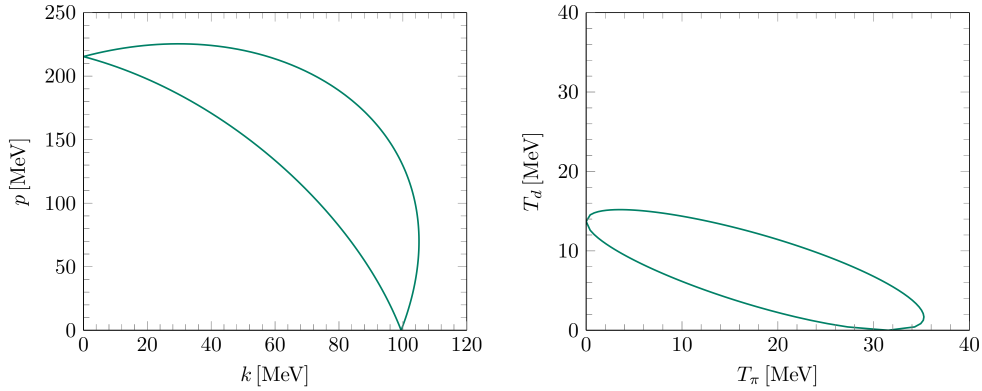

Figure 6.7.: Allowed momenta and kinetic energies in the T_d-T_π plane. The phase space density only allows momenta or kinetic energy combination that are within the curves. Note: the kinetic energy of the nucleon can be reconstructed out of the other two.

implementation, which comes in handy, but also allows us to rewrite the integral. There are two distinguished points. The maximum allowed value for k, k_{max}, and the point k_0 where $p\left(k_0\right)=0$. In order to integrate over this area we need to split up the integration for the upper limit associated with ϕ^-. Labeling the rest of the integrand $f\left(k,p\right)$, we obtain

$$\begin{aligned}\int\int \mathrm{d}k\,\mathrm{d}p\,f\left(k,p\right)\Theta\left(\phi^-\right)\mapsto&\int_0^{k_{max}}\mathrm{d}k\int_0^{p_+^-(k)}\mathrm{d}p\,f\left(k,p\right)\\&-\int_{k_0}^{k_{max}}\mathrm{d}k\int_0^{p_-^-(k)}\mathrm{d}p\,f\left(k,p\right),\end{aligned}\tag{6.33}$$

where $p_\pm^-\left(k\right)$ is the parametrization of the upper part of the integration border. Since both are solutions of ϕ^- with respect to p, they have the form $p_\pm^-\left(k\right)=a\left(k\right)\pm\sqrt{b\left(k\right)}$. For the lower limit no split-up is needed, therefore we obtain for the full integral with $p_+^+\left(k\right)$ the paremtrization of the lower limit

$$\begin{aligned}\int\int \mathrm{d}k\,\mathrm{d}p\,f\left(k,p\right)\left(\Theta\left(\phi^-\right)-\Theta\left(\phi^+\right)\right)=&\int_0^{k_{max}}\mathrm{d}k\int_0^{p_+^-(k)}\mathrm{d}p\,f\left(k,p\right)\\&-\int_{k_0}^{k_{max}}\mathrm{d}k\int_0^{p_-^-(k)}\mathrm{d}p\,f\left(k,p\right)\\&-\int_0^{k_0}\mathrm{d}k\int_0^{p_+^+(k)}\mathrm{d}p\,f\left(k,p\right).\end{aligned}\tag{6.34}$$

Due to the plus-minus structure of $\phi^\pm$ we find, however, that $p_+^+\left(k\right)=-q_-^-$, which allows us to directly connect the upper limit with the lower limit of integration, this simplifies the integration. Indeed we can even simplify this expression even further as long as the primitive function of $f\left(k,p\right)$ is invariant under the transition $k\mapsto -k$ as for example in the case for vanishing final state interactions.

$$\int\int \mathrm{d}k\,\mathrm{d}p\,f\left(k,p\right)\left(\Theta\left(\phi^--\Theta\left(\phi^+\right)\right)\right)=\int_0^{k_{max}}\mathrm{d}k\int_{p_-^-(k)}^{p_+^-(k)}\mathrm{d}p\,f\left(k,p\right)\tag{6.35}$$

In principle a similar expression can be obtained by swapping the k and the p integration. Explicit expressions for the borders of integration are given in App. E.3

6.3. Helium/Triton Channel

In this channel, as we are neglecting pionic final state interactions, only one diagram is contributing to the width, depicted in Fig. 6.8. As in the case for the free Λ, the outgoing momentum of the pion is fixed, therefore the $\Gamma_{^3\mathrm{He}}$ phase space looks similar to the free one

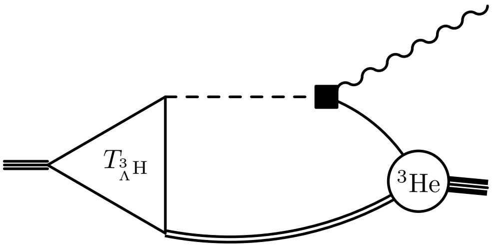

Figure 6.8.: Diagram contributing to the hypertriton width with an outgoing ^{3}He state. A similar diagram with an outgoing triton exists in the neutral decay channel.

$$\begin{aligned}\Gamma_{^3\mathrm{He}} =& \int\int \frac{\mathrm{d}^3p}{(2\pi)^3}\frac{\mathrm{d}^3k}{(2\pi)^3}\frac{1}{2\omega(k)}\frac{1}{2} \\ &\times \sum_{m_{^3\mathrm{He}},m_{^3_\Lambda\mathrm{H}}} \left|\mathcal{M}_{^3\mathrm{He}}\right|^2 (2\pi)^4 \delta^{(3)}(\boldsymbol{p}+\boldsymbol{k})\,\delta\left(\Delta - \omega(k) - \frac{p^2}{2M_{^3\mathrm{He}}}\right),\end{aligned} \tag{6.36}$$

with $\Delta = M_{^3_\Lambda\mathrm{H}} - M_{^3\mathrm{He}}$ and $\boldsymbol{p}$ is now the momentum of the outgoing ^{3}He nucleus. $Z_{^3\mathrm{He}}$ is the ^{3}He wave function renormalization, constructed in a similar way to the hypertriton one. In fact we can reuse the calculation for the phase space from the free Λ width together with the loop analysis done before for the Nd case. We obtain

$$\begin{aligned}\Gamma_{^3\mathrm{He}} =& \frac{G_F^2 M_\pi^4}{2\pi}\frac{\bar{k}m_{^3\mathrm{He}}}{m_{^3\mathrm{He}}+\omega(\bar{k})} Z(B_\Lambda)\,Z_{^3\mathrm{He}} \\ &\times (B_{^3\mathrm{He}})\left(A_\pi^2 + \frac{1}{9}\left(\frac{B_\pi}{M_\Lambda + m}\right)^2 \bar{k}^2\right)\left|I_q(\bar{k},B_\Lambda)\right|^2.\end{aligned} \tag{6.37}$$

Using pure relativistic kinematics, we can fix the momentum of the outgoing pion to be

$$\bar{k} = \frac{\sqrt{\left(M^2_{{}^3_\Lambda\mathrm{H}} + M^2_{{}^3\mathrm{He}} - M^2_\pi\right)^2 - 4M^2_{{}^3_\Lambda\mathrm{H}}M^2_{{}^3\mathrm{He}}}}{2M_{{}^3_\Lambda\mathrm{H}}}. \tag{6.38}$$

Note that the difference of using relativistic kinematics compared to semi-relativistic kinematics are negligibly small, however the representation is much more compact in a relativistic framework.

6.4. Results

Now, we discuss the results of our calculations for the hypertriton width. We start our evaluation utilizing the empiric isospin rule relating the charged and the uncharged channel. Further on we will discuss corrections to our calculations.

6.4.1. Results with Isospin Rule

In our calculation we use the lifetime and Λ decay parameter to calculate the values for A_π and B_π according to Ch. 6.1.1, these are given in Tab. 6.1. We perform the remaining momentum integrals numerically, thereby we exploit the correlation between charged and uncharged decay channels. The importance of final state interaction can be visualized very nicely by plotting $\frac{\mathrm{d}\Gamma_{\mathrm{Nd}}}{\mathrm{d}k}$, which is obtained by evaluating everything but the final pion momentum integration for a fixed binding energy. The result for $B_\Lambda = 0.13$ MeV is depicted in Fig. 6.9.

Table 6.1.: Values for A_π and B_π for different α_- and $\tau_\Lambda = 263.2$ ps. The parameters are also depicted in Fig. 6.4

α_-	A_π	B_π
$\alpha_-^{2018} = 0.642$	1.05996	-7.94169
$\alpha_-^{\mathrm{KP}} = 0.721$	1.03759	-9.11119
$\alpha_-^{\mathrm{BESIII}} = 0.750$	1.02789	-9.56708

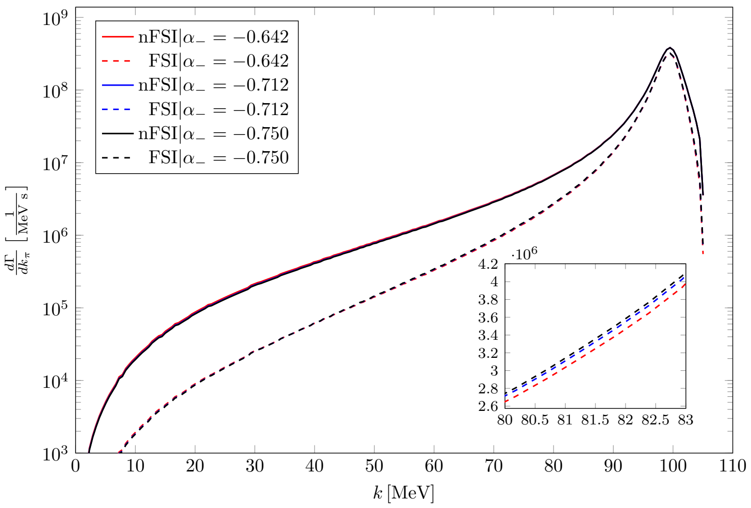

Figure 6.9.: Semi-logarithmic plot of $\frac{\mathrm{d}\Gamma_{\mathtt{Nd}}}{\mathrm{d}k}$ for different values of α_- at a fixed binding energy of $B_\Lambda = 0.13$ MeV. Results including final state interactions are dashed. The solid line neglects final state interactions. The inset magnifies and shows that the partial decay width indeed depends on α_-.

The new larger decay parameter shifts the partial widths upwards by a few percent. The newest results concerning the weak Λ decay parameter, which contains information for the contribution of the parity conserving and parity violating contribution to the width, let us expect a moderate change of the width. Indeed the change of up to 17% of the decay parameter shifts the contribution of the parity conserving part moderately, as indicated by Fig. 6.10. The parity violating part is less dominant over all k. Furthermore, at the most critical point, where the partial decay width peaks (and a severe amount of the contribution comes from) the relative change starts decreasing again. Hence, although the relative contribution of the parity violating term and the parity conserving term change moderately, the result of the sum only changes slightly as illustrated in Fig. 6.9. We expected this behavior from the fitting procedure and the scaling behavior best depicted in the result for the Helium width, see also Eq. (6.37). This trend is also reflected in Tab. 6.2.

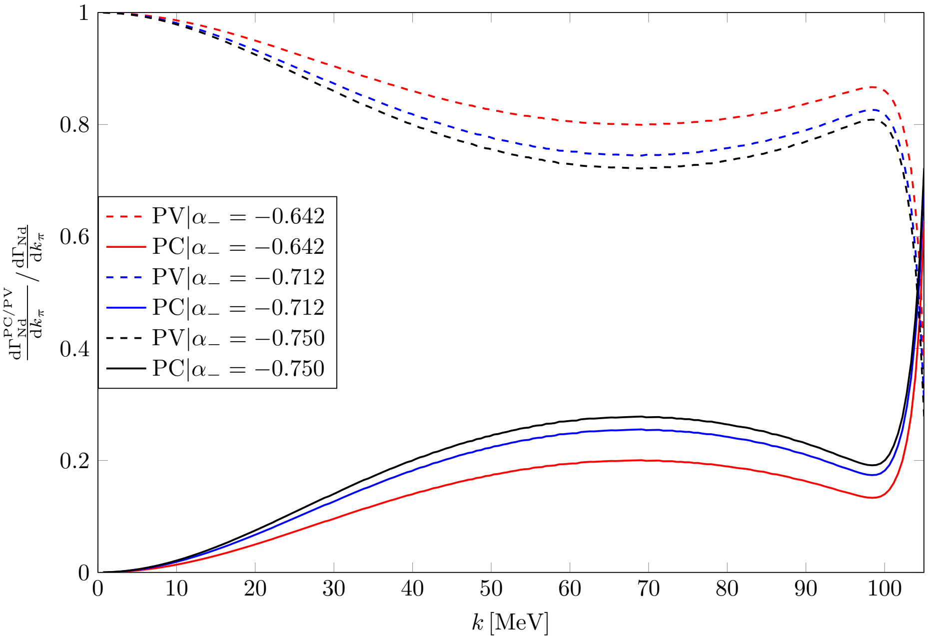

Figure 6.10.: Contribution of the parity conserving (PC) part and parity violating part (PV) of Fig. 6.9 in the same color scheme as before.

The results for the different partial widths are shown in Fig. 6.11. The two prominent values for $B_\Lambda = 0.13 \pm 0.05$ MeV [5] and $B_\Lambda = 0.41 \pm 0.12 \pm 0.11$ MeV [8] are the shaded green and blue area respectively. The calculated widths and ratios are given by the colored bands, which cover the parameter space of $-0.750 \leq \alpha_- \leq -0.642$. For an more detailed comparison in terms of the weak decay parameter see also App. E.4. As expected for very small B_Λ the Nd channel is dominating, since the allowed phase space for the decay into a bound state is small. As B_Λ is increasing, the decay into a bound state becomes more and more dominant. Note that for $B_\Lambda \mapsto \Delta$ both partial decay widths go to zero as expected and the hypertriton becomes stable against the weak interaction, since the energy release at the weak vertex would be below the binding energy of the Λ. While the hypertriton width $\Gamma_{^3_\Lambda\text{H}}$ does only moderately depend on the binding energy, and hence the correlation seems small, the partial width depends strongly on it and therefore the experimentally measured ratio $\Gamma_{^3\text{He}}/\left(\Gamma_{^3\text{He}} + \Gamma_{pd}\right)$ as well. Hence this quantity might be the better one to correlate the binding energy B_Λ with than the total width [50].

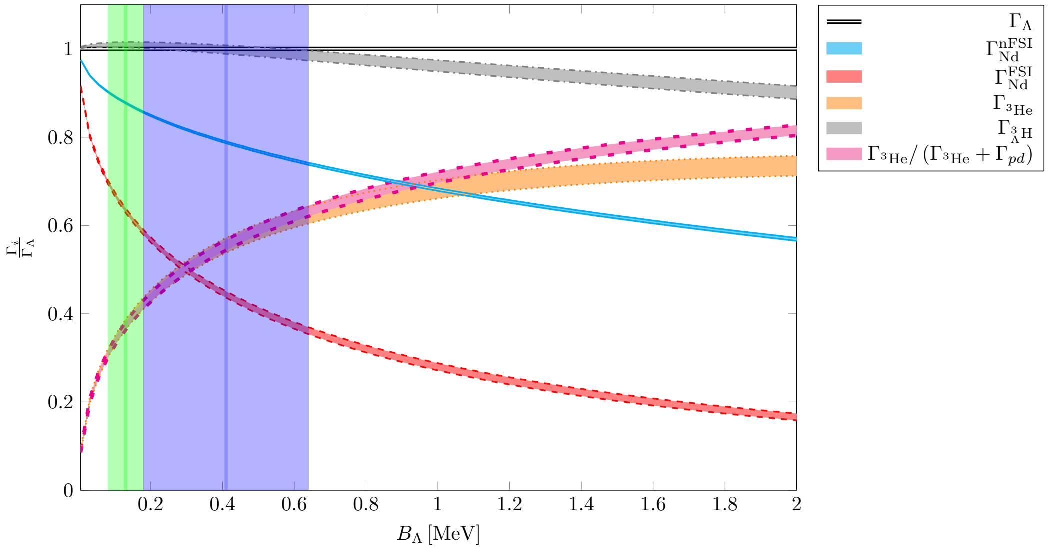

Figure 6.11.: Partial decay widths Γ_i as a function of the binding energy B_Λ over the free Λ width, together with the ratio $\Gamma_{^3\text{He}}/\left(\Gamma_{^3\text{He}} + \Gamma_{pd}\right)$. The boundaries of the bands correspond to the limits of the Λ weak decay parameter.. The regions for different suggested B_Λ (including uncertainties) are shaded green for Ref. [5] and blue for Ref. [8].

The results for the most prominent Λ binding energies $B_\Lambda = 0.13$ MeV and $B_\Lambda = 0.41$ MeV are shown in Tab. 6.2. Our results with α_-^{2018} compare very well with the result obtained by [114]. Note that the peak of the differential decay width is slightly shifted due to the different particle thresholds. Only evaluating the phase space it seems reasonable that the width is decreasing for larger B_Λ since the available phase space gets smaller. The result obtained by Congleton [50] using a similar closure approximation is in agreement for the ratio $\Gamma_{^3\text{He}}/\left(\Gamma_{^3\text{He}} + \Gamma_{pd}\right)$, however, the total width is about 13% higher. Although the decay constant changes by up to 17% compared to the old value α_-^{2018}, the impact on the decay rates is much smaller for small binding energies B_Λ. While the change of the partial decay width is in the order of a few percent, the total width changes barely at all. So far the Coulomb interaction is not included in this calculation, which might shift the lifetime in the charged channel. In principle our calculation supports the picture that coming from the limit $B_\Lambda \mapsto 0$ the lifetime of the hypertriton should be mainly determined by the free Λ lifetime. For small B_Λ our three-body calculation done in the previous chapter confirm the simple two-body picture that the Λ and the other nucleons are indeed far apart.

Table 6.2.: Experimentally known branching ratios and lifetimes for two binding energies for three different α_-. The results assume the empirical isospin rule. The widths are given in percent of the Λ free width which corresponds to $\tau_\Lambda = 263.2$ ps. The resulting total and partial lifetimes are given in ps, where the bottom two corresponds to the single decay channels.

Observable	$B_\Lambda = 0.13$ MeV			$B_\Lambda = 0.41$ MeV		
α_-	0.642	0.721	0.750	0.642	0.721	0.750
$\Gamma_{\text{Nd}}/\Gamma_\Lambda$	0.629	0.636	0.640	0.438	0.446	0.451
$(\Gamma_{^3\text{He}} + \Gamma_\text{H})/\Gamma_\Lambda$	0.387	0.371	0.364	0.574	0.550	0.538
$\Gamma_{^3_\Lambda\text{H}}/\Gamma_\Lambda$	1.016	1.007	1.003	1.012	0.994	0.989
$\Gamma_{^3\text{He}}/\left(\Gamma_{^3\text{He}} + \Gamma_\text{pd}\right)$	0.362	0.368	0.365	0.563	0.551	0.544
$\tau_{^3_\Lambda\text{H}}$/ps	259.1	261.4	262.4	259.9	264.8	266.1
τ_Nd/ps	418.55	413.65	411.60	601.13	589.49	583.77
$\tau_{^3\text{He+H}}$/ps	680.08	709.71	723.17	458.61	480.33	489.45

The results of this work compare differently to different recent heavy-ion collision experiments. The results for low binding energy B_Λ lie within error bars of the results close to the free Λ width [56], while other results tend to lie lower [48, 54, 55, 57]. Despite giving values for the lifetime within a large area $60 - 400$ ps (see also Fig.4.3), older emulsion experiments give relatively consistent experimental values for the ratio $R = \Gamma_{^3\text{He}}/\left(\Gamma_{^3\text{He}} + \Gamma_{pd}\right)$ starting from $R = 0.30 \pm 0.07$ to 0.39 ± 0.07 [59, 61, 63, 119]. Both and therefore the average are in agreement with our result obtained for $B_\Lambda = 0.13$ MeV, while the ratio $R_{B_\Lambda = 0.41} \approx 0.55$ is much larger, see also Tab. 6.2. Since this ratio is much more sensitive towards the binding energy it might be a good idea to solve the binding energy puzzle by combining lifetime branching ratio data and binding energy data. If the experimental results for R are correct, this would according to our calculation favor smaller binding energies up to $B_\Lambda = 0.20$ MeV and hence the established result for the binding energy of $B_\Lambda = 0.13 \pm 0.05$ MeV [5]. This border would lie relatively close to the end of the uncertainty band for recent STAR collaboration measurements of the binding energy $B_\Lambda = 0.41 \pm 0.12 \pm 0.11$ MeV [8].

6.4.2. Corrections to Results

In this part we want to Check how good are the assumptions we made before and look at the impact of possible corrections.

6.4.2.1. Isospin Breaking

A first Idea is to check the validity of the isospin correlation between the charged and uncharged channel. So far we used an average nucleon mass and 139.57 MeV pions and are neglecting Coulomb, which indeed could shift this result due to the repulsion of a deuteron and a proton. Still neglecting Coulomb for the charged case, we fix our final state interaction for the uncharged channel now by reproducing the triton binding energy. This leads to an effective correction of the final state scattering length by around 10%, resulting in a new value for $a_{nc} = 2.22$ fm, compared to the one given in Ch. 6.2. We also need to correct our coupling according to the different pion masses of $M_{\pi^\pm} = 139.57$ MeV and $M_{\pi^0} = 134.99$ MeV. Furthermore, we include now the mass splitting between the neutron and proton produced in the weak decay. Therefore the free width is now given by $\Gamma_\Lambda = \Gamma_\Lambda^{\mathrm{c}} + \Gamma_\Lambda^{\mathrm{cn}}$. This changes the amplitudes A_π and B_π. Since we want to resolve the isospin dependency explicitly, it is now crucial to define two sets of the amplitudes A_π and B_π. Using the actual branching ratio of the two channels, which is according to Ref. [7] $\Gamma_\Lambda\left(n\pi^0\right)/\Gamma_\Lambda\left(N\pi\right) = 0.359 \pm 0.005$ directly implies that there are corrections to the ratio $2/1$. Further on, according to Ref. [7] the ratio $\alpha_0/\alpha_- = 1.01$ seems to be independent of α_-. We obtain for example for α_-^{2018}, see also Tab. 6.1, for the charged channel

$$A_\pi^c = 1.02562 \quad \text{and} \quad B_\pi^c = -7.68275. \tag{6.39}$$

In contrast to that, with the sign swap the contribution to the uncharged channel, we obtain

$$A_\pi^{nc} = -0.788035 \quad \text{and} \quad B_\pi^{nc} = 5.98044, \tag{6.40}$$

which is a puzzling result at first glance. But remember we resolved this feature by construction before, see also Ch. 3.2. Nonetheless the contribution of the parity violating part seems to be slightly stronger affected than the contribution of the parity conserving one. This change, however, is absorbed completely by kinematic changes and differences in the masses, yet proving our choice to be solid. Compared to our assumption with an average nucleon mass and 139.57 MeV pions we obtain the following results:

$$\Gamma_{\mathrm{Nd}}/\Gamma_{\Lambda} = 0.398 + 0.232 = 0.629 \tag{6.41}$$

$$\Gamma_{\mathrm{He/T}}/\Gamma_{\Lambda} = 0.242 + 0.132 = 0.374 \tag{6.42}$$

$$\Gamma_{{}^{3}_{\Lambda}\mathrm{H}}/\Gamma_{\Lambda} = 0.640 + 0.363 = 1.003 \tag{6.43}$$

We obtain a shift by $< 0.1\%$ upwards for the sum of the channels decaying into a deuteron, the decay width into the two-body bound state goes downwards by about 3%, hence the correction to the total width is negligibly small ($\sim 1\%$). This, however, shifts the ratio R up by 4%, resulting in $R = 0.378$. Although the corrections to our obtained results are small, it is interesting to look at the isospin splitting between the two channels.

We directly see that the actually assumed ratio coming from the branching ratio of the Λ is about $\approx 10\%$ off the assumed value. Starting by around 3% splitting for the charged Nd channel as depicted in Fig. 6.12 the contribution of the charged channel is decreasing with increasing B for reasonable binding energies with respect to the ratio of the charged to the uncharged channel coming from Λ data. A similar behavior can be observed for the decay into a bound state, the splitting, however, is much stronger with increasing B_{Λ}. Due to the relative strength of the channels to each other the splitting for the total width is, however, relatively small, approximately 1.5% for B_{Λ}, at least with respect to the assumed symmetry with respect to the free Λ. Interestingly the rather huge shift from the assumed ratio of 2/1 seems to barely affect the result at all. This confirms our assumption that the decay of the hypertriton is mainly determined by the width of the free Λ. How the width is split up into the different channels barely influences the result, implying that the assumed ratio of 2/1 is a good assumption to calculate this decay, at least when neglecting Coulomb. Hence isospin symmetry seems to be a good symmetry for this system.

6.4.2.2. Introduction of a Form Factor

A second option is the introduction of a form factor $F(\boldsymbol{k})$ that corrects the weak vertex depending on the outgoing pion momentum. For their three-body calculation Kamada

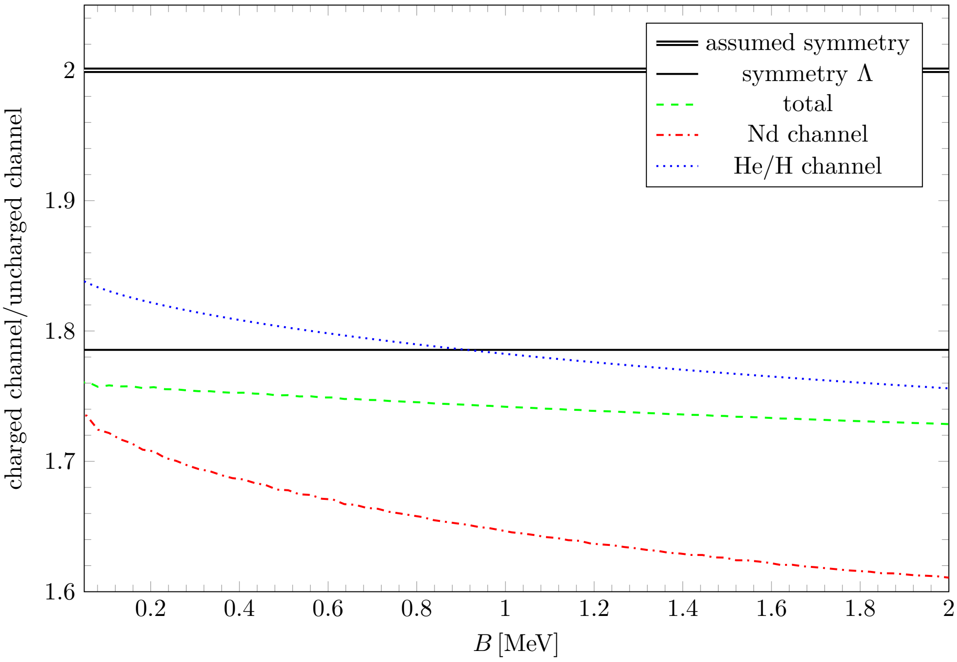

Figure 6.12.: Ratio of the charged and uncharged channel as a function of the binding energy of the Λ to the deuteron. The assumed ratio in our calculations is 2.

et al. used a form factor of the monopole type [114]

$$F(\boldsymbol{k}) = \frac{\xi^2 - M_\pi^2}{\xi^2 + \boldsymbol{k}^2} \tag{6.44}$$

with $\xi = 1300$ MeV. The value of ξ was chosen to match the cutoff of the Nijmegen interactions on which their strong and weak coupling constants are based on [53]. We, however, do not fix to such a potential. Nonetheless, this value might be a good value for the introduction of such a form factor in our theory. The form factor suppresses large pion momenta. However, very large pion momenta are forbidden anyway by the phase space restrictions, see also Fig. 6.7. Hence $F(\boldsymbol{k})$ is smaller but close to 1, the form factor assumed so far, for all $\boldsymbol{k}$. We therefore assume the effect to be minimal. As reference point we choose once more our calculation assuming isospin symmetry. Since we fix the weak interaction by reproducing Γ_Λ, we expect the absolute value for both

A_π and B_π to go up, which is indeed the case. Although the amplitudes A_π and B_π change moderately:

$$A_\pi = 1.0599 \mapsto 1.07851 \quad \text{and} \quad B_\pi = -7.942 \mapsto -8.079, \tag{6.45}$$

for $\alpha_- = \alpha_-^{2018}$ the effect is as expected minimal. The contribution in the Nd channel increases for $B_\Lambda = 0.13$ MeV barely up to 0.632 of the free Λ width. The decay width into the bound state remain unchanged. Therefore the total width is increased to $1.018\,\Gamma_\Lambda$. This is a change by less than one percent. Hence the impact of a form factor of the monopole type is negligible for this theory and confirming our choice of neglecting it in the first place.

6.4.3. Outlook: the Deuteron Break Up and Wave Functions

Another part that is not included in our theory is the breakup of the deuteron. Including this within our theory would change the approach drastically, however, the impact is possibly minimal. For the calculations done before, we would need to replace the two-body final state interaction with the full three-body problem and consider taking the deuteron dynamically into account. However, at this point we just give a little insight that contributions from the so far neglected process are driven by the three-body scattering amplitude. Fortunately we already calculated a dimer propagator for the deuteron in our EFT analysis of the structure of the hypertriton. Since we expect the final state interaction to act similarly for this process and therefore decreasing the width or be at least of the same order of magnitude, it is sufficient to calculate the matrix element without final state interactions for illustrative purposes. For a diagrammatic visualization of such a process see Fig. 6.13.

Labeling the weak decay nucleon momentum $\boldsymbol{k}_1$ and the pion momentum $\boldsymbol{k}$ we obtain for the width the following expression

$$\begin{aligned}\Gamma_{\mathrm{Npn}} = \int & \frac{\mathrm{d}^3 k_1}{(2\pi)^3} \frac{\mathrm{d}^3 k}{(2\pi)^3} \frac{\mathrm{d}^3 p_1}{(2\pi)^3} \frac{\mathrm{d}^3 p_2}{(2\pi)^3} \frac{1}{2\omega(k)} (2\pi)^4 \delta\left(\boldsymbol{k} + \boldsymbol{k}_1 + \boldsymbol{p}_1 + \boldsymbol{p}_2\right) \\ & \times \delta\left(\Delta - B_d - B_\Lambda - \omega(k) - \frac{k_1^2}{2m} - \frac{p_1^2}{2m} - \frac{p_2^2}{2m}\right) \frac{1}{2} \sum_{m_{Hyp}, m_f} \left|\mathcal{M}_{\mathrm{Npn}}\right|^2\end{aligned} \tag{6.46}$$

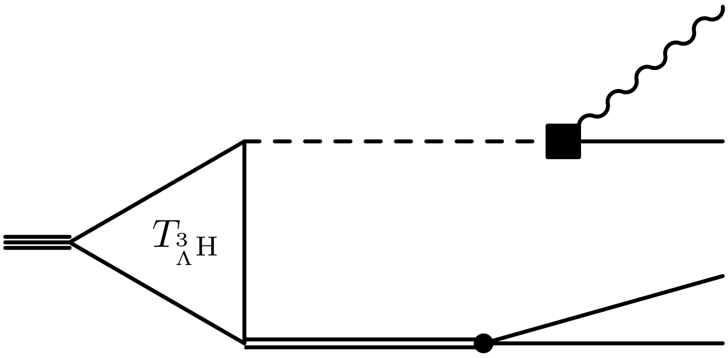

Figure 6.13.: Deuteron breakup contribution without including a full three-body amplitude, hence there are no important final state interactions.

with $\boldsymbol{p}_{1/2}$ the two deuteron nucleon momenta and

$$^S\mathcal{M}_{\mathrm{Npn}} = S_\Lambda\left(-B_\Lambda - \frac{\boldsymbol{p}_1^2 + \boldsymbol{p}_2^2}{2m}, -\boldsymbol{p}_1 - \boldsymbol{p}_2\right) D_d\left(\frac{\boldsymbol{p}_1^2 + \boldsymbol{p}_2^2}{2m}, \boldsymbol{p}_1 + \boldsymbol{p}_2\right) \mathcal{W}(k)\, Z(B_\Lambda) \tag{6.47}$$

the scalar part of the matrix element. We can reduce the complexity of the phase space by introducing a set of 2-d Jacobi coordinates $\boldsymbol{p}_r$ and $\boldsymbol{p}_s$ for the outgoing nucleons of the deuteron system. We obtain a phase space that looks similar to the one obtained in the Nd channel with an extra three momentum integration due to the extra outgoing particle. However, due to the variable transformation the amount of explicit angle dependencies is not increased. Note that one might think about doing a similar transformation for the decay nucleon and the pion, this unfortunately is not possible due to the mixture of relativistic and non-relativistic kinematics. We obtain for the energy delta function

$$\delta\left(\Delta - B_d - B_\Lambda - \omega(k) - \frac{p_r^2}{m} - \frac{p_s^2}{4m} - \frac{(\boldsymbol{k} + \boldsymbol{p}_s)^2}{2m}\right). \tag{6.48}$$

The scalar matrix elements then reads

$$^S\mathcal{M}_{\mathrm{Npn}} = S_\Lambda\left(-B_\Lambda - \frac{\boldsymbol{p}_s^2}{4m} - \frac{\boldsymbol{p}_r^2}{m}, -\boldsymbol{p}_s\right) D_d\left(\frac{\boldsymbol{p}_s^2}{4m} - \frac{\boldsymbol{p}_r^2}{m}, \boldsymbol{p}_s\right) \mathcal{W}(k)\, Z(B_\Lambda). \tag{6.49}$$

Calculating the partial width $\frac{\mathrm{d}\Gamma_{\mathrm{Npn}}}{\mathrm{d}k}$, we obtain a similar result as achieved by Kamada et al. in Ref. [114], which we used for the assumption to neglect this process. For the result neglecting final state interaction we obtain 9.7% of the free width. However, final interactions are expected to be crucial, even more crucial than in the Nd channel. However, we cannot make any final conclusions for this channel without solving the three-body problem explicitly. Following the results of the three-body calculations of Ref. [114], we can expect final state interactions to suppress by one order of magnitude resulting in a total contribution of about 1% of the free width and therefore can be expected to be negligible for the considered binding energies.

An important note at this point is that the result obtained here should not be seen with reference to the results obtained before, since this process in not included in the theory before and there is also no systematic way of including it. However, in principle although we consider this channel to be small, it is still contributing to the total width.

Further on, in principle we could use the wave functions obtained in our structure analysis in Ch. 5.7, instead of the wave function renormalization used so far. This is inconsistent in the framework we used so far, treating the hypertriton as a two-body problem, yet undermining the wave function reconstruction of the two-body problem as used in the limit $B_\Lambda \mapsto 0$. However, moving from a two-body calculation to a three-body the wave functions obtained by us should be reconstructed in a rigorous effective field theory approach. Nonetheless due to the inconsistent total lifetime data from experiment, it is questionable that the total width is a good quantity to test wave functions.

6.5. Chapter Summary

In this chapter we discussed the dependence of the lifetime of the hypertriton on the binding energy in a deuteron closure approximation in leading order pionless effective field theory. Calculating the main decay channels of the hypertriton, our results are in good agreement with the results obtained in a rigorous Fadeev approach in the isospin symmetry limit using realistic potentials [114]. This indicates that the closure approximation is reasonable at leading order pionless EFT. Giving up the isospin symmetry limit shows only small corrections to the result. Furthermore, we looked at the impact of the new results on the weak Λ decay parameter α_-. Despite the change of α_- up to 17%, the impact for reasonable binding energies B_Λ is small, although the contribution of the parity violating part is increasing moderately.

In addition, we performed an intensive study of the binding energy dependence of the decay widths. Looking at the same range $B_\Lambda \leq 1$ MeV the dependence of the total width $\Gamma_{^3_\Lambda\mathrm{H}}$ of B_Λ, changing only by a few percent of the free Λ width, is small. In contrast to that the contribution of a singular channel depends strongly on B_Λ, changing up to 75% of the total width in a span over 1 MeV, meaning also the ratio $R = \Gamma_{^3\mathrm{He}} / \left(\Gamma_{^3\mathrm{He}} + \Gamma_{pd}\right)$, which is experimentally accessible and has been already measured, is mainly driven by the binding energy of the Λ particle. Therefore it might be worthwhile to combine lifetime and binding energy data. Based on this calculation, combined with old bubble chamber results, a small $B_\Lambda \leq 0.20$ MeV would be favored. As expected from the limit $B_\Lambda \mapsto 0$, the contribution of the decay into a bound two-body state (consisting out three nucleons) is increasing with B_Λ for reasonable binding energies. Meanwhile the contribution from a decay into a deuteron is decreasing. Analyzing the partial decay with $\frac{\mathrm{d}\Gamma_{\mathrm{Nd}}}{\mathrm{d}k}$ we find that the main contribution is coming from high pion momenta. The decay rate into the two-body bound state is also fixed at a relativistic pion momentum, which once again justifies the relativistic inclusion of the pion.

Possible corrections to the results presented here, as for example the introduction of a form factor or giving up the isospin symmetry, offer only small corrections to the result. Although not performing a full three-body calculation, the results obtained here are indeed comparable to results obtained with realistic nucleon-nucleon interactions [114]. Following the approach of a three-body breakup might also give further insight into the nature of the Λnn state [66].

7. Summary

In this thesis, we presented a detailed analysis of the structure of three-body hypernuclei. We thereby focused on the two most important systems, the hypertriton and the Λnn system, both offering an opportunity to study physics beyond the up- and down-quark sector. The first of them, the hypertriton, has been established in theory and experiments over decades, yet offering challenges and open questions. The second, Λnn is accessed experimentally rather recently [9]. Its actual nature however is up to debate until today.

In the first part of the thesis we did an extensive analysis of the structure of both systems. In a pionless effective field theory we found both systems to be bound due to the Efimov effect, hence both systems display universal properties. We studied those in a dimer field approach studying Λd (nn) scattering, obtaining the Phillips line, a correlation between the binding energy and the scattering length. This allows us to tackle the impact of one of the current questions regarding the binding energy of the hypertriton. The new proposed value by the STAR collaboration [8] would decrease the value of the Λ-d scattering length by roughly 40% compared to the obtained $15.4^{+4.3}_{-2.3}$ fm for the challenged value $B_\Lambda = 0.13 \pm 0.05$ MeV [5]. This small binding energy is often used to express that the hypertriton is shallowly bound. In our consecutive calculation of the three-body wave function and matter radii we find the assumed picture of a rather closely bound deuteron core with a far away Λ particle present. We find a large separation of 10.79 fm of these two components, compared to all other matter radii present within the system. This is in good agreement with the results obtained from a simple two-body estimate. As the scattering length before, the matter radius is once more directly connected to the binding energy, which allows us to directly connect those properties. As for the scattering length, the impact of the proposed binding energy is large. The simple two-body picture and hence the large separation of the Λ from the n-p pair, however, remains a reasonable picture.

In comparison, the results for the Λnn do not exhibit this halo type structure of the hypernucleus. This becomes immediately clear due to the lack of a bound two-body core substructure, since the di-neutron is considered to be unbound. Therefore all matter radii extracted are of similiar size. A present feature of this theory is that the binding energy is an input parameter of the theory offering a correlation between binding energy and matter radius which could be exploited. However as a QCD parameter analysis indicates the possibility of a bound Λnn is only about 6% and therefore rather unlikely. However, the manifestation as a resonance is still up for debate. Nonetheless, we can find similar universal correlations for a, if bound, Λnn assuming an non-physical bound nn system.

In the second project of this thesis we approached another open question about the hypertriton, the lifetime. Experimental data of this observable are available from two different sources, bubble chamber experiments and heavy ion collisions. However, results coming from both sources are inconsistent, not only between both types of experiments but also within themselves, covering a huge area of possible results. We therefore addressed this problem, in the light of the new binding energy result of the STAR colloboration [8], with the intention to analyze the impact of the Λ binding energy. We did this in a deuteron closure approximation stressing the impact of the Λ binding energy.

We calculated the two most important channels, the decay into a deuteron and the decay into a bound system containing three nucleons assuming an isospin symmetry between the charged and uncharged channel. However, the total lifetime is barely impacted by the binding energy B_Λ for reasonable B_Λ and is very close to the lifetime of the free Λ. This result is in good agreement with the result obtained in the first part of this thesis where we found that the Λ is indeed far apart from the nucleon pair. Therefore the result can be seen as a correction to the free Λ lifetime. Corrections due to isospin splitting are small strengthening the picture as a correction to the free Λ lifetime.

However, the ratio R of the decay into ^{3}He and a π^- over all charged channels depends strongly on the binding energy covering almost 75% of the possible values over a span of 1 MeV. This observable is experimentally accessible and therefore might be a better observable to combine binding energy data with than the total lifetime. If results obtained for R in emulsion experiments are correct, based on our calculation smaller binding energies, smaller than $B_\Lambda \approx 0.20$ MeV, are preferred compared to higher binding energies.

In the future it might be worthwhile to extend the EFT discussion for the hypertriton and the Λnn to next-to-leading order and rotate the procedure to the complex plane for the Λnn system to cover possible and debated resonance states. Further on it might be elucidating to combine EFT methods with input for unphysical pion masses obtained from lattice QCD to analyze the structure of hypernuclei at unphysical pion masses. In addition, the wave functions obtained in our calculation, including the full three-body structure of the hypertriton, could be used in coalescence models for the production in heavy ion collisions.

The combination of the three-body results obtained in the first part of this thesis could be combined with the width calculation by moving to a full three-body calculation. In principle, it would also be interesting to include pionic final state interactions, as recent analysis shows that they could shift the result by up to 6% of the free Λ with, which would lead to solving a four-body problem. Here, the use of a deuteron closure approximation as done in this thesis could be used to reduce the complexity of the system to a three-body system with one pion, one nucleon and a fundamental deuteron.

Experimentally, a result for the ratio R coming from heavy ion experiments would be interesting to test and further study the dependency of the binding energy. Nonetheless, interesting experiments are coming up as a proposed lifetime measurement of the hypertriton as well as other hypernuclei in recent J-PARC proposals. Further on, we can expect new results from the upcoming LHC runs. For the third run, a large increase of statistics is expected [120–122]. For the hypertriton the expected peak of possible events is according to Ref. [100] approximately 440000. In addition to that a different approach to measure the hypertriton binding energy at high precision is for example proposed for MAMI [123].

For the Λnn, if it is bound, it should be observable in other experiments, such as ALICE [65]. However the recently completed JLab E12-17-003 experiment may give further insight into the nature of the Λnn [124].

A. Theoretical Background Details

A.1. Effective Potentials

From textbook physics [10] it is known that the analytic solution of the Lippmann-Schwinger equation for any separable potential is given by

$$\left\langle \boldsymbol{p} \middle| T\left(z\right) \middle| \boldsymbol{p}' \right\rangle = \lambda v\left(p\right) v\left(p'\right) \tau\left(z\right) \tag{A.1}$$

with

$$\tau = \left(1 - \lambda \int \frac{\mathrm{d}^3 q}{\left(2\pi\right)^3} \frac{v^2\left(\boldsymbol{q}\right)}{z - E_q}\right)^{-1} . \tag{A.2}$$

The energy E_q is the energy associated to the momentum q. In order to calculate the full solution we need to solve the integral given in Eq. (A.2). With the principal value $\mathcal{P}$, see also App. B.2, we obtain that

$$\int_0^{\Lambda_c} \frac{\mathrm{d}^3 q}{\left(2\pi\right)^3} \frac{1}{E - q^2/\left(2m\right) + i\epsilon} = \frac{m}{\pi^2}\left(-\Lambda_c + \int_0^{\Lambda_c} \mathrm{d}q \, \frac{2mE\mathcal{P}}{2mE - q^2} - \frac{i\pi m E}{\sqrt{2mE}}\right) . \tag{A.3}$$

Evaluating the principal value integral and setting $\sqrt{2mE} = p$ we obtain for $T\left(p,p\right)$ the following expression

$$T\left(p,p\right) = -\frac{2m}{\pi}\left(-\frac{2\pi}{m g_0} - \frac{2\Lambda_c}{\pi} + \frac{2p}{\pi} \operatorname{arccoth}\left(\frac{\Lambda_c}{p}\right) - ip\right)^{-1} . \tag{A.4}$$

Comparing the obtained result with the effective range expansion Eq. (2.8) at threshold we obtain for the scattering length a and the coupling constant g

$$a = \frac{1}{2\pi} \frac{mg}{1 + \Lambda_c m g} \quad \text{and} \quad g = \frac{2\pi}{m} \frac{a}{1 - 2a\pi\Lambda_c} \tag{A.5}$$

respectively [125]. These expressions are plotted for a mass of 1 MeV in Fig. 2.4. Note that the prefactors may change in differnt conventions.

A.2. Efimov-Effect

The binding energy of an Efimov trimer according to Ref. [11] is given by the transcendental equation

$$B_i^{\text{Ef}} + \frac{\hbar^2}{ma^2} = \left(e^{-\frac{2\pi}{s_0}}\right)^{n-n*} e^{\Delta(\xi)/s_0} \frac{\hbar^2 \kappa_*^2}{m} \tag{A.6}$$

with $n, n*$ numbering the Efimov states, k_* a three-body parameter and $\Delta(\xi)$ the universal function obtained from [25]. The angle ξ is defined by

$$\tan(\xi) = -\sqrt{mB_i^{\text{Ef}}}\frac{a}{\hbar}. \tag{A.7}$$

The energy spectrum shown in Fig. 2.6 is now obtained by solving Eq. (A.6). In this framework $K = \tan(\xi)/a$ and the scattering length now can be rewritten in the following way

$$K = H \sin(\xi) \quad \text{and} \quad 1/a = H \cos(\xi). \tag{A.8}$$

Typical Efimov plots are then re-scaled in this case the axis are $H^{\frac{1}{4}} \cos(\xi)$ and $H^{\frac{1}{4}} \sin(\xi)$ although labeled otherwise, note that in literature also other re-scaling procedures are used.

A.3. Cutting Rules

It is straightforward to calculate the two-body scattering amplitude, using the propagator given in the main part and the Feynmanrule for the contact interaction $-ig$, the equation for $\mathcal{A}$ reads

$$\begin{aligned}
i\mathcal{A} =& - ig + (ig) \int \frac{\mathrm{d}^4 q}{(2\pi)^4} \frac{i}{q_0 + E - \frac{q^2}{2m_1} + i\epsilon} \frac{i}{-q_0 - \frac{q^2}{2m_2} + i\epsilon} \\
=& - ig + (ig)(-2\mu)\, i \underbrace{\int \frac{\mathrm{d}^3 q}{(2\pi)^3} \frac{1}{\frac{q^2}{2\mu} - 2\mu E - i\epsilon}}_{=-\frac{1}{4\pi}\sqrt{-2\mu E - i\epsilon}} \\
=& - ig - ig\mathcal{I}i\mathcal{A} \quad \Rightarrow \\
\mathcal{A} =& \frac{1}{-1/g - i\mathcal{I}}
\end{aligned} \tag{A.9}$$

utilizing the methods described in App. B.1. The cut through the loop can be calculated by using standard relations of the δ function. We start with the expression for

$$i\mathcal{I} = i\int \frac{\mathrm{d}^4 q}{(2\pi)^4} \frac{i}{q_0 + E - \frac{q^2}{2m_1} + i\epsilon} \frac{i}{-q_0 - \frac{q^2}{2m_2} + i\epsilon} \tag{A.10}$$

and now apply the cutting rules, recognizing that we can cut through these two operators. In the next step we replace them by the corresponding δ functions

$$\cancel{i\mathcal{I}} = - i\frac{\mathrm{d}^4 q}{(2\pi)^4} \delta\left(q_0 + E - \frac{q^2}{2m_1}\right) \delta\left(q_0 + \frac{q^2}{2m_2}\right) \tag{A.11}$$

$$= \frac{i}{\pi} \int \mathrm{d}q\, q^2 \delta\left(\frac{q^2}{2\mu} - E\right) \tag{A.12}$$

$$= \frac{i}{\pi} \mu \sqrt{2\mu E} = 2i\mathcal{I}, \tag{A.13}$$

where we rewrote the $\delta\left(f\left(q\right)\right)$ into a sum of δ functions and directly eliminated those that are not part of the integration area.

B. Calculation Details

In this part of the Appendix we present often used mathematical techniques in our calculations. We will not discuss or prove this technique in all generality, instead we will focus on the cases that are relevant for this thesis.

B.1. Residue Theorem

Often we need to integrate integrals that are shifted into the complex plane, especially propagators by the means of contour integration. The typical case is the energy integration over two or more propagators of the type

$$iS\left(P_0, \boldsymbol{p}\right) = \frac{i}{P_0 - \frac{p^2}{2m} + i\epsilon} \tag{B.1}$$

within loops. The residue theorem states that any closed contour integration over a simple connected subset of the complex plane does only depend on the residue of the singularities within this subset, in other words the function f is holomorph except at the singularities. The contribution of this integration over the contour $\mathcal{C}$ is then given by

$$\int_{\mathcal{C}} f = 2\pi i \sum_a \omega\left(a\right) \mathrm{Res}_a\left(f\right), \tag{B.2}$$

where $\omega\left(a\right)$ is the winding number of $\mathcal{C}$ around the point a and $\mathrm{Res}_a\left(f\right)$ the residue of the function f at this point. The typical case within this work is the case where we can select one out of two poles. The typical structure is depicted in Fig. B.1. Note, if the rest of the integral does not depend on the integration variable, the contribution of the contour $\mathcal{C}$ vanishes if we send the radius of the arc in Fig. B.1 to infinity.

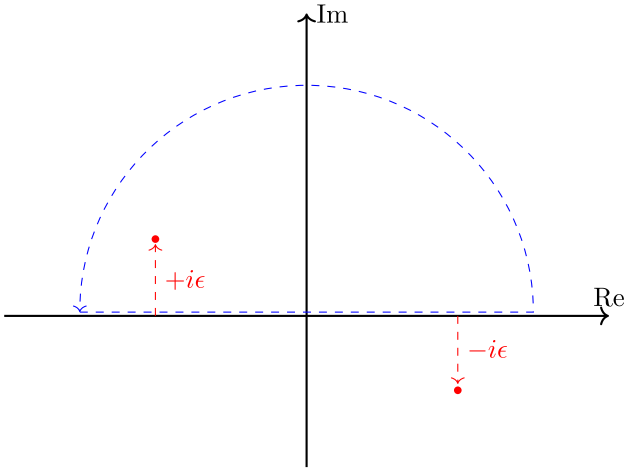

Figure B.1.: Typical case of the residue theorem applying in the thesis. Two shifted propagators, while one pole is lying in the upper half of the complex plane, the other one is not. Note that in principle we integrate along the real axis, hence the shift as indicated is only for visibility.

B.2. Principal Value Integral

Another method that can be used to integrate integrands of the type $g\left(x\right)=\frac{1}{x}$ is the principal value method, which can be symbolically written as

$$\frac{1}{x+i\epsilon}=\mathcal{P}\frac{1}{x}\mp\frac{i\pi}{\delta\left(x\right)}, \tag{B.3}$$

where $\mathcal{P}$ denotes the principal value of the integral. At this point we imply that the smooth function f we consider falls off quickly in the limit $|x|\mapsto\infty$ and does not have a pole on the real axis, to be precise, we utilize the following expression

$$\lim_{\zeta\mapsto 0}\int_{-\infty}^{\infty}\mathrm{d}x\,\frac{f\left(x\right)}{x\pm i\epsilon}=\lim_{\zeta\mapsto 0}\left[\int_{-\infty}^{-\zeta}\mathrm{d}x\,\frac{f}{x}+\int_{\zeta}^{\infty}\mathrm{d}x\,\frac{f}{x}\right]\mp i\pi\int_{-\infty}^{\infty}\delta\left(x\right)f\left(x\right). \tag{B.4}$$

Important at this point is to recognize that in general a lot of functions can be evaluated with both approaches introduced in App. B.1 and here, but not all. This is the case since either the contribution of the contour is not vanishing or the principal value is not finite. The principal value method is generally only valid for poles of exactly this structure.

C. Calculation Details Lambda-Sigma Conversions

C.1. Momentum Scale Calculation

In order to calculate the typical momentum scale, we need to evaluate the loop integrals $I_{\Lambda \mathrm{N}}$ and $I_{\Sigma \mathrm{N}}$. The diagrams needed to be evaluated are of the following type:

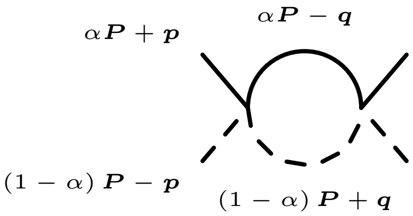

Figure C.1.: Typical loop with split momentum distribution according to the mass ratio α or the constituent particles.

The in Fig. C.1 defined variables and the reduced mass μ are given by

$$\boldsymbol{p} = \mu \left(\frac{1}{M_n} \boldsymbol{p}_{\mathrm{N}} - \frac{1}{m_\Lambda} \boldsymbol{p}_\Lambda \right), \qquad \mu = \frac{M_n M_\Lambda}{M_n + M_\Lambda}, \qquad \alpha = \frac{\mu}{M_\Lambda}. \tag{C.1}$$

We then can calculate $I_{\Lambda \mathrm{N}}$ and $I_{\Sigma \mathrm{N}}$, we obtain (note the integral $I_{\Lambda \mathrm{N}}$ differs only in the non-existence of the mass shift $\Delta_{\Sigma\Lambda}$)

$$
\begin{aligned}
iI_{\Sigma\backslash\Lambda n} &= \int \frac{d^D q}{(2\pi)^D} \frac{i}{-q_0 - \frac{(\alpha \boldsymbol{P} - \boldsymbol{q})^2}{2M_n} + i\epsilon} \frac{i}{E + q_0 - \frac{((1-\alpha)\boldsymbol{P} + \boldsymbol{q})^2}{2M_\Lambda} - \Delta_{\Sigma\Lambda} + i\epsilon} \\
&= i \int \frac{d^d q}{(2\pi)^d} \frac{1}{E - \frac{(\alpha \boldsymbol{P} - \boldsymbol{q})^2}{2M_n} - \frac{((1-\alpha)\boldsymbol{P} + \boldsymbol{q})^2}{2M_\Lambda} - \Delta_{\Sigma\Lambda} + i\epsilon} \\
&= i \int \frac{d^d q}{(2\pi)^d} \frac{1}{E - \Delta_{\Sigma\Lambda} - \frac{q^2}{2\mu} - \frac{P^2}{2(M_n + M_\Lambda)} + i\epsilon} \\
&= -2\mu i \int \frac{d^d q}{(2\pi)^d} \frac{1}{q^2 + 2\mu\left(-E - i\epsilon + \Delta_{\Sigma\Lambda} + \frac{P^2}{2(M_n + M_\Lambda)}\right)} .
\end{aligned}
\tag{C.2}
$$

Defining now $E_{cm} = \frac{P^2}{2(M_n + M_\Lambda)}$ then we obtain

$$
iI_{\Sigma\backslash\Lambda n} = -2\mu i \int \frac{d^d q}{(2\pi)^d} \frac{1}{q^2 - 2\mu\left(E_{cm} + i\epsilon - \Delta_{\Sigma\Lambda}\right)} . \tag{C.3}
$$

and evaluating the integral in dimensional regularisation yields the result:

$$
iI_{\Sigma\backslash\Lambda n} = i\frac{\mu}{2\pi}\sqrt{-2\mu\left(E_{cm} + i\epsilon - \Delta_{\Sigma\Lambda}\right)} + \mathcal{O}\left(d - 3\right) . \tag{C.4}
$$

D. EFT Calculation Details

D.1. Calculation of the Two-Body Propagators

As stated in the main text, we need to sum up to all baryon loops as of Fig. 5.3. The bare propagator is given by i/Δ. Labeling the loops according to their propagating particles A, B I^j_{AB}, we obtain the following equation

$$\begin{aligned} iD^j_{AB} =& \frac{i}{\Delta} + \frac{i}{\Delta} iI^j_{AB} \frac{i}{\Delta} + \frac{i}{\Delta} iI^j_{AB} \frac{i}{\Delta} iI^j_{AB} \frac{i}{\Delta} + \dots \\ =& \frac{i}{\Delta} \sum_n \left(-\frac{I^j_{AB}}{\Delta} \right)^n \\ =& \frac{i}{\Delta} \frac{1}{1 + \frac{I^j_{AB}}{\Delta}}, \end{aligned} \tag{D.1}$$

where we used the closed expression for a geometric series from the second to the third line and $j = 2S + 1$ or a reference to a state. Hence the dimer propagator only depends on the evaluation of a single loop. In case of the three-body system discussed within this theses, four different loops need to be calculated. The general idea of how to calculate such an integral is already presented in App. C. In contrast to a general integral we now take spin explicitly into consideration. Starting from

$$iI_{AB} = -i\mathcal{S}^j_{AB} \frac{\mu_{AB}}{2\pi} \sqrt{-2\mu_{AB} \left(E - \frac{\boldsymbol{p}^2}{2\left(M_A + M_B\right)} + i\epsilon \right)} \tag{D.2}$$

where $\mathcal{S}^j_{AB}$ is a "spin" factor determined by particle type, spin, isospin and the coupling constant g_{AB} for the dimer break up. The reduced mass of the particles A and B is given by $\mu_{AB} = M_A M_B/(M_A + M_B)$. Evaluating now the result of the geometric series

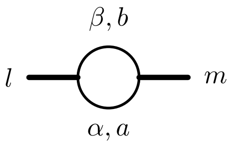

Figure D.1.: Baryon loop for the case of a ${}^3S_1(NN)$, l, m are spin 1, α, β spin $1/2$ indices. a and b are the corresponding isospin indices.

Eq. (D.1) by inserting Eq. (D.2) we obtain

$$iD^j_{AB} = \frac{2\pi i}{\mathcal{S}^j_{AB}\mu_{AB}} \frac{-1}{\frac{2\pi\Delta}{-\mu_{AB}\mathcal{S}^j_{AB}} + \sqrt{-2\mu_{AB}\left(E - \frac{\boldsymbol{p}^2}{2(M_A+M_B)} + i\epsilon\right)}} \tag{D.3}$$

In a final step we now need to evaluate the spin factors $\mathcal{S}^j_{AB}$ explicitly. The spin/isospin structure of such a system is shown representatively for the $\mathcal{S}^3_{NN}$ case in Fig. D.1. We obtain

$$\begin{aligned} \mathcal{S}^3_{NN} =& 2\frac{g_d}{2}\frac{g_d}{2}\left(\tau_2\right)_{ab}\left(\tau_2\right)_{ba}\left(\sigma_l\sigma_2\right)_{\alpha\beta}\left(\sigma_2\sigma_m\right)_{\beta\alpha} \\ =& \frac{g_d^2}{4}\operatorname{Tr}\left(\tau_2\tau_2\right)\operatorname{Tr}\left(\sigma_l\sigma_2\sigma_2\sigma_m\right) = 2g_d^2\delta_{lm}. \end{aligned} \tag{D.4}$$

In similiar fashion it is now possible to obtain the values for the other spin factors. Note that $S^3_{NN} = S^1_{NN}$ because isospin and spin "flip" their roles. We then obtain for the $\mathcal{S}$ containing Λ-Baryons

$$S^3_{\Lambda N} = g_3^2\left(\sigma_l\sigma_2\right)_{\alpha\beta}\left(\sigma_2\sigma_m\right)_{\beta\alpha} = g_3^2\operatorname{Tr}\left(\sigma_l\sigma_2\sigma_2\sigma_m\right) = 2g_3^2\delta_{lm}, \tag{D.5}$$

$$S^1_{\Lambda N} = g_1^2\left(\sigma_2\right)_{\alpha\beta}\left(\sigma_2\right)_{\beta\alpha} = g_3^2\operatorname{Tr}\left(\sigma_2\sigma_2\right) = 2g_1^2, \tag{D.6}$$

where we changed the notation of the coupling constants to those used in the main text. The nucleon-nucleon propagator then reads (setting $l = m$)

$$iD^{s,d}_{NN} = \frac{2\pi}{g^2_{d,s}M} \frac{-i}{-\frac{2\pi\Delta}{Mg^2_{s,d}} + \sqrt{-M\left(E - \frac{\boldsymbol{p}^2}{4M} + i\epsilon\right)}}, \tag{D.7}$$

with $\gamma_{d/s} = 2\pi\Delta/(Mg^2_{s,d})$ we obtain the dimer-propagators given in Eq. (5.6) where we dropped the particle and lowered the upper indices. The same procedure is used for the ΛN propagators, those are then given by

$$iD_{\Lambda N}^{1,3} = \frac{\pi}{\mu_{\Lambda N} g_{1,3}^2} \frac{-i}{-\frac{\pi\Delta}{\mu_{\Lambda N} g_{1,3}^2} + \sqrt{-2\mu_{\Lambda N}\left(E - \frac{\boldsymbol{p}^2}{2(M_\Lambda + M)} + i\epsilon\right)}} . \tag{D.8}$$

At this point it is worth mentioning that the expression $\gamma_{1/3} = \pi\Delta/(\mu_{\Lambda N} g_{1,3}^2)$ differs by a factor of 2 at first glance, but is indeed identical since $\mu_{NN} = M/2$. Note that this result differs by a factor of 2 compared to the result obtained in Ref. [83].

D.2. Choice of a Cutoff

For numerical purposes it is convenient to set the three-body force to zero that can be achieved by a specific choice of the cutoff given in Eq. (5.28). That the cutoff indeed vanishes for this choice can be easily seen by setting Eq. (5.18) to zero:

$$H^I\left(\Lambda_c\right) = -\frac{\sin\left(s_0 \ln\left(\frac{\Lambda_c}{\Lambda_*^I}\right) - \arctan\left(\frac{1}{s_0}\right)\right)}{\sin\left(s_0 \ln\left(\frac{\Lambda_c}{\Lambda_*^{I=0}}\right) + \arctan\left(\frac{1}{s_0}\right)\right)} = 0 \tag{D.9}$$

Evaluating the enumerator of Eq. (D.9) and utilizing the periodicity of the sine function, as condition for the cutoff we obtain

$$s \log\left(\frac{\Lambda_c}{\Lambda_*^I}\right) - \arctan\left(\frac{1}{s}\right) = n\pi \tag{D.10}$$

with $n > 0$ is an integer. Solving now for Λ_c returns Eq. (5.28), the condition for cutoffs at which the three-body force vanishes. Since the sine is periodic, it becomes immediately clear why the parameter Λ_*^I is only determined up to a factor of $\exp\left(n\pi/s\right)$.

D.3. Hypertriton Integral Equations

Starting from the Lagrangian Eq. (5.3) we now want to give some details on the derivation of the hypertriton integral equations in the unequal mass case. This calculation was already done in Ref. [95], but needs to be corrected by a factor $1/2$. The details of the calculation thereby are similar to Ref. [95]. The amplitudes are given by the following set of equations:

$$\begin{aligned}\left[t_A^{ij}\left(\boldsymbol{k},\boldsymbol{p}\right)_{\alpha\beta}\right] =& g_d g_3 \int \frac{\mathrm{d}^3 q}{(2\pi)^3}\left[t_B^{i,l'}\left(\boldsymbol{k},\boldsymbol{q}\right)_{\alpha\beta'}\right]\frac{\left(\sigma_j\sigma_{l'}\right)_{\beta'\beta} D_3\left(E-\frac{q^2}{2m},\boldsymbol{q}\right)}{E-\frac{p^2}{2M_\Lambda}-\frac{q^2}{2M}-\frac{(\boldsymbol{q}+\boldsymbol{p})^2}{2M}+i\epsilon}\\ &+ g_d g_1 \int \frac{\mathrm{d}^3 q}{(2\pi)^3}\left[t_C^{i}\left(\boldsymbol{k},\boldsymbol{q}\right)_{\alpha\beta'}\right]\frac{\left(\sigma_j\right)_{\beta'\beta} D_1\left(E-\frac{q^2}{2m},\boldsymbol{q}\right)}{E-\frac{p^2}{2M_\Lambda}-\frac{q^2}{2M}-\frac{(\boldsymbol{q}+\boldsymbol{p})^2}{2M}+i\epsilon}\end{aligned} \tag{D.11}$$

$$\begin{aligned}\left[t_B^{i,j}\left(\boldsymbol{k},\boldsymbol{q}\right)_{\alpha\beta}\right] =& -2g_d g_3 \frac{\left(\sigma_j\sigma_i\right)_{\alpha\beta}}{E-\frac{k^2}{2M_\Lambda}-\frac{p^2}{2m}-\frac{(\boldsymbol{k}+\boldsymbol{p})^2}{2M}+i\epsilon}\\ &+ 2g_d g_3 \int \frac{\mathrm{d}^3 q}{(2\pi)^3}\left[t_A^{i,l'}\left(\boldsymbol{k},\boldsymbol{q}\right)_{\alpha\beta'}\right]\frac{\left(\sigma_j\sigma_{l'}\right)_{\beta'\beta} D_d\left(E-\frac{q^2}{2m},\boldsymbol{q}\right)}{E-\frac{p^2}{2M}-\frac{q^2}{2M_\Lambda}-\frac{(\boldsymbol{q}+\boldsymbol{p})^2}{2M}+i\epsilon}\\ &+ g_3^2 \int \frac{\mathrm{d}^3 q}{(2\pi)^3}\left[t_B^{i,l'}\left(\boldsymbol{k},\boldsymbol{q}\right)_{\alpha\beta'}\right]\frac{\left(\sigma_j\sigma_{l'}\right)_{\beta'\beta} D_3\left(E-\frac{q^2}{2m},\boldsymbol{q}\right)}{E-\frac{p^2+q^2}{2M}-\frac{(\boldsymbol{q}+\boldsymbol{p})^2}{2M_\Lambda}+i\epsilon}\\ &- g_3 g_1 \int \frac{\mathrm{d}^3 q}{(2\pi)^3}\left[t_C^{i}\left(\boldsymbol{k},\boldsymbol{q}\right)_{\alpha\beta'}\right]\frac{\left(\sigma_j\right)_{\beta'\beta} D_1\left(E-\frac{q^2}{2m},\boldsymbol{q}\right)}{E-\frac{p^2+q^2}{2M}-\frac{(\boldsymbol{q}+\boldsymbol{p})^2}{2M_\Lambda}+i\epsilon}\end{aligned} \tag{D.12}$$

$$\begin{aligned}\left[t_C^{i}\left(\boldsymbol{k},\boldsymbol{q}\right)_{\alpha\beta}\right] =& -2g_d g_1 \frac{\left(\sigma_i\right)_{\alpha\beta}}{E-\frac{k^2}{2M_\Lambda}-\frac{p^2}{2m}-\frac{(\boldsymbol{k}+\boldsymbol{p})^2}{2M}+i\epsilon}\\ &+ 2g_d g_3 \int \frac{\mathrm{d}^3 q}{(2\pi)^3}\left[t_A^{i,l'}\left(\boldsymbol{k},\boldsymbol{q}\right)_{\alpha\beta'}\right]\frac{\left(\sigma_{l'}\right)_{\beta'\beta} D_d\left(E-\frac{q^2}{2m},\boldsymbol{q}\right)}{E-\frac{p^2}{2M}-\frac{q^2}{2M_\Lambda}-\frac{(\boldsymbol{q}+\boldsymbol{p})^2}{2M}+i\epsilon}\\ &- g_3 g_1 \int \frac{\mathrm{d}^3 q}{(2\pi)^3}\left[t_B^{i,l'}\left(\boldsymbol{k},\boldsymbol{q}\right)_{\alpha\beta'}\right]\frac{\left(\sigma_{l'}\right)_{\beta'\beta} D_3\left(E-\frac{q^2}{2m},\boldsymbol{q}\right)}{E-\frac{p^2+q^2}{2M}-\frac{(\boldsymbol{q}+\boldsymbol{p})^2}{2M_\Lambda}+i\epsilon}\\ &+ g_1^2 \int \frac{\mathrm{d}^3 q}{(2\pi)^3}\left[t_C^{i}\left(\boldsymbol{k},\boldsymbol{q}\right)_{\alpha\beta'}\right]\frac{\delta_{\beta'\beta} D_1\left(E-\frac{q^2}{2m},\boldsymbol{q}\right)}{E-\frac{p^2+q^2}{2M}-\frac{(\boldsymbol{q}+\boldsymbol{p})^2}{2M_\Lambda}+i\epsilon}\end{aligned} \tag{D.13}$$

At this point we already absorbed the isospin dependence of the amplitudes t_B and t_c within them via the definition

$$t_{B/C} = t^{ab}_{B/C} \left(\tau_2\right)_{ba} , \tag{D.14}$$

where we suppressed all other dependencies of the amplitudes. This can only be done for the hypertriton case. In case of the Λnn case, we need to explicitly resolve this isospin, see also App. D.4. The indices a and b are isospin indices. In the equations above, we use Greek letters for isospin $1/2$ indicies and Latin ones for spin 1. Intermediate quantum numbers are marked with a prime. We project onto total $J = 1/2$ by applying the following definitions

$$t_{A/B}\left(\boldsymbol{k},\boldsymbol{p}\right)\delta_{\alpha\beta} = \frac{1}{3}\left(\sigma_i\right)_{\alpha\alpha'} t^{i,j}_{A/B}\left(\boldsymbol{k},\boldsymbol{p}\right)_{\alpha'\beta'}\left(\sigma_j\right)_{\beta'\beta} , \tag{D.15}$$

$$t_{C}\left(\boldsymbol{k},\boldsymbol{p}\right)\delta_{\alpha\beta} = \frac{1}{3}\left(\sigma_i\right)_{\alpha\alpha'} t^{i,j}_{C}\left(\boldsymbol{k},\boldsymbol{p}\right)_{\alpha'\beta} . \tag{D.16}$$

Further on, we project onto relative S-waves. We can account for the wave function renormalization of the deuteron by refining the amplitudes once more. We obtain

$$T_A = Z_d t_A \quad T_B = \frac{g_3}{g_d} Z_d T_B, T_C = \frac{gd}{g_1} t_c, \tag{D.17}$$

with

$$\frac{1}{Z_d} = i\frac{\partial}{\partial P_0}\left[iD_d\left(P_0,\boldsymbol{p}\right)\right]^{-1}\Big|_{P_0=-\frac{\gamma_d^2}{M},\boldsymbol{p}=0} = \frac{M^2 g_d^2}{4\pi\gamma_d}. \tag{D.18}$$

The integral equations for the hypertriton for general mass ratios $y \neq 0$ then are

$$\begin{aligned}
T_A^{I=0}\left(k,p\right) =& \frac{-1}{2\pi\left(1+y\right)}\int_0^{\Lambda_c} dqq^2\left[\tilde{L}_B\left(p,q,E\right)T_B^{I=0}\left(k,q\right) - 3\tilde{L}_C\left(p,q,E\right)T_C^{I=0}\left(k,q\right)\right]\\
T_B^{I=0}\left(k,p\right) =& -\frac{4\pi\gamma_d}{M}L_I\left(p,k,E\right) - \frac{1}{\pi}\int_0^{\Lambda_c} dqq^2 L_A\left(p,q,E\right)T_A^{I=0}(k,q)\\
&- \frac{1}{2\pi\left(1-y\right)}\int_0^{\Lambda_c} dqq^2\left[L_B\left(p,q,E\right)T_B^{I=0}\left(k,q\right) + 3L_C\left(p,q,E\right)T_C^{I=0}\left(k,q\right)\right]\\
T_C^{I=0}\left(k,p\right) =& \frac{4\pi\gamma_d}{M}L_I\left(p,k,E\right) + \frac{1}{\pi}\int_0^{\Lambda_c} dqq^2 L_A\left(p,q,E\right)T_A^{I=0}(k,q)\\
&- \frac{1}{2\pi\left(1-y\right)}\int_0^{\Lambda_c} dqq^2\left[L_B\left(p,q,E\right)T_B^{I=0}\left(k,q\right) - L_C\left(p,q,E\right)T_C^{I=0}\left(k,q\right)\right] ,
\end{aligned} \tag{D.19}$$

where in addition to the corrected factor of two, also the sign in the prefactor of the integral in the first equation was flipped $(1-y) \to (1+y)$ compared to the derivation given in Ref. [83]. (See also the discussion for the $I=1$ case in Appendix D.4.) The y-dependent functions $L(p,q,E,(y))$ are given by

$$\begin{aligned}
L_I &= \frac{1}{pk}\log\left(\frac{k^2/(1+y)+p^2+pk-ME}{k^2/(1+y)+p^2-pk-ME}\right) \\
L_A &= \frac{1}{pq}\log\left(\frac{q^2/(1+y)+p^2+pq-ME}{q^2/(1+y)+p^2-pq-ME}\right) \\
&\quad\cdot\left[-\gamma_{d/s}+\sqrt{\frac{3-y}{4\,(1+y)}q^2-ME-i\epsilon}\right]^{-1} \\
\tilde{L}_{B/C} &= \frac{1}{pq}\log\left(\frac{q^2+p^2/(1+y)+pq-ME}{q^2+p^2/(1+y)-pq-ME}\right) \\
&\quad\cdot\left[-\gamma_{3/1}+\sqrt{\frac{3+2y-y^2}{4}q^2-ME(1+y)-i\epsilon}\right]^{-1} \\
L_{B/C} &= \frac{1}{pq}\log\left(\frac{q^2+p^2+pq(1-y)-ME(1+y)}{q^2+p^2-pq(1-y)-ME(1+y)}\right) \\
&\quad\cdot\left[-\gamma_{3/1}+\sqrt{\frac{3+2y-y^2}{4}q^2-ME(1+y)-i\epsilon}\right]^{-1}\,.
\end{aligned} \tag{D.20}$$

D.4. Λnn Integral Equations

Starting from the Lagrangian Eq. (5.3) and using the same conventions and definitions for the L_i as for the hypertriton, we obtain from the Feynman diagrams in Fig. 5.4 the following equations:

$$\begin{aligned}
\left[t_A^{ij}\left(\boldsymbol{k},\boldsymbol{p}\right)_{\alpha\beta}\right] =& g_s g_3 \int \frac{\mathrm{d}^3 q}{(2\pi)^3}\left[t_B^{i,l'}\left(\boldsymbol{k},\boldsymbol{q}\right)^{a'b'}_{\alpha\beta'}\right]\frac{\left(\sigma_{l'}\right)_{\beta'\beta}\left(\tau_j\tau_2\right)_{b'a'}D_3\left(E-\frac{q^2}{2m},\boldsymbol{q}\right)}{E-\frac{p^2}{2M_\Lambda}-\frac{q^2}{2M}-\frac{(\boldsymbol{q}+\boldsymbol{p})^2}{2M}+i\epsilon} \\
&+ g_s g_1 \int \frac{\mathrm{d}^3 q}{(2\pi)^3}\left[t_C^{i}\left(\boldsymbol{k},\boldsymbol{q}\right)^{a'b'}_{\alpha\beta'}\right]\frac{\delta_{\beta'\beta}\left(\tau_j\tau_2\right)_{b'a'}D_1\left(E-\frac{q^2}{2m},\boldsymbol{q}\right)}{E-\frac{p^2}{2M_\Lambda}-\frac{q^2}{2M}-\frac{(\boldsymbol{q}+\boldsymbol{p})^2}{2M}+i\epsilon}
\end{aligned} \tag{D.21}$$

$$
\begin{aligned}
\left[t_B^{i,l}\left(\boldsymbol{k},\boldsymbol{q}\right)^{ab}_{\alpha\beta}\right] =& -g_s g_3 \frac{\left(\sigma_l\right)_{\alpha\beta}\left(\tau_2\tau_i\right)_{ab}}{E-\frac{k^2}{2M_\Lambda}-\frac{p^2}{2m}-\frac{(\boldsymbol{k}+\boldsymbol{p})^2}{2M}+i\epsilon} \\
&+ g_s g_3 \int \frac{\mathrm{d}^3q}{(2\pi)^3}\left[t_A^{i,j'}\left(\boldsymbol{k},\boldsymbol{q}\right)_{\alpha\beta'}\right]\frac{\left(\sigma_l\right)_{\beta'\beta}\left(\tau_2\tau_{j'}\right)_{ab}D_d\left(E-\frac{q^2}{2m},\boldsymbol{q}\right)}{E-\frac{p^2}{2M}-\frac{q^2}{2M_\Lambda}-\frac{(\boldsymbol{q}+\boldsymbol{p})^2}{2M}+i\epsilon} \\
&+ g_3^2 \int \frac{\mathrm{d}^3q}{(2\pi)^3}\left[t_B^{i,l'}\left(\boldsymbol{k},\boldsymbol{q}\right)^{a'b'}_{\alpha\beta'}\right]\frac{\left(\sigma_l\sigma_{l'}\right)_{\beta'\beta}\delta_{b'b}\delta_{a'a}D_3\left(E-\frac{q^2}{2m},\boldsymbol{q}\right)}{E-\frac{p^2+q^2}{2M}-\frac{(\boldsymbol{q}+\boldsymbol{p})^2}{2M_\Lambda}+i\epsilon} \\
&- g_3 g_1 \int \frac{\mathrm{d}^3q}{(2\pi)^3}\left[t_C^{i}\left(\boldsymbol{k},\boldsymbol{q}\right)^{a'b'}_{\alpha\beta'}\right]\frac{\left(\sigma_l\right)_{\beta'\beta}\delta_{b'b}\delta_{a'a}D_1\left(E-\frac{q^2}{2m},\boldsymbol{q}\right)}{E-\frac{p^2+q^2}{2M}-\frac{(\boldsymbol{q}+\boldsymbol{p})^2}{2M_\Lambda}+i\epsilon}
\end{aligned}
\tag{D.22}
$$

$$
\begin{aligned}
\left[t_C^{i}\left(\boldsymbol{k},\boldsymbol{q}\right)^{ab}_{\alpha\beta}\right] =& -g_s g_1 \frac{\delta_{\alpha\beta}\left(\tau_2\tau_i\right)_{ab}}{E-\frac{k^2}{2M_\Lambda}-\frac{p^2}{2m}-\frac{(\boldsymbol{k}+\boldsymbol{p})^2}{2M}+i\epsilon} \\
&+ g_s g_3 \int \frac{\mathrm{d}^3q}{(2\pi)^3}\left[t_A^{i,j'}\left(\boldsymbol{k},\boldsymbol{q}\right)_{\alpha\beta'}\right]\frac{\delta_{\beta'\beta}\left(\tau_2\tau_{j'}\right)_{ab}D_d\left(E-\frac{q^2}{2m},\boldsymbol{q}\right)}{E-\frac{p^2}{2M}-\frac{q^2}{2M_\Lambda}-\frac{(\boldsymbol{q}+\boldsymbol{p})^2}{2M}+i\epsilon} \\
&- g_3 g_1 \int \frac{\mathrm{d}^3q}{(2\pi)^3}\left[t_B^{i,l'}\left(\boldsymbol{k},\boldsymbol{q}\right)^{a'b'}_{\alpha\beta'}\right]\frac{\left(\sigma_{l'}\right)_{\beta'\beta}\delta_{b'b}\delta_{a'a}D_3\left(E-\frac{q^2}{2m},\boldsymbol{q}\right)}{E-\frac{p^2+q^2}{2M}-\frac{(\boldsymbol{q}+\boldsymbol{p})^2}{2M_\Lambda}+i\epsilon} \\
&+ g_1^2 \int \frac{\mathrm{d}^3q}{(2\pi)^3}\left[t_C^{i}\left(\boldsymbol{k},\boldsymbol{q}\right)^{a'b'}_{\alpha\beta'}\right]\frac{\delta_{\beta'\beta}\delta_{b'b}\delta_{a'a}D_1\left(E-\frac{q^2}{2m},\boldsymbol{q}\right)}{E-\frac{p^2+q^2}{2M}-\frac{(\boldsymbol{q}+\boldsymbol{p})^2}{2M_\Lambda}+i\epsilon}
\end{aligned}
\tag{D.23}
$$

where a, b and i, j are isospinor (isovector) indices while α, β and l are the corresponding indices in the spin space. Intermediate states are marked with a prime. While it is possible to absorb the isospin dependence in the amplitude for the hypertriton (cf. App. D.3 and Ref. [83]), a specific choice for all isospin indices is needed for the Λnn system. We must choose all incoming and outgoing states to be two neutrons ($a = b = -1/2$) or part of the nn partial wave ($i = -j = 1$). For the tree level diagrams this choice then yields

$$
\left(\tau_2\tau_+\right)_{-1/2-1/2} = i. \tag{D.24}
$$

In a similar way one can obtain the prefactors for the first equations, since $a = b = -1/2$ is the only contributing element, when setting $j = -1$. The same procedure can be applied for the intermediate j' the other way around. Choosing $a = b = -1/2$ for the resulting isospinor indices one receives $j' = 1$ as only contributing part left. In order to obtain the correct spin only one projection is needed for t_b. We choose

$$\left[t^l_B\left(\boldsymbol{k},\boldsymbol{q}\right)\right]\delta_{\alpha\beta} = \left[t^l_B\left(\boldsymbol{k},\boldsymbol{q}\right)_{\alpha\beta'}\right]\frac{\left(\sigma_l\right)_{\beta'\beta}}{3} \tag{D.25}$$

$$\left[t_{A/C}\left(\boldsymbol{k},\boldsymbol{q}\right)\right]\delta_{\alpha\beta} = \left[t_{A/C}\left(\boldsymbol{k},\boldsymbol{q}\right)_{\alpha\beta}\right]. \tag{D.26}$$

Projection on relative S-waves and defining the amplitudes

$$\begin{aligned} T^{I=1}_A\left(k,p\right) &= Z_s t_A\left(k,p\right) \\ T^{I=1}_B\left(k,p\right) &= i\frac{g_s}{g_3} Z_s t_B\left(k,p\right) \\ T^{I=1}_C\left(k,p\right) &= i\frac{g_s}{g_1} Z_s t_C\left(k,p\right) \end{aligned} \tag{D.27}$$

where $Z_s^{-1} = \frac{M^2 g_s^2}{4\pi\gamma_s}$ is the wave function renormalization of the nn-system leads to the set of integral equations

$$\begin{aligned} T^{I=1}_A\left(k,p\right) =& \frac{1}{2\pi\left(y+1\right)}\int \mathrm{d}q\, q^2\left[3\tilde{L}_B\left(p,q,E\right)T^{I=1}_B\left(k,q\right) + \tilde{L}_C\left(p,q,E\right)T^{I=1}_C\left(k,q\right)\right] \\ T^{I=1}_B\left(k,p\right) =& +\frac{4\pi\gamma_{\mathrm{nn}}}{M}L_I\left(p,q,E\right) + \frac{1}{\pi}\int \mathrm{d}q\, q^2 L_A\left(q,p,E\right)T^{I=1}_A\left(k,q\right) \\ & + \frac{1}{2\pi\left(1-y\right)}\int \mathrm{d}q\left[L_B\left(p,q,E\right)T^{I=1}_B\left(k,q\right) + L_C\left(p,q,E\right)T^{I=1}_C\left(k,q\right)\right] \\ T^{I=1}_C\left(k,p\right) =& +\frac{4\pi\gamma_{\mathrm{nn}}}{M}L_I\left(p,q,E\right) + \frac{1}{\pi}\int \mathrm{d}q\, q^2 L_A\left(q,p,E\right)T^{I=1}_A\left(k,q\right) \\ & + \frac{1}{2\pi\left(1-y\right)}\int \mathrm{d}q\left[3L_B\left(p,q,E\right)T^{I=1}_B\left(k,q\right) - L_C\left(p,q,E\right)T^{I=1}_C\left(k,q\right)\right]\ , \end{aligned} \tag{D.28}$$

where the L_i are the same as in Appendix D.3. Taking the limit $y \to 0$ results in the integral equations shown in Eq. (5.11).

D.5. Three-Body Lagrangians

$I = 0$ Channel

The most general form of the Lagrangian for the non-derivative part of the three-body force for the hypertriton is given by

$$\begin{aligned}\mathcal{L}_{3Hyp} =& \frac{AMH\left(\Lambda_c\right)}{\Lambda_c^2}\left(C_d \cdot g_d^2 \left[d_l^* \Lambda_\alpha \left(\sigma_l \sigma_m\right)_{\alpha\beta} \Lambda_\beta^* d_m\right]\right.\\ &+ C_{ii}\left(g_3^2\left[\left(u_l^3\right)_a^* N_{\alpha a}\left(\sigma_l \sigma_m\right)_{\alpha\beta} N_{\beta b}^*\left(u_m^3\right)_b\right] - 3g_1^2\left[\left(u^1\right)_a^* N_{\alpha,a}\delta_{\alpha\beta}N_{\beta,b}^*\left(u^1\right)_b\right]\right)\\ &+ C_{3d}\cdot g_3 g_d\left[d_l^* N_{\alpha a}\left(\sigma_l\sigma_m\right)_{\alpha\beta}\Lambda_\beta^*\left(\tau_2\right)_{ab}\left(u_m^3\right)_b + H.c.\right]\\ &+ C_{13}\cdot g_1 g_3\left[\left(u_l^3\right)_a^* N_{\alpha a}\left(\sigma_l\right)_{\alpha\beta} N_{\beta b}^*\left(u^1\right)_b + H.c.\right]\\ &+ C_{1d}\cdot g_1 g_d\left[d_l^* N_{\alpha a}\left(\sigma_l\right)_{\alpha\beta}\Lambda_\beta^*\left(\tau_2\right)_{ab}\left(u^1\right)_b + H.c.\right] \ ,\end{aligned} \tag{D.29}$$

where A is a constant. It is possible to reconstruct the free parameters by evaluating the three-body force in the coupled integral equations in Ch. 5.4. This can be done by doing the transformations and projections used to derive the one-parameter three-body force backwards. The matrices S and S^{-1} denote the transformation matrices between the old and the new amplitudes $\tilde{T}_{A/B/C}$ and $T_{1/2/3}$, see also Eq. (5.14). The matrix J is the kernel of the set of decoupled integral equations. With the introduction of the three-body force $J_0 = \text{diag}(0, 0, 1)$ in T_3 one obtains for the backwards transformation of the amplitudes

$$S \cdot J \cdot J_0 \cdot S^{-1} = \frac{1}{3}\begin{pmatrix} 2 & -1 & 3 \\ -2 & 1 & -3 \\ 2 & -1 & 3 \end{pmatrix} . \tag{D.30}$$

Inverting the spin and isospin projections that were done for the original amplitudes $T_{A/B/C}$, see also [83], leads to

$$C_{ij} = \frac{1}{3}\begin{pmatrix} 4 & 1 & 1 \\ 1 & -1 & -1 \\ 1 & -1 & 3 \end{pmatrix} , \tag{D.31}$$

where we have matched the different loop-diagrams to the interactions. Since the Lagrangian is hermitian, the matrix C_{ij} must be symmetric. Matching the coefficients yields

$$\begin{aligned} A &= \frac{1}{3}, & C_d \quad &= 4, & C_{ii} &= -1, \\ C_{13} &= -1, & C_{1d} &= 1, & C_{3d} \ &= 1 \ , \end{aligned}$$

which fully determines the structure of the three-body force in the $I = 0$ channel.

$I = 1$ Channel

For the Λnn system we follow the same procedure as in $I = 0$ channel. The resulting structure of the three-body force in the $I = 1$ channel is

$$\begin{aligned} \mathcal{L}_{\Lambda \mathrm{nn}} =& \frac{2MH}{3\Lambda_c^2} \left(2g_n^2 \left[s_i^* \Lambda_\alpha \left(\tau_i \tau_j\right)_{\alpha\beta} \Lambda_\beta^* d_m\right]\right. \\ &+ \left(3g_3^2 \left[\left(u_l^3\right)_a^* N_{\alpha a} \left(\sigma_l \sigma_m\right)_{\alpha\beta} N_{\beta b}^* \left(u_m^3\right)_b\right] - g_1^2 \left[\left(u^1\right)_a^* N_{\alpha,a} \delta_{\alpha\beta} N_{\beta,b}^* \left(u^1\right)_b\right]\right) \\ &+ g_3 g_d \left[s_i^* N_{\alpha a} \left(\sigma_m\right)_{\alpha\beta} \Lambda_\beta^* \left(\tau_i \tau_2\right)_{ab} \left(u_m^3\right)_b + H.c.\right] \\ &+ g_1 g_3 \left[\left(u_l^3\right)_a^* N_{\alpha a} \left(\sigma_l\right)_{\alpha\beta} N_{\beta b}^* \left(u^1\right)_b + H.c.\right] \\ &+ g_1 g_s \left[s_i^* N_{\alpha a} \delta_{\alpha\beta} \Lambda_\beta^* \left(\tau_i \tau_2\right)_{ab} \left(u^1\right)_b + H.c.\right] \ . \end{aligned} \tag{D.32}$$

E. Width Calculation Details

E.1. Spin Structure of the Matrix Element

We need to evaluate the following spin sum

$$\begin{aligned}\frac{1}{2J+1}\sum_{m_{i,f}}\left|\mathcal{M}^{\mathrm{tot}}_{\mathrm{Nd}}\right|^2 =& \frac{1}{2J+1}\sum_{m_d,m_N,m_{\mathrm{Hyp}}}\left|\mathcal{M}^{\mathrm{FSI}}_{\mathrm{Nd}}+\mathcal{M}_{\mathrm{Nd}}\right|^2 = \frac{1}{2}\sum_{m_d,m_p,m_{\mathrm{Hyp}}}\\ &\Bigg|\sum_{m_\Lambda}\left[C\left(\begin{array}{c|cc}1/2 & 1 & 1/2\\ m_{\mathrm{Hyp}} & m_d & m_\Lambda\end{array}\right)(A+B\sigma_i k_i)_{m_\Lambda,m_p}\mathcal{M}_1\right]\\ &+\sum_{\substack{m_\Lambda,m'_p,\\ m'_d,m_A}}\left[C\left(\begin{array}{c|cc}1/2 & 1 & 1/2\\ m_{\mathrm{Hyp}} & m'_d & m_\Lambda\end{array}\right)(A+B\sigma_i k_i)_{m_\Lambda,m'_p}\right.\\ &\left.\times\, C\left(\begin{array}{c|cc}1/2 & 1 & 1/2\\ m_A & m'_d & m'_p\end{array}\right)C\left(\begin{array}{c|cc}1/2 & 1 & 1/2\\ m_A & m_d & m_p\end{array}\right)\mathcal{M}_2\right]\Bigg|^2,\end{aligned}\tag{E.1}$$

with the standard Clebsch-Gordon coefficient C

$$\sum_{m_1,m_2}\langle j_1,m_1;j_2,m_2|\,C\left(\begin{array}{c|cc}J & j_1 & j_2\\ M & m_1 & m_2\end{array}\right)=|J,M;j_1,j_2\rangle\tag{E.2}$$

representing the coupling of the product base into the eigen base $\langle J,M;j_1,j_2|$. The mixing occurs since both matrix elements have the same incoming and outgoing states. Evaluating all the sums returns the result of the main text.

E.2. Evaluation of $I_q\left(k, B_\Lambda\right)$

In order to evaluate the loop integral given in Eq. 6.24, we perform the q_0 integration with the means of standard contour integration resulting in an integral containing two factors

$$I_q\left(k, B_\Lambda\right) = \int \frac{\mathrm{d}^3 q}{\left(2\pi\right)^3}\left[-B_\Lambda - \frac{q^2}{2\mu_{d\Lambda}}\right]^{-1}\left[\Delta - B_\Lambda - \omega\left(k\right) - \frac{q^2}{2m_d} - \frac{\left(\boldsymbol{q}-\boldsymbol{k}\right)^2}{2m}\right]^{-1}. \tag{E.3}$$

Due to the positive energy Δ and the dependence on $\boldsymbol{q}\cdot\boldsymbol{k}$ the second term has a complex pole structure with up to two poles, which can in principle fall on top of each other, depending on the angle between the loop momentum $\boldsymbol{q}$ and the external momentum of the pion $\boldsymbol{k}$. In contrast, the first term is always negative, therefore never shows a pole structure, hence it is adroit to shift the angular dependence to the first term

$$\begin{aligned}I_q\left(k, B_\Lambda\right) = \int \frac{\mathrm{d}^3 q}{\left(2\pi\right)^3}&\left[-B_\Lambda - \frac{q^2}{2\mu_{d\Lambda}} - \frac{\mu_{\mathrm{Nd}}\boldsymbol{q}\cdot\boldsymbol{k}}{m\mu_{d\Lambda}} - \frac{\mu_{\mathrm{Nd}}^2}{2m^2\mu_{d\Lambda}^2}k^2\right]^{-1}\\ &\times\left[\Delta - B_\Lambda - \omega\left(k\right) - \frac{q^2}{2\mu_{\mathrm{Nd}}} + \frac{\mu k^2}{2m^2} - \frac{k^2}{2m}\right]^{-1}.\end{aligned} \tag{E.4}$$

Solving now the denominator of the second line with respect to q and performing the angular integration, which now can be done independently of the second propagator and therefore poleless, returns the expression Eq. (6.25) from the main part.

E.3. Integration of the Phase Space

We solve the equation $\phi^\pm\left(k, p\right) = 0$ with respect to p. We obtain the following results

$$p_-^\pm = \frac{1}{2}\mu\left(\sqrt{\frac{4k^2}{m^2} - \frac{4\left(2B - 2\Delta + \frac{k^2}{m} + 2\omega\right)}{\mu}} \pm \frac{2k}{m}\right), \tag{E.5}$$

$$p_+^\pm = -\frac{1}{2}\mu\left(\sqrt{\frac{4k^2}{m^2} - \frac{4\left(2B - 2\Delta + \frac{k^2}{m} + 2\omega\right)}{\mu}} \pm \frac{2k}{m}\right) \tag{E.6}$$

It can easily be seen that $p^{\pm}_{-} = -p^{\pm}_{+}$. The value k_0 is determined by the roots of the function

$$\frac{4\left(2B - 2\Delta + \frac{k^2}{m} + 2\omega\right)}{\mu}, \tag{E.7}$$

since $p^{\pm}_{\pm} \mapsto 0$ due to the structure of the square roots given in the equations before, solving with respect to k yields

$$k_0 = \sqrt{2}\sqrt{-\sqrt{-m^2\left(2Bm - m^2 - 2\Delta m - M_\pi^2\right)} - Bm + m^2 + \Delta m}. \tag{E.8}$$

Setting the complete square root in the expressions for $p^{\pm}_{\pm} = 0$ and solving with respect to k yields the maximum value of integration

$$\begin{aligned} k_{max} =& \frac{1}{m-\mu}\Big(2m^2(\mu(B-\Delta) + m(-B+\Delta+m)) \\ & - 2\sqrt{m^4\left(m^2\left(m(-2B+2\Delta+m) + M_\pi^2\right) + 2\mu m\left(Bm - \Delta m - M_\pi^2\right) + \mu^2 M_\pi^2\right)}\Big)^{\frac{1}{2}} \end{aligned} \tag{E.9}$$

E.4. Alternative Representations for Partial Widths

We present an alternative Plot for the partial and total widths for the hypertriton decays. In this plot we make the assumed values for α_- explicit. Following the same color scheme as before. Therefore the old value α_-^{2018} is depicted in red, the more recent values are depicted blue and black, where we suppressed the index 3 and ${}^{3}_{\Lambda}\mathrm{H}$ Hyp.

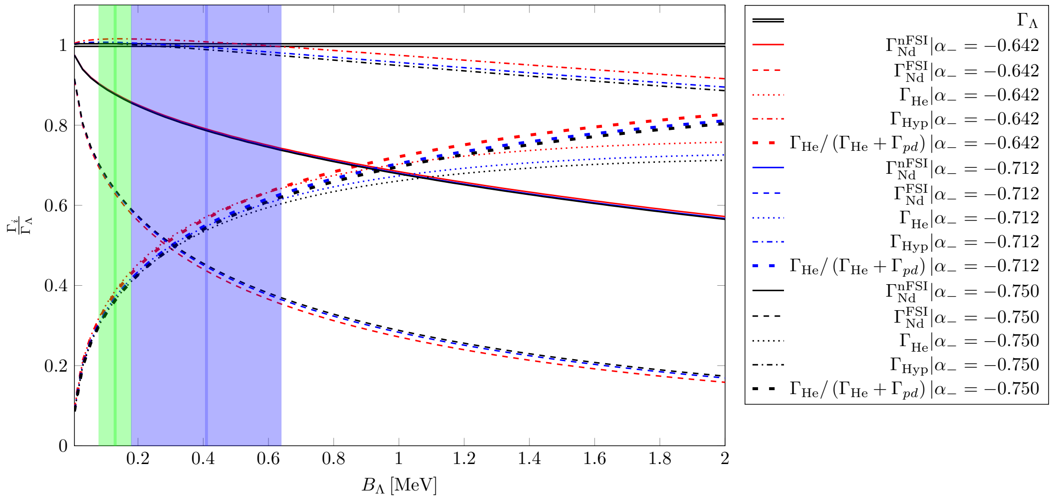

Figure E.1.: Alternative representation of Fig. 6.11. The color scheme is the same as for Fig. 6.9

Bibliography

[1] G. D. Rochester and C. C. Butler, “Evidence for the Existence of New Unstable Elementary Particles,” *Nature*, vol. 160, pp. 855–857, 1947.

[2] M. E. Peskin and D. V. Schroeder, *An Introduction to quantum field theory*. Reading, USA: Addison-Wesley, 1995.

[3] S. Durr *et al.*, “Ab-Initio Determination of Light Hadron Masses,” *Science*, vol. 322, pp. 1224–1227, 2008.

[4] A. Gal, E. V. Hungerford, and D. J. Millener, “Strangeness in nuclear physics,” *Rev. Mod. Phys.*, vol. 88, no. 3, p. 035004, 2016.

[5] M. Juric *et al.*, “A new determination of the binding-energy values of the light hypernuclei (15>=a),” *Nucl. Phys.*, vol. B52, pp. 1–30, 1973.

[6] A. Gal and H. Garcilazo, “Towards resolving the $^{3}_{\Lambda}$H lifetime puzzle,” *Phys. Lett.*, vol. B791, pp. 48–53, 2019.

[7] M. Tanabashi *et al.*, “Review of Particle Physics,” *Phys. Rev.*, vol. D98, no. 3, p. 030001, 2018.

[8] J. Adam *et al.*, “Precise measurement of the mass difference and the binding energy of hypertriton and antihypertriton,” 2019.

[9] C. Rappold *et al.*, “Search for evidence of $^{3}_{\Lambda}n$ by observing $d + \pi^-$ and $t + \pi^-$ final states in the reaction of $^{6}Li +^{12} C$ at 2A GeV,” *Phys. Rev.*, vol. C88, no. 4, p. 041001, 2013.

[10] J. J. Sakurai and J. Napolitano, *Modern Quantum Mechanics*. Quantum physics, quantum information and quantum computation, Cambridge: Cambridge University Press, 2017.

[11] E. Braaten and H. W. Hammer, "Universality in few-body systems with large scattering length," *Phys. Rept.*, vol. 428, pp. 259–390, 2006.

[12] B. Lippmann and J. Schwinger, "Variational Principles for Scattering Processes. I," *Phys. Rev.*, vol. 79, pp. 469–480, 1950.

[13] H. Bethe, "Theory of the Effective Range in Nuclear Scattering," *Phys. Rev.*, vol. 76, pp. 38–50, 1949.

[14] J. J. de Swart, C. P. F. Terheggen, and V. G. J. Stoks, "The Low-energy n p scattering parameters and the deuteron," in *3rd International Symposium on Dubna Deuteron 95 Dubna, Russia, July 4-7, 1995*, 1995.

[15] Q. Chen *et al.*, "Measurement of the neutron-neutron scattering length using the pi-d capture reaction," *Phys. Rev.*, vol. C77, p. 054002, 2008.

[16] G. A. Miller, B. M. K. Nefkens, and I. Slaus, "Charge symmetry, quarks and mesons," *Phys. Rept.*, vol. 194, pp. 1–116, 1990.

[17] J. Haidenbauer, S. Petschauer, N. Kaiser, U. G. Meissner, A. Nogga, and W. Weise, "Hyperon-nucleon interaction at next-to-leading order in chiral effective field theory," *Nucl. Phys.*, vol. A915, pp. 24–58, 2013.

[18] J. Haidenbauer and U.-G. Meissner, "The Julich hyperon-nucleon model revisited," *Phys. Rev.*, vol. C72, p. 044005, 2005.

[19] T. A. Rijken, V. G. J. Stoks, and Y. Yamamoto, "Soft core hyperon - nucleon potentials," *Phys. Rev.*, vol. C59, pp. 21–40, 1999.

[20] L. D. Faddeev, "Scattering theory for a three particle system," *Sov. Phys. JETP*, vol. 12, pp. 1014–1019, 1961. [Zh. Eksp. Teor. Fiz.39,1459(1960)].

[21] S. Weinberg, "Phenomenological Lagrangians," *Physica*, vol. A96, no. 1-2, pp. 327–340, 1979.

[22] P. F. Bedaque, H. W. Hammer, and U. van Kolck, "The Three boson system with short range interactions," *Nucl. Phys.*, vol. A646, pp. 444–466, 1999.

[23] H. W. Hammer, C. Ji, and D. R. Phillips, "Effective field theory description of halo nuclei," *J. Phys.*, vol. G44, no. 10, p. 103002, 2017.

[24] V. Efimov, "Energy levels arising form the resonant two-body forces in a three-body system," *Phys. Lett.*, vol. 33B, pp. 563–564, 1970.

[25] M. Gattobigio, M. Göbel, H. W. Hammer, and A. Kievsky, “More on the universal equation for Efimov states,” *Few Body Syst.*, vol. 60, no. 2, p. 40, 2019.

[26] G. Danilov, “On the three-body problem with short-range forces,” *J. Exp. Theor. Phys.*, vol. 13, p. 349, 1961.

[27] R. D. Amado and J. V. Noble, “On Efimov’s effect: A new pathology of three-particle systems,” *Phys. Lett.*, vol. 35B, pp. 25–27, 1971.

[28] R. D. Amado and J. V. Noble, “Efimov’s effect - a new pathology of three-particle systems. ii,” *Phys. Rev.*, vol. D5, pp. 1992–2002, 1972.

[29] T. Kraemer, M. Mark, P. Waldburger, J. G. Danzl, C. Chin, B. Engeser, A. D. Lange, K. Pilch, A. Jaakkola, H. C. Naegerl, and R. Grimm, “Evidence for efimov quantum states in an ultracold gas of cesium atoms,”

[30] M. Kunitski *et al.*, “Observation of the Efimov state of the helium trimer,” *Science*, vol. 348, pp. 551–555, 2015.

[31] S.-K. Tung, K. Jimenez-Garcia, J. Johansen, C. V. Parker, and C. Chin, “Geometric scaling of Efimov states in a ^{6}Li-^{133}Cs mixture,” *Phys. Rev. Lett.*, vol. 113, no. 24, p. 240402, 2014.

[32] R. Pires, J. Ulmanis, S. Häfner, M. Repp, A. Arias, E. D. Kuhnle, and M. Weidemüller, “Observation of Efimov Resonances in a Mixture with Extreme Mass Imbalance,” *Phys. Rev. Lett.*, vol. 112, no. 25, p. 250404, 2014.

[33] C. H. Schmickler, H. W. Hammer, and E. Hiyama, “Tetramer Bound States in Heteronuclear Systems,” *Phys. Rev.*, vol. A95, no. 5, p. 052710, 2017.

[34] P. Naidon and S. Endo, “Efimov Physics: a review,” *Rept. Prog. Phys.*, vol. 80, no. 5, p. 056001, 2017.

[35] F. Giacosa, “The Lee model: a tool to study decays,” 1 2020.

[36] R. E. Cutkosky, “Singularities and discontinuities of Feynman amplitudes,” *J. Math. Phys.*, vol. 1, pp. 429–433, 1960.

[37] M. Danysz and J. Pniewski, “Delayed disintegration of a heavy nuclear fragment: I,” *The London, Edinburgh, and Dublin Philosophical Magazine and Journal of Science*, vol. 44, no. 350, pp. 348–350, 1953.

[38] "National Nuclear Data Center, Information extracted from the NuDat 2 database", “http://www.nndc.bnl.gov/nudat2/.”

[39] S. Weinberg, “Nuclear forces from chiral Lagrangians,” *Phys. Lett.*, vol. B251, pp. 288–292, 1990.

[40] S. Weinberg, “Effective chiral Lagrangians for nucleon - pion interactions and nuclear forces,” *Nucl. Phys.*, vol. B363, pp. 3–18, 1991.

[41] H. Polinder, J. Haidenbauer, and U.-G. Meissner, “Hyperon-nucleon interactions: A Chiral effective field theory approach,” *Nucl. Phys.*, vol. A779, pp. 244–266, 2006.

[42] J. Haidenbauer and U. G. Meißner, “Predictions for the strangeness S = -3 and -4 baryon-baryon interactions in chiral effective field theory,” *Phys. Lett.*, vol. B684, pp. 275–280, 2010.

[43] J. Haidenbauer, U.-G. Meißner, and S. Petschauer, “Strangeness S = -2 baryon–baryon interaction at next-to-leading order in chiral effective field theory,” *Nucl. Phys.*, vol. A954, pp. 273–293, 2016.

[44] S. Petschauer, N. Kaiser, J. Haidenbauer, U.-G. Meißner, and W. Weise, “Leading three-baryon forces from SU(3) chiral effective field theory,” *Phys. Rev.*, vol. C93, no. 1, p. 014001, 2016.

[45] S. R. Beane, E. Chang, S. D. Cohen, W. Detmold, H. W. Lin, T. C. Luu, K. Orginos, A. Parreno, M. J. Savage, and A. Walker-Loud, “Light Nuclei and Hypernuclei from Quantum Chromodynamics in the Limit of SU(3) Flavor Symmetry,” *Phys. Rev.*, vol. D87, no. 3, p. 034506, 2013.

[46] J. Donoghue, E. Golowich, and B. R. Holstein, *Dynamics of the standard model*, vol. 2. CUP, 2014.

[47] B. R. Holstein, *Weak interactions in nuclei*. 1985.

[48] J. Adam *et al.*, “$^{3}_{\Lambda}\mathrm{H}$ and $^{3}_{\bar{\Lambda}}\overline{\mathrm{H}}$ production in Pb-Pb collisions at $\sqrt{s_{\mathrm{NN}}} = 2.76$ TeV,” *Phys. Lett.*, vol. B754, pp. 360–372, 2016.

[49] B. Dönigus, “(Anti-)matter and hyper-matter production at the LHC with ALICE,” *Nucl. Phys.*, vol. A904-905, pp. 547c–550c, 2013.

[50] J. G. Congleton, “A Simple model of the hypertriton,” *J. Phys.*, vol. G18, pp. 339–357, 1992.

[51] B. Povh, K. Rith, C. Scholz, F. Zersche, and W. Rodejohann, *Particles and nuclei: An Introduction to the physical concepts*. Graduate Texts in Physics, Springer, 1995.

[52] J. Cohen, “Weak Non-mesonic Decays of Λ Hypernuclei,” *Prog. Part. Nucl. Phys.*, vol. 25, pp. 139–234, 1990.

[53] J. Golak, K. Miyagawa, H. Kamada, H. Witala, W. Gloeckle, A. Parreno, A. Ramos, and C. Bennhold, “The Non-mesonic weak decay of the hypertriton,” *Phys. Rev.*, vol. C55, pp. 2196–2213, 1997. [Erratum: Phys. Rev.C56,2892(1997)].

[54] B. I. Abelev *et al.*, “Observation of an Antimatter Hypernucleus,” *Science*, vol. 328, pp. 58–62, 2010.

[55] L. Adamczyk *et al.*, “Measurement of the ${}^{3}_{\Lambda}\mathrm{H}$ lifetime in Au+Au collisions at the BNL Relativistic Heavy Ion Collider,” *Phys. Rev.*, vol. C97, no. 5, p. 054909, 2018.

[56] S. Acharya *et al.*, “${}^{3}_{\Lambda}\mathrm{H}$ and ${}^{3}_{\bar{\Lambda}}\overline{\mathrm{H}}$ lifetime measurement in Pb-Pb collisions at $\sqrt{s_{\mathrm{NN}}} =$ 5.02 TeV via two-body decay,” 2019.

[57] C. Rappold *et al.*, “Hypernuclear spectroscopy of products from 6Li projectiles on a carbon target at 2 AGeV,” *Nucl. Phys.*, vol. A913, pp. 170–184, 2013.

[58] R. J. Prem and P. H. Steinberg, “Lifetimes of hypernuclei, ${}_{\Lambda}\mathrm{H}^{3}$, ${}_{\Lambda}\mathrm{H}^{4}$, ${}_{\Lambda}\mathrm{H}^{5}$,” *Phys. Rev.*, vol. 136, pp. B1803–B1806, Dec 1964.

[59] G. Keyes, M. Derrick, T. Fields, L. G. Hyman, J. G. Fetkovich, J. Mckenzie, B. Riley, and I. T. Wang, “Properties of (lambda)he-3,” *Phys. Rev.*, vol. D1, pp. 66–77, 1970.

[60] G. Bohm *et al.*, “On the lifetime of the ${}^{3}_{\Lambda}\mathrm{H}$ hypernucleus,” *Nucl. Phys.*, vol. B16, pp. 46–52, 1970. [Erratum: Nucl. Phys.B16,523(1970)].

[61] G. Keyes, J. Sacton, J. H. Wickens, and M. M. Block, “A measurement of the lifetime of the (lambda)h-3 hypernucleus,” *Nucl. Phys.*, vol. B67, pp. 269–283, 1973.

[62] M. M. Block, R. Gessaroli, J. Kopelman, S. Ratti, M. Schneeberger, L. Grimellini, T. Kikuchi, L. Lendinara, L. Monari, W. Becker, and E. Harth, “Hyperfragment studies in the helium bubble chamber,” 1964.

[63] G. Keyes, M. Derrick, T. Fields, L. G. Hyman, J. G. Fetkovich, J. McKenzie, B. Riley, and I. T. Wang, “New Measurement of the H La-3mda Lifetime,” *Phys. Rev. Lett.*, vol. 20, pp. 819–821, 1968.

[64] R. E. Phillips and J. Schneps, “Lifetimes of light hyperfragments. ii,” *Phys. Rev.*, vol. 180, pp. 1307–1318, 1969.

[65] A. Mastroserio, "Search for a Λnn bound state in Pb-Pb collisions with ALICE at the LHC," *EPJ Web Conf.*, vol. 192, p. 00045, 2018.

[66] A. Gal and H. Garcilazo, "Is there a bound Λnn?," *Phys. Lett.*, vol. B736, pp. 93–97, 2014.

[67] H. Garcilazo and A. Valcarce, "Nonexistence of a Λnn bound state," *Phys. Rev.*, vol. C89, no. 5, p. 057001, 2014.

[68] J.-M. Richard, Q. Wang, and Q. Zhao, "Lightest neutral hypernuclei with strangeness -1 and -2," *Phys. Rev.*, vol. C91, no. 1, p. 014003, 2015.

[69] E. Hiyama, S. Ohnishi, B. F. Gibson, and T. A. Rijken, "Three-body structure of the $nn\Lambda$ system with $\Lambda N - \Sigma N$ coupling," *Phys. Rev.*, vol. C89, no. 6, p. 061302, 2014.

[70] B. W. Downs and R. H. Dalitz, "Analysis of the Λ-hypernuclear three-body systems," *Phys. Rev.*, vol. 114, pp. 593–602, Apr 1959.

[71] V. Belyaev, S. Rakityansky, and W. Sandhas, "Three-body resonances λnn and $\lambda\lambda$n," *Nuclear Physics A*, vol. 803, no. 3, pp. 210 – 226, 2008.

[72] B. F. Gibson and I. R. Afnan, "Conjecture Regarding a Possible $nn\Lambda$ Resonance," *JPS Conf. Proc.*, vol. 17, p. 012001, 2017.

[73] H. Kamada, K. Miyagawa, and M. Yamaguchi, "A Λnn three-body resonance," *EPJ Web Conf.*, vol. 113, p. 07004, 2016.

[74] S.-I. Ando, U. Raha, and Y. Oh, "Investigation of the $nn\Lambda$ bound state in pionless effective theory," *Phys. Rev.*, vol. C92, no. 2, p. 024325, 2015.

[75] J. Fujita and H. Miyazawa, "Pion Theory of Three-Body Forces," *Prog. Theor. Phys.*, vol. 17, pp. 360–365, 1957.

[76] H.-W. Hammer, A. Nogga, and A. Schwenk, "Three-body forces: From cold atoms to nuclei," *Rev. Mod. Phys.*, vol. 85, p. 197, 2013.

[77] O. N. I.G. Kaplan, "The role of non-additive forces in atomic and nuclear interactions," *Rev.Mex.Fis.*, vol. 40, p. 108, 1994.

[78] I. R. Afnan and B. F. Gibson, "$\Lambda N - \Sigma N$ Coupling in (Λ) ^{3}H," *Phys. Rev.*, vol. C40, pp. R7–R9, 1989.

[79] I. R. Afnan and B. F. Gibson, "Hypertriton: Lambda <—> Sigma conversion and tensor forces," *Phys. Rev.*, vol. C41, pp. 2787–2799, 1990.

[80] M. J. Savage, “The Delta Delta intermediate state in s wave singlet N N scattering from effective field theory,” *Phys. Rev.*, vol. C55, pp. 2185–2190, 1997.

[81] F. Hildenbrand and H.-W. Hammer, “Three-Body Hypernuclei in Pionless Effective Field Theory,” *Phys. Rev. C*, vol. 100, no. 3, p. 034002, 2019. [Erratum: Phys.Rev.C 102, 039901 (2020)].

[82] P. F. Bedaque and U. van Kolck, “Effective field theory for few nucleon systems,” *Ann. Rev. Nucl. Part. Sci.*, vol. 52, pp. 339–396, 2002.

[83] H. W. Hammer, “The Hypertriton in effective field theory,” *Nucl. Phys.*, vol. A705, pp. 173–189, 2002.

[84] N. Barnea, B. Bazak, E. Friedman, and A. Gal, “Onset of η-nuclear binding in a pionless EFT approach,” *Phys. Lett.*, vol. B771, pp. 297–302, 2017. [Erratum: Phys. Lett.B775,364(2017)].

[85] N. Barnea, E. Friedman, and A. Gal, “Onset of η-meson binding in the He isotopes,” *Nucl. Phys.*, vol. A968, pp. 35–47, 2017.

[86] L. Contessi, N. Barnea, and A. Gal, “Resolving the Λ Hypernuclear Overbinding Problem in Pionless Effective Field Theory,” *Phys. Rev. Lett.*, vol. 121, no. 10, p. 102502, 2018.

[87] S.-I. Ando, G.-S. Yang, and Y. Oh, “${}_{\Lambda\Lambda}{}^{4}$H in halo effective field theory,” *Phys. Rev.*, vol. C89, no. 1, p. 014318, 2014.

[88] S.-I. Ando and Y. Oh, “${}_{\Lambda\Lambda}^{6}$He in cluster effective field theory,” *Phys. Rev.*, vol. C90, no. 3, p. 037301, 2014.

[89] S.-I. Ando, “Hypernuclei in Halo/Cluster Effective Field Theory,” *Int. J. Mod. Phys.*, vol. E25, no. 05, p. 1641005, 2016.

[90] D. B. Kaplan, M. J. Savage, and M. B. Wise, “A new expansion for nucleon-nucleon interactions,” *Physics Letters B*, vol. 424, no. 3–4, pp. 390 – 396, 1998.

[91] U. van Kolck, “Effective field theory of short-range forces,” *Nuclear Physics A*, vol. 645, no. 2, pp. 273 – 302, 1999.

[92] P. F. Bedaque, H. W. Hammer, and U. van Kolck, “Renormalization of the three-body system with short range interactions,” *Phys. Rev. Lett.*, vol. 82, pp. 463–467, 1999.

[93] P. Bedaque, H.-W. Hammer, and U. van Kolck, “Effective theory of the triton,” *Nuclear Physics A*, vol. 676, no. 1–4, pp. 357 – 370, 2000.

[94] P. F. Bedaque, H. W. Hammer, and U. van Kolck, “Effective theory for neutron deuteron scattering: Energy dependence,” *Phys. Rev.*, vol. C58, pp. R641–R644, 1998.

[95] H. W. Hammer and T. Mehen, “A Renormalized equation for the three-body system with short range interactions,” *Nucl. Phys.*, vol. A690, pp. 535–546, 2001.

[96] A. C. Phillips, “Consistency of the low-energy three-nucleon observables and the separable interaction model,” *Nucl. Phys.*, vol. A107, pp. 209–216, 1968.

[97] A. Cobis, A. S. Jensen, and D. V. Fedorov, “The simplest strange three-body halo,” *Journal of Physics G: Nuclear and Particle Physics*, vol. 23, no. 4, p. 401, 1997.

[98] H. W. Hammer and S. König, “Constraints on a possible dineutron state from pionless EFT,” *Phys. Lett.*, vol. B736, pp. 208–213, 2014.

[99] A. Gardestig, “Extracting the neutron-neutron scattering length - recent developments,” *J. Phys.*, vol. G36, p. 053001, 2009.

[100] P. Braun-Munzinger and B. Dönigus, “Loosely-bound objects produced in nuclear collisions at the LHC,” *Nucl. Phys. A*, vol. 987, pp. 144–201, 2019.

[101] J. Chen, D. Keane, Y.-G. Ma, A. Tang, and Z. Xu, “Antinuclei in Heavy-Ion Collisions,” *Phys. Rept.*, vol. 760, pp. 1–39, 2018.

[102] I. R. Afnan and A. W. Thomas, “Fundamentals of Three-Body Scattering Theory,” *Top. Curr. Phys.*, vol. 2, pp. 1–47, 1977.

[103] W. Glöckle, *The Quantum Mechanical Few-Body Problem*. Springer, Berlin, Heidelberg, 1983.

[104] B. Acharya, C. Ji, and D. R. Phillips, “Implications of a matter-radius measurement for the structure of Carbon-22,” *Phys. Lett.*, vol. B723, pp. 196–200, 2013.

[105] D. L. Canham and H. W. Hammer, “Universal properties and structure of halo nuclei,” *Eur. Phys. J.*, vol. A37, pp. 367–380, 2008.

[106] M. Göbel, H. W. Hammer, C. Ji, and D. R. Phillips, “Momentum-space probability density of ^{6}He in Halo Effective Field Theory,” *Few Body Syst.*, vol. 60, no. 4, p. 61, 2019.

[107] M. Schäfer, B. Bazak, N. Barnea, and J. Mareˇ s, “The Continuum Spectrum of Hypernuclear Trios,” 3 2020.

[108] L. Contessi, N. Barnea, and A. Gal, “$B_\Lambda({}^{5}_{\Lambda}\text{He})$ from short range effective field theory,” *AIP Conf. Proc.*, vol. 2130, no. 1, p. 040012, 2019.

[109] Z. Zhang and C. M. Ko, “Hypertriton production in relativistic heavy ion collisions,” *Phys. Lett.*, vol. B780, pp. 191–195, 2018.

[110] N. Barnea, L. Contessi, D. Gazit, F. Pederiva, and U. van Kolck, “Effective Field Theory for Lattice Nuclei,” *Phys. Rev. Lett.*, vol. 114, no. 5, p. 052501, 2015.

[111] F. Hildenbrand and H.-W. Hammer, “On the lifetime of the hypertriton,” *arXiv 2007.10122*, 2020.

[112] M. Rayet and R. Dalitz, “Lifetime of H-3,” *Nuovo Cim. A*, vol. 46, pp. 786–794, 1966.

[113] B. Ram and W. Williams, “Decay rate and branching ratio (pi- he-3)/(all pi-modes) of (lambda)h-3,” *Nucl. Phys. B*, vol. 28, pp. 566–572, 1971.

[114] H. Kamada, J. Golak, K. Miyagawa, H. Witala, and W. Gloeckle, “Pi mesonic decay of the hypertriton,” *Phys. Rev.*, vol. C57, pp. 1595–1603, 1998.

[115] A. Pérez-Obiol, A. Nogga, and D. R. Entem, “Non-Mesonic Weak Decay of the Hypertriton with Effective Field Theory,” *JPS Conf. Proc.*, vol. 17, p. 022002, 2017.

[116] M. Ablikim *et al.*, “Polarization and Entanglement in Baryon-Antibaryon Pair Production in Electron-Positron Annihilation,” *Nature Phys.*, vol. 15, pp. 631–634, 2019.

[117] D. Ireland, M. Döring, D. Glazier, J. Haidenbauer, M. Mai, R. Murray-Smith, and D. Rönchen, “Kaon Photoproduction and the Λ Decay Parameter α_-,” *Phys. Rev. Lett.*, vol. 123, no. 18, p. 182301, 2019.

[118] M. Schmidt, M. Jansen, and H.-W. Hammer, “Threshold Effects and the Line Shape of the X(3872) in Effective Field Theory,” *Phys. Rev. D*, vol. 98, no. 1, p. 014032, 2018.

[119] M. Block in *Sienna International Conference on Elementary Particles* (G. Bernandini and G. Puppi, eds.), p. 62, Societa de Fisicia, 1963.

[120] The ALICE Collaboration, "Addendum to the Technical Design Report for the Upgrade of the ALICE Time Projection Chamber," 2 2015.

[121] B. Abelev *et al.*, "Technical Design Report for the Upgrade of the ALICE Inner Tracking System," *J. Phys. G*, vol. 41, p. 087002, 2014.

[122] B. Abelev *et al.*, "Upgrade of the ALICE experiment: Letter of intent," *Journal of Physics G: Nuclear and Particle Physics*, vol. 41, p. 087001, jul 2014.

[123] P. Achenbach, S. Bleser, J. Pochodzalla, and M. Steinen, "High-precision measurement of the hypertriton mass," *PoS*, vol. Hadron2017, p. 207, 2018.

[124] L. Tang, F. Garibaldi, P. Markowitz, S. Nakamura, J.Reinhold, and G. Urciuoli, "Proposal to Jefferson Lab PAC 45, Determining the Unknown Λ-n Interaction by Investigating the Λ nn Resonance." Project Proposal, 2017.

[125] F. Hildenbrand, "Effektive Theorien in der Quantenmechanik." Bachelors' Thesis, 2014.

Curriculum Vitae

Fabian Hildenbrand

Date of Birth	July 20, 1990
Address	Erbacherstr. 4 64283 Darmstadt
Email	hildenbrand@theorie.ikp.physik.tu-darmstadt.de

Working Experience

2016-present	Institut für Kernphysik der TU Darmstadt (Darmstadt, Germany) Scientific employee (June-present)
2012-2016	TU Darmstadt Student teaching assistant (Sep.-May)
2010-2011	Kreis Wesel (Wesel, Germany) Social Service (Sep.-Feb.)

Education

2016-present	TU Darmstadt doctoral studies (June-present)
2014-2016	TU Darmstadt M.Sc. in Physics (Dec.-May)
2011-2014	TU Darmstadt B.Sc. in Physics (April-Nov.)
2002-2010	Gymnasium Voerde (Voerde, Germany) Abitur (July-June)

Acknowledgements

Mein besonderer Dank gilt meinem Doktorvater Hans-Werner Hammer, der mich bereits seit meiner Bachelorarbeit durch mein Studium und meine wissenschaftliche Arbeit begleitet. Hans-Werner hatte die Tür für mich in den letzten fast 7 Jahren stets geöffnet und war auch stets offen für andere Meinungen und Ansichten. Der Dank gilt dabei nicht nur der wissenschaftlichen Expertise sondern auch für diverse Gruppenaktivitäten.

Bei Jens Braun möchte ich mich nicht nur dafür Bedanken, dass er diese Arbeit begutachtet, sondern insbesondere dafür, dass er als unbestrittener Meister im einbauen von Trailern in die Quantenfeldtheorie-Vorlesungen mir dieses Physikfeld verständlich nahe gebracht hat. Auch hat er mich in meiner Skepsis gegenüber grüner Kreide bestätigt.

Herzlich bedanken möchte ich bei den vielen Kollegen die mich im Laufe meiner Zeit hier am IKP begleitet haben. Insbesondere möchte ich dabei bei Marcel Schmidt, Wael Elkamhawy und Matthias Göbel bedanken, welche nicht nur diese Dissertation Korrektur gelesen haben, sondern mir gemeinsam mit Artem Volosniev stets beim Vernichten von Kreide behilflich gewesen sind. Ich wünsche Ihnen allen für Ihre Zukunft alles Gute.

Ganz herzlich bedanken möchte ich mich auch bei Laura Mertes für unsere gemeinsamen Bestrebungen theoretische Physik auch jungen Menschen im Rahmen der deutschen SchülerAkademie nahe zu bringen.

Mein größten Dank möchte ich meinen Eltern Astrid und Martin und meinem Bruder Dennis aussprechen, die mich in meinem Leben stets mit all Ihrer Kraft unterstützt haben und ohne die diese Dissertation gar nicht möglich gewesen wäre. Bei meiner Cousine Mona möchte ich mich für Ihr offenes Ohr und ihren Rat herzlich bedanken.